FORMATION OF CADMIUM SULFIDE THIN FILMS ON DIFFERENT SUBSTRATES USING ELECTROCHEMICAL ATOMIC LAYER DEPOSITION (E-ALD)

by

SHENG SHEN

(Under the Direction of John L. Stickney)

ABSTRACT

This dissertation discussed the layer-by-layer growth of CdS thin film using electrochemical atomic layer deposition (E-ALD) as well as the investigations into the possible fabrication of both substrate and superstrate configurations of CdTe/CdS solar cells. E-ALD is the electrochemical equivalence of gas phase atomic layer deposition (ALD). Similar to ALD, E-ALD allows for the layer-by-layer deposition of materials using surface-limited reaction. Underpotential deposition (UPD) is usually used in E-ALD, allowing for atomically thick layers of materials to be deposited on a second material at a potential before the potential needed for the element to deposit on itself. In this report, CdS thin films with different thicknesses were grown using E-ALD. Results indicated that the E-ALD grown CdS on Au was stoichiometric, crystalline, uniform, and is N-type. Formation of CdS on Ag substrates and on ITO was also studied.

Preliminary studies on the fabrication of CdS/CdTe photovoltaic device with both superstrate and substrate configuration were also performed. In the substrate configuration, CdTe was first deposited onto Au substrates using 15 minutes of codeposition at -700 mV, followed by electrochemical atomic layer deposition (E-ALD) of CdS on CdTe/Au. In the superstrate

configuration, the ITO substrate was first patterned with 1x1 mm^2 squares using photolithography, and then treated with electrochemical methods to form Cu nucleation sites on the ITO surface. CdS E-ALD was performed on the treated ITO substrate. CdTe thin films were deposited onto CdS/ITO using pulse plating atomic layer deposition (PP-ALD). A layer of Au was deposited electrochemically on CdTe/CdS/ITO as the back contact. Photoelectrochemical measurements on the substrate configuration showed good P-type response and clean dark current. XRD showed CdTe zinc blend <111> and CdS zinc blend <111> structure. SEM images of the CdTe/CdS/ITO showed compact deposits covering the whole surface. Work on collecting more information on cell performance is on the way.

INDEX WORDS: electrochemical atomic layer deposition, cadmium telluride, cadmium sulfide, Ag nanorods, indium-tin oxide, thin-film, UPD, photovoltaics, XRD, EPMA, cyclic voltammetry, p-n junction, electrodeposition

FORMATION OF CADMIUM SULFIDE THIN FILMS ON DIFFERENT SUBSTRATES USING ELECTROCHEMICAL ATOMIC LAYER DEPOSITION (E-ALD)

by

SHENG SHEN

BS, Wuhan University, China, 2012

A Dissertation Submitted to the Graduate Faculty of The University of Georgia in Partial Fulfillment of the Requirements for the Degree

DOCTOR OF PHILOSOPHY

ATHENS, GEORGIA

2018

FORMATION OF CADMIUM SULFIDE THIN FILMS ON DIFFERENT SUBSTRATES

USING ELECTROCHEMICAL ATOMIC LAYER DEPOSITION (E-ALD)

by

SHENG SHEN

Major Professor:	John L. Stickney
Committee:	Tina Salguero
	Jeffrey Urbauer

Electronic Version Approved:

Suzanne Barbour
Dean of the Graduate School
The University of Georgia
May 2018

DEDICATION

To everyone who has helped me along this long walk.

ACKNOWLEDGEMENTS

I would like to thank Dr. John Stickney for being a great mentor in all aspects. He has not only taught me science and research skills, but also a broader attitude towards life in general. His patience, motivation, and enthusiasm will always be guidance in my future growth. I would also like to thank my past and present group members for all their help and support through the years.

TABLE OF CONTENTS

Page

CHAPTER 1

INTRODUCTION AND LITERATURE REVIEW

With the energy crisis people are faced with today, researchers are actively searching for alternative energy sources other than fossil fuels. One of the most promising solutions is solar energy[1]. By 2050, people will need 23 terawatts (TW) of energy to sustain the lifestyle of the total world population[2]. There are 120,000 TW of solar energy hitting the earth every year. Despite of this massive resource, the energy produced from solar remains less than 0.01% of the total world energy demand.

Photovoltaic describes a group of device that converts solar energy to electricity. It usually consists of an electron-rich n-type semiconductor and a hole-rich p-type semiconductor. When the semiconductors are brought together and in contact with each other, the electrons in the n-type semiconductor diffuse across the semiconductor interface and the same behavior happens for the hole in the p-type semiconductor. As the electrons and hole diffuse and neutralize, the fixed ion cores left behind at the interface is going to set up an electric field called the depletion region. When the equilibrium is reestablished, a p-n junction is formed, and the Fermi levels of the two semiconductors are going to align, causing bending of the valence band and the conduction band. This band bending sets up a potential barrier. When the p-n junction is illuminated by light, energy from photons is going to be absorbed, exciting the electrons, and electron-hole pairs are generated. Because of the potential barrier, the electrons and holes can only go a certain direction, and this movement of electrons and holes creates current. Only photons with energy higher than the bandgap will be absorbed.

The first generation solar cells are based on Si wafers[3], including both single crystals and bulk polycrystalline Si wafers[4]. In today's solar cell market, 80-90% of the technology is dominated by silicon-based materials[5]. As an indirect bandgap material, in order for an electron to absorb a photon to be excited to the conduction band, the assistance of a phonon needed. This has led to the low absorption coefficient of Si wafers, which require the material thickness to be a few hundred μm to absorb most of the incident light. The high manufacturing cost associated with the large amount of materials needed is the major factor hindering the development of Si solar cells.

To reduce the cost and achieve high efficiency, researchers have developed 2nd generation of solar cells that are based on thin film materials such as CdTe[6-11], Cu_2ZnSnS_4 (CZTS)[12-20], Cu(In,Ga)Se (CIGS)[21-26], etc. These semiconductors are possible candidates for solar cells because they have bandgaps near the optimal 1.5 eV and have theoretical efficiency limit of 30%[27-28]. The basic advantages thin film solar cells have over their crystalline counterparts are materials utilization, mass production and integrated module fabrication: this has been the driving force for their development since the early sixties[29]. In structure of a typical thin film solar cell, the p-type absorber material is usually partnered with the n-type semiconductor CdS to form a p-n junction. The light comes in from the front transparent conducting oxide (TCO) and passes through semi-transparent CdS layer and eventually be absorbed by the p-type absorber layer. Electron-hole pairs are generated at the p-n junction and are conducted out to the external circuit by the back contact. CdTe is one of the most prevailing absorber material used in thin film solar cells. It has a large absorption coefficient ($>1x10^4$ cm^{-1})[30-31], and only a few micron is sufficient to absorb 90% of the light with energy above CdTe's

bandgap (1.4 eV). The reduced thickness gives rise to an intense electric field, which facilitates carrier generation and collection.

Another critical component of CdTe solar cell is CdS. CdS is the most widely used n-type material in thin film solar cell. The major function of CdS layer is to allow the maximum amount of light to pass through and to form p-n junction with the absorber layer. For high optical throughput, an ideal candidate for the n-type material should have a high bandgap and thickness as low as possible thus to absorb the minimum amount of light and to maintain low series resistance[32]. CdS also facilitates the formation of large bandgap $CdTe_{1-x}S_x$ mixed crystal layer near the CdS-CdTe interface[33].

The common methods for forming CdS thin films include spray pyrolysis[34-39], closed-space sublimation (CSS)[8, 40-44], atomic layer deposition (ALD)[45], chemical bath deposition (CBD)[22, 46-51], etc. The principle of spray pyrolysis is the process of spraying very fine aqueous dispersion of the salt of interest onto a heated substrate, where the salt decomposes and forms a thermally resistant compound of the metal with sulphur[52]. The reactants are selected such that the products, other than the desired compound, are volatile at the temperature of deposition[53]. Since the deposition is made at a high temperature, no post-fabrication annealing is required. Similar to spray pyrolysis, decomposition under high temperature also occurs in closed-space sublimation, where the source dissociates into elements, which recombine at the substrate surface, forming CdS. The driving force for compound formation in CSS is the temperature difference between the source and the substrate, along with the surface energy of the substrate. Atomic layer deposition (ALD) is where monoatomic layers of elemental Cd and S are deposited sequentially by periodically alternating a gas flow between a Cd containing and an S containing inert carrier gas. Each deposition cycle is limited to one atomic layer at a time. This method allows for

precise control of the CdS/CdTe intermixing region, by controlling the number of atomic layers. All of the aforementioned deposition techniques require high temperature and most of them require vacuum chambers, which significant increase the fabrication cost.

A popular method for fabricating CdS thin film is chemical bath deposition (CBD), where the growth of CdS is realized by ion-by-ion condensation of Cd^{2+} and S^{2-} on the surface of the substrate. A Cd source in the form of a salt is dissolved in the solution and slowly releases Cd^{2+}. The S^{2-} in the solution generated by thiosulfate will precipitate with the Cd^{2+}, forming CdS on the substrate surface. The entire process can be done with a beaker on a hotplate. Thin, compact CdS thin films have been fabricated using chemical bath deposition.

Another low cost method for forming CdS thin film at ambient condition is electrodeposition[54-57]. Since the dual damascene method was developed to fabricate high quality copper interconnects in microprocessors, electrodeposition has been proven to meet the industry requirements for large-scale production[58]. The film quality and composition can be controlled by varying the precursor concentration, pH, deposition potential, and temperature. The problem of conventional electrodeposition is that bulk deposition usually results in rough surface morphology and limited control of thickness.

Electrochemical atomic layer deposition (E-ALD)[59-64] was developed by this group and is the electrochemical equivalent of gas phase ALD. Similar to ALD, E-ALD uses surface limited reaction, which is referred to as underpotential deposition (UPD). UPD allows for atomically thick layers of materials to be deposited on a second material at a potential before the potential needed for the element to deposit on itself[65]. This is explained by the negative free energy change for compound formation, which stabilizes the element on the second material[66-68]. In a typical E-ALD cycle, a solution containing the ionic form of the element of interest is introduced

to the cell, and is deposited at a potential where only less than a monolayer of deposit should form. A monolayer is defined as one adsorbate atom per surface atom. After the reaction is completed, a blank solution is introduced to cell to rinse away any excess precursor ions, and a new solution containing the second element is introduced at its UPD and forms an atomic layer on the surface of the first element. After the reaction is completed, the solution is rinse away with a blank solution, and a bilayer of the compound of interest is formed on the substrate. This cycle can be repeated many times until the desired film thickness is reached. This method significantly increases the deposit morphology and prevents 3D growth, at the same time gives precise control of the deposit composition and thickness. E-ALD formation of absorber layers such as CdTe[66] and CIGS[64] has been studied by this group.

This dissertation involves the growth and characterization of CdS thin films on different substrates using E-ALD, and the fabrication of CdTe/CdS by electrochemical methods. In these studies the films were grown using an automated flow cell system (Electrochemical ALD L.C., Athens, GA). The system consists of solution bottles containing different precursor solutions and blank rinse solutions. All of the bottles were connected to a distribution valve, which distributes solutions to the flowcell. A pump was connected to the flow cell to pump the solution into and out from the cell. All waste was pumped to a waste container. The flow cell has an Au wire inlayed as the auxiliary electrode. The working electrode is the substrate used for electrodeposition, with an area of 2.1 cm^2. An Ag/AgCl reference electrode was used to form the 3-electrode setup. The potentials are measured using a potentiostat. The pump, the valves and the potentiostat are automated using an in house LabVIEW-based program called “SEQUENCER”. During the electrodeposition process, the solution bottles and the valves were continuously purged with nitrogen to minimized oxygen gas in the system.

Chapter 2 of the dissertation presents the study of E-ALD formation of CdS on Au substrates. The electrochemical behavior of Cd and S were studied using cyclic voltammetry (CV). Deposits formed at different potentials and flow speeds were made and the dependence of film composition on deposition potential was investigated. The films were analyzed with a variety of thin film characterization techniques including electron probe microanalysis (EPMA), X-ray diffraction (XRD), spectroscopic elliposometry (SE), scanning electron microscopy (SEM), and photoelectrochemistry to probe different aspects of the film. The growth rate was found to be linear with respect to the deposition cycle numbers. A sharp CdS zinc blend <111> crystal pattern was observed in XRD. The growth rate was determined to be 0.56 ML/cycle. SEM of the deposits showed conformal coating over the substrate and the morphology of the deposits followed that of the substrate. Photoelectrochemical measurements showed that the deposit was n-type semiconductor with a very clean dark current, suggesting good film quality.

Chapter 3 describes the study of E-ALD of CdS on Ag substrates, on both planar and nanorod form. The deposition differs from that on Au in that Ag is more reactive and at open circuit forms bulk Ag_2S, so the potential for CdS growth on Ag needs to be more carefully controlled. The electrochemical behavior of Cd and S on Ag planar films was studied using cyclic voltammetry. The more complicated morphology of nanorods also posed challenges to the conformal growth of the thin film. The deposition potentials for both Cd and S were found to work best at -600 mV. The films of CdS fabricated on both planar Ag films and on Ag nanorods were characterized using EPMA and SEM. The SEM of Ag nanorods before and after deposition showed distinct difference, and the CdS seemed to coat all sides and direction of the exposed Ag nanorods.

Chapter 4 of this dissertation investigates the possibility of using E-ALD to form CdS on Indium-Tin-Oxide (ITO) substrates, because ITO is the most widely used front contact material in making photovoltaic devices. The difficulty in this study lies in the heterogeneity nature of ITO. There are several different kinds of oxygen and indium atoms on the surface of ITO. Neither Cd nor S showed UPD behavior on ITO substrates. The proposed method in this dissertation is to first reduce a small amount of ITO to indium metal, which can act as nucleation sites for Cd and S UPD growth. But indium metal is not stable at the potential where Cd deposits, so Cu is used to replace indium as a more stable nucleation site. This method not only increased the density of nucleation sites on ITO surface by over an order of magnitude, but also improves the adhesion between the CdS thin film and the ITO substrate.

Chapter 5 involves the CdTe/CdS photovoltaic device fabrication with superstrate configuration. It is a step forward from chapter 4 after CdS is deposited onto ITO substrate, so that subsequent layers can be deposited and a complete device could be fabricated. Photolithography was first used to divide the surface of ITO into 1x1 mm^2 squares so that each square can act as its own individual photovoltaic device. If there is a defect or short circuit in one square, the performance of other squares won't be affected. CdS thin film was deposited onto the ITO substrate using the method described in chapter 4. CdTe absorber layer was deposited onto CdS/ITO by a lab mate Xiaoyue Zhang using Pulse-Plating Atomic Layer Deposition (PP-ALD) method. And finally Au back contact was electrochemically deposited on to CdTe/CdS/ITO, so that a complete device was fabricated.

Chapter 6 involves the deposition of an ultra-thin Au layer on triple junction amorphous silicon solar cell for protection purpose. The method used for the deposition follows the same idea in chapter 4, where a minimum amount of ITO is reduced to In metal and a more stable

metal Au is introduced for the redox exchange at open circuit. The Au coverage on the surface increases as the cycle number increases and eventually plateaued after reaching a full monolayer. The Au layer covers the TJSC surface evenly with no visible defects under SEM. The Au-coated TJSC is stable in pH 13 solution for over an hour. Future studies can be done on characterizing the PEC performance of the Au-coated TJSC for catalyst attachment and water splitting.

References

1. Weisz, P. B., Basic choices and constraints on long-term energy supplies. *PHYSICS TODAY*. **2004,** *57* (7), 47-52.

2. Kamat, P. V., Meeting the Clean Energy Demand: Nanostructure Architectures for Solar Energy Conversion. *The Journal of Physical Chemistry C* **2007,** *111* (7), 2834-2860.

3. Goetzberger, A.; Knobloch, J.; Voss, B., *Crystalline silicon solar cells*. Wiley Online Library: 1998.

4. Badawy, W. A., A review on solar cells from Si-single crystals to porous materials and quantum dots. *Journal of advanced research* **2015,** *6* (2), 123-132.

5. Rahman, M. Z., Advances in surface passivation and emitter optimization techniques of c-Si solar cells. *Renewable and Sustainable Energy Reviews* **2014,** *30*, 734-742.

6. Durose, K.; Edwards, P.; Halliday, D., Materials aspects of CdTe/CdS solar cells. *Journal of Crystal Growth* **1999,** *197* (3), 733-742.

7. Mathew, X.; Enriquez, J. P.; Romeo, A.; Tiwari, A. N., CdTe/CdS solar cells on flexible substrates. *Sol. Energy* **2004,** *77* (6), 831-838.

8. Aramoto, T.; Kumazawa, S.; Higuchi, H.; Arita, T.; Shibutani, S.; Nishio, T.; Nakajima, J.; Tsuji, M.; Hanafusa, A.; Hibino, T., 16.0% efficient thin-film CdS/CdTe solar cells. *Japanese Journal of Applied Physics* **1997,** *36* (10R), 6304.

9. Britt, J.; Ferekides, C., Thin‐film CdS/CdTe solar cell with 15.8% efficiency. *Applied Physics Letters* **1993,** *62* (22), 2851-2852.

10. Sites, J.; Pan, J., Strategies to increase CdTe solar-cell voltage. *Thin Solid Films* **2007,** *515* (15), 6099-6102.

11. Mitchell, K. W.; Fahrenbruch, A. L.; Bube, R. H., Evaluation of the CdS/CdTe heterojunction solar cell. *Journal of Applied Physics* **1977,** *48* (10), 4365-4371.

12. Katagiri, H.; Jimbo, K.; Maw, W. S.; Oishi, K.; Yamazaki, M.; Araki, H.; Takeuchi, A., Development of CZTS-based thin film solar cells. *Thin Solid Films* **2009,** *517* (7), 2455-2460.

13. Malerba, C.; Biccari, F.; Azanza Ricardo, C. L.; Valentini, M.; Chierchia, R.; Müller, M.; Santoni, A.; Esposito, E.; Mangiapane, P.; Scardi, P.; Mittiga, A., CZTS stoichiometry effects on the band gap energy. *Journal of Alloys and Compounds* **2014,** *582* (0), 528-534.

14. Suryawanshi, M. P.; Agawane, G. L.; Bhosale, S. M.; Shin, S. W.; Patil, P. S.; Kim, J. H.; Moholkar, A. V., CZTS based thin film solar cells: a status review. *Materials Technology* **2013,** *28* (1/2), 98-109.

15. Jiang, M.; Yan, X., *Cu2ZnSnS4 Thin Film Solar Cells: Present Status and Future Prospects*. 2013.

16. Minlin, J.; Dhakal, R.; Yong, L.; Thapaliya, P.; Xingzhong, Y. In *Cu2ZnSnS4 (CZTS) polycrystalline thin films prepared by sol-gel method*, Photovoltaic Specialists Conference (PVSC), 2011 37th IEEE, 19-24 June 2011; 2011; pp 001283-001286.

17. Kask, E.; Raadik, T.; Grossberg, M.; Josepson, R.; Krustok, J., Deep defects in Cu2ZnSnS4 monograin solar cells. *Energy Procedia* **2011,** *10* (0), 261-265.

18. Araki, H.; Kubo, Y.; Jimbo, K.; Maw, W. S.; Katagiri, H.; Yamazaki, M.; Oishi, K.; Takeuchi, A., Preparation of Cu2ZnSnS4 thin films by sulfurization of co-electroplated Cu-Zn-Sn precursors. *physica status solidi (c)* **2009,** *6* (5), 1266-1268.

19. Tatsuo, F.; Shin, T.; Tadayoshi, I., Enhancement of Conversion Efficiency of Cu 2 ZnSnS 4 Thin Film Solar Cells by Improvement of Sulfurization Conditions. *Applied Physics Express* **2013,** *6* (6), 062301.

20. Chen, S.; Walsh, A.; Gong, X.-G.; Wei, S.-H., Classification of Lattice Defects in the Kesterite Cu2ZnSnS4 and Cu2ZnSnSe4 Earth-Abundant Solar Cell Absorbers. *Advanced Materials* **2013,** *25* (11), 1522-1539.

21. Naghavi, N.; Spiering, S.; Powalla, M.; Cavana, B.; Lincot, D., High‐efficiency copper indium gallium diselenide (CIGS) solar cells with indium sulfide buffer layers deposited by atomic layer chemical vapor deposition (ALCVD). *Progress in Photovoltaics: Research and Applications* **2003,** *11* (7), 437-443.

22. Chirilă, A.; Reinhard, P.; Pianezzi, F.; Bloesch, P.; Uhl, A. R.; Fella, C.; Kranz, L.; Keller, D.; Gretener, C.; Hagendorfer, H., Potassium-induced surface modification of Cu (In, Ga) Se2 thin films for high-efficiency solar cells. *Nature Materials* **2013,** *12* (12), 1107-1111.

23. Repins, I.; Contreras, M. A.; Egaas, B.; DeHart, C.; Scharf, J.; Perkins, C. L.; To, B.; Noufi, R., 19•9%‐efficient ZnO/CdS/CuInGaSe2 solar cell with 81•2% fill factor. *Progress in Photovoltaics: Research and applications* **2008,** *16* (3), 235-239.

24. Ramanathan, K.; Contreras, M. A.; Perkins, C. L.; Asher, S.; Hasoon, F. S.; Keane, J.; Young, D.; Romero, M.; Metzger, W.; Noufi, R., Properties of 19.2% efficiency ZnO/CdS/CuInGaSe2 thin‐film solar cells. *Progress in Photovoltaics: research and applications* **2003,** *11* (4), 225-230.

25. Nakada, T.; Mizutani, M., 18% efficiency Cd-free Cu (In, Ga) Se2 thin-film solar cells fabricated using chemical bath deposition (CBD)-ZnS buffer layers. *Japanese Journal of Applied Physics* **2002,** *41* (2B), L165.

26. Islam, M. M.; Ishizuka, S.; Yamada, A.; Sakurai, K.; Niki, S.; Sakurai, T.; Akimoto, K., CIGS solar cell with MBE-grown ZnS buffer layer. *Solar Energy Materials and Solar Cells* **2009,** *93* (6), 970-972.

27. Triboulet, R., Progress in Crystal Growth and Characterization of Materials. *Progress in Crystal Growth and Characterization of Materials* **2014,** *60*, 1-14.

28. Shah, A.; Torres, P.; Tscharner, R.; Wyrsch, N.; Keppner, H., Photovoltaic technology: the case for thin-film solar cells. *science* **1999,** *285* (5428), 692-698.

29. Poortmans, J.; Arkhipov, V., *Thin film solar cells: fabrication, characterization and applications*. John Wiley & Sons: 2006; Vol. 5.

30. Lee, J.; Im, H., Effects of junction formation conditions on the photovoltaic properties of sintered CdS/CdTe solar cells. *Journal of materials science* **1986,** *21* (3), 980-984.

31. Bai, Z.; Yang, J.; Wang, D., Thin film CdTe solar cells with an absorber layer thickness in micro-and sub-micrometer scale. *Applied Physics Letters* **2011,** *99* (14), 143502.

32. McCandless, B.; Hegedus, S. In *Influence of CdS window layers on thin film CdS/CdTe solar cell performance*, Photovoltaic Specialists Conference, 1991., Conference Record of the Twenty Second IEEE, IEEE: 1991; pp 967-972.

33. Kumar, S. G.; Rao, K. K., Physics and chemistry of CdTe/CdS thin film heterojunction photovoltaic devices: fundamental and critical aspects. *Energy & Environmental Science* **2014,** *7* (1), 45-102.

34. Ma, Y. Y.; Bube, R. H., Properties of CdS Films Prepared by Spray Pyrolysis. *J. Electrochem. Soc.* **1977,** *124* (9), 1430-1435.

35. HyukáIm, S.; HyeokáPark, J., CdS or CdSe decorated TiO 2 nanotube arrays from spray pyrolysis deposition: use in photoelectrochemical cells. *Chem. Commun.* **2010,** *46* (14), 2385-2387.

36. Ma, Y. Y.; Fahrenbruch, A. L.; Bube, R. H., Photovoltaic properties of n‐CdS/p‐CdTe heterojunctions prepared by spray pyrolysis. *Applied Physics Letters* **1977,** *30* (8), 423-424.

37. Hiie, J.; Dedova, T.; Valdna, V.; Muska, K., Comparative study of nano-structured CdS thin films prepared by CBD and spray pyrolysis: annealing effect. *Thin Solid Films* **2006,** *511*, 443-447.

38. Kumar, N.; Komarala, V. K.; Dutta, V., In-situ synthesis of Au–CdS plasmonic photocatalyst by continuous spray pyrolysis and its visible light photocatalysis. *Chemical Engineering Journal* **2014,** *236*, 66-74.

39. Dhawankar, S. H.; Suryavanshi, B. M., Characterization of cadmium sulphide (CdS) thin film deposited by spray pyrolysis technique. *International Journal of Physical Research* **2016,** *4* (2), 58-61.

40. Schaffner, J.; Motzko, M.; Tueschen, A.; Swirschuk, A.; Schimper, H.-J.; Klein, A.; Modes, T.; Zywitzki, O.; Jaegermann, W., 12% efficient CdTe/CdS thin film solar cells deposited by low-temperature close space sublimation. *Journal of Applied Physics* **2011,** *110* (6), 064508.

41. Feldmeier, E. M.; Fuchs, A.; Schaffner, J.; Schimper, H. J.; Klein, A.; Jaegermann, W., Comparison between the structural, morphological and optical properties of CdS layers prepared by Close Space Sublimation and RF magnetron sputtering for CdTe solar cells. *Thin Solid Films* **2011,** *519* (21), 7596-7599.

42. Han, J.-f.; Fu, G.-h.; Krishnakumar, V.; Schimper, H.-J.; Liao, C.; Jaegermann, W.; Besland, M., Studies of CdS/CdTe interface: Comparison of CdS films deposited by close space sublimation and chemical bath deposition techniques. *Thin Solid Films* **2015,** *582*, 290-294.

43. Paudel, N. R.; Xiao, C.; Yan, Y., Close-space sublimation grown CdS window layers for CdS/CdTe thin-film solar cells. *Journal of Materials Science. Materials in Electronics* **2014,** *25* (4), 1991.

44. Plaza, J.; Martínez, O.; Rubio, S.; Hortelano, V.; Diéguez, E., Growth of CdS and CdTe films by close space vapour sublimation by using SiC resistive elements. *CrystEngComm* **2013,** *15* (12), 2314-2318.

45. Dasgupta, N. P.; Meng, X.; Elam, J. W.; Martinson, A. B., Atomic layer deposition of metal sulfide materials. *Accounts of chemical research* **2015,** *48* (2), 341-348.

46. Pavaskar, N.; Menezes, C.; Sinha, A., Photoconductive CdS films by a chemical bath deposition process. *J. Electrochem. Soc.* **1977,** *124* (5), 743-748.

47. Wang, W.; Winkler, M. T.; Gunawan, O.; Gokmen, T.; Todorov, T. K.; Zhu, Y.; Mitzi, D. B., Device characteristics of CZTSSe thin ‐ film solar cells with 12.6% efficiency. *Advanced Energy Materials* **2014,** *4* (7).

48. Ortega ‐ Borges, R.; Lincot, D., Mechanism of Chemical Bath Deposition of Cadmium Sulfide Thin Films in the Ammonia ‐ Thiourea System In Situ Kinetic Study and Modelization. *J. Electrochem. Soc.* **1993,** *140* (12), 3464-3473.

49. Khallaf, H.; Oladeji, I. O.; Chai, G.; Chow, L., Characterization of CdS thin films grown by chemical bath deposition using four different cadmium sources. *Thin Solid Films* **2008,** *516* (21), 7306-7312.

50. Alexander, J. N.; Higashiya, S.; Caskey, D.; Efstathiadis, H.; Haldar, P., Deposition and characterization of cadmium sulfide (CdS) by chemical bath deposition using an alternative chemistry cadmium precursor. *Solar Energy Materials and Solar Cells* **2014,** *125*, 47-53.

51. Ghosh, B.; Kumar, K.; Singh, B. K.; Banerjee, P.; Das, S., Growth of CdS thin films on indium coated glass substrates via chemical bath deposition and subsequent air annealing. *Applied Surface Science* **2014,** *320*, 309-314.

52. Krunks, M.; Mellikov, E.; Sork, E., Formation of CdS films by spray pyrolysis. *Thin Solid Films* **1986,** *145* (1), 105-109.

53. Patil, P. S., Versatility of chemical spray pyrolysis technique. *Materials Chemistry and physics* **1999,** *59* (3), 185-198.

54. Sasikala, G.; Dhanasekaran, R.; Subramanian, C., Electrodeposition and optical characterisation of CdS thin films on ITO-coated glass. *Thin solid films* **1997,** *302* (1-2), 71-76.

55. Zarębska, K.; Skompska, M., Electrodeposition of CdS from acidic aqueous thiosulfate solution—Invesitigation of the mechanism by electrochemical quartz microbalance technique. *Electrochimica Acta* **2011,** *56* (16), 5731-5739.

56. Izgorodin, A.; Winther-Jensen, O.; Winther-Jensen, B.; MacFarlane, D. R., CdS thin-film electrodeposition from a phosphonium ionic liquid. *Physical chemistry chemical physics* **2009,** *11* (38), 8532-8537.

57. Dennison, S., Studies of the cathodic electrodeposition of CdS from aqueous solution. *Electrochimica acta* **1993,** *38* (16), 2395-2403.

58. Carlà, F.; Loglio, F.; Resta, A.; Felici, R.; Lastraioli, E.; Innocenti, M.; Foresti, M. L., Electrochemical atomic layer deposition of CdS on Ag single crystals: Effects of substrate orientation on film structure. *The Journal of Physical Chemistry C* **2014,** *118* (12), 6132-6139.

59. Stickney, J. L., Electrochemical atomic layer epitaxy (EC-ALE): Nanoscale control in the electrodeposition of compound semiconductors. *Advances in Electrochemical Science and Engineering* **2002,** *7*, 1-106.

60. Gregory, B. W.; Suggs, D. W.; Stickney, J. L., Conditions for the deposition of CdTe by electrochemical atomic layer epitaxy. *J. Electrochem. Soc.* **1991,** *138* (5), 1279-1284.

61. Villegas, I.; Stickney, J. L., Preliminary studies of GaAs deposition on Au (100),(110), and (111) surfaces by electrochemical atomic layer epitaxy. *J. Electrochem. Soc.* **1992,** *139* (3), 686-694.

62. Vaidyanathan, R.; Cox, S. M.; Happek, U.; Banga, D.; Mathe, M. K.; Stickney, J. L., Preliminary studies in the electrodeposition of PbSe/PbTe superlattice thin films via electrochemical atomic layer deposition (ALD). *Langmuir* **2006,** *22* (25), 10590-10595.

63. Colletti, L. P.; Flowers, B. H.; Stickney, J. L., Formation of thin films of CdTe, CdSe, and CdS by electrochemical atomic layer epitaxy. *J. Electrochem. Soc.* **1998,** *145* (5), 1442-1449.

64. Banga, D.; Jarayaju, N.; Sheridan, L.; Kim, Y.-G.; Perdue, B.; Zhang, X.; Zhang, Q.; Stickney, J., Electrodeposition of CuInSe2 (CIS) via electrochemical atomic layer deposition (E-ALD). *Langmuir* **2012,** *28* (5), 3024-3031.

65. Gregory, B. W.; Norton, M. L.; Stickney, J. L., Thin-layer electrochemical studies of the underpotential deposition of cadmium and tellurium on polycrystalline Au, Pt and Cu electrodes. *Journal of Electroanalytical Chemistry and Interfacial Electrochemistry* **1990,** *293* (1), 85-101.

66. Perdue, B.; Czerniawski, J.; Anthony, J.; Stickney, J., Optimization of Te Solution Chemistry in the Electrochemical Atomic Layer Deposition Growth of CdTe. *J. Electrochem. Soc.* **2014,** *161* (7), D3087-D3092.

67. Czerniawski, J. M.; Perdue, B. R.; Stickney, J. L., Potential Pulse Atomic Layer Deposition of Cu2Se. *Chemistry of Materials* **2016,** *28* (2), 583-591.

68. Gregory, B. W.; Stickney, J. L., Electrochemical atomic layer epitaxy (ECALE). *Journal of electroanalytical chemistry and interfacial electrochemistry* **1991,** *300* (1-2), 543-561.

CHAPTER 2

FORMATION OF CADMIUM SULFIDE USING ELECTROCHEMICAL ATOMIC LAYER DEPOSITION (E-ALD) AND SUCCESSIVE IONIC LAYER ADSORPTION REACTION (SILAR)[1]

[1]S. Shen, X. Zhang, B. Perdue, J. Stickney, To be submitted to *Journal of the electrochemical society*

Abstract

Cadmium sulfide (CdS) thin films were electrochemically formed on polycrystalline Au films, using electrochemical atomic layer deposition (E-ALD) and successive ionic layer adsorption reaction (SILAR). In developing a E-ALD cycle for CdS, voltammetric studies of the individual precursors on Au electrodes were used to determine potentials ranges for the underpotential deposition (UPD) of Cd and S. Subsequent potential optimization was performed by nanofilm growth, systematically varying the deposition potential of one element and examining the resulting Cd/S stoichiometry using electron probe microanalysis, and microscopy of deposit morphology. Optimized deposits displayed a linear growth dependence on cycle number, characterized using spectroscopy ellipsometry, and expected for an ALD process. The 1LO Raman peak was observed at 303 cm^{-1} using 514 nm light. The X-ray diffraction pattern was consistent with a strongly preferred zinc blend <111> orientation. For SILAR deposits, formed using the same flow system used for E-ALD, the CdS existed as porous clusters, as viewed using SEM, whereas E-ALD deposits were conformal and compact coatings. The comparison between E-ALD and SILAR deposits, formed using the flow cell system, indicated some degree of homogeneous precipitation near the surface in the case of SILAR, which appeared to be eliminated using the E-ALD growth cycle, leading to both a higher growth rate and film quality.

Introduction

The II-VI compound semiconductor cadmium sulfide (CdS) is the most widely used buffer layer material for second generation thin film solar cells. It is an n-type semiconductor, with a band gap of 2.4 eV, good optical transmittance, low resistivity, and has been used by the PV industry to form p-n junctions with various absorber layers, such CdTe[1-3] and $Cu(In,Ga)Se_2$

(CIGS)[4-5]. For an ideal thin-film solar cell configuration, a CdS buffer layer should have a thickness sufficient to avoid pinholes and short circuits, but thin enough for high optical transmission. As a result, good uniformity and limited defects are needed. The microstructure and morphology of CdS thin films are a function of the deposition method. CdS thin layer can be fabricated using a number of methods, such close-spaced sublimation (CSS)[3, 6-7], chemical bath deposition (CBD)[5, 8-11], electrodeposition[12], and successive ionic layer adsorption and reaction (SILAR)[13] .

SILAR is considered as a modified version of CBD. It was first introduced by Nicolau[13] in 1985, and gained popularity when applied to the making of core-shell nanocrystals in quantum dot sensitized solar cells[14]. The basis of the SILAR process involves alternate immersions of the substrate in separate solutions containing the precursor cations (Cd^{2+}) and the precursor anions (S^{2-}). When the S^{2-} coated substrate is immersed in Cd^{2+} solution, they react ideally at the solid liquid interface, forming a layer of CdS.

In the subsequent rinse step, the excess Cd^{2+} is quickly washed away by convection. The resulting growth rate appears dependent on the rinsing process and duration. Subsequent dipping in the S^{2-} solution leads to adsorption of S^{2-} ions, and the process is repeated. CdS thin films have been made using SILAR under a variety of conditions. Table 1 summarizes the parameters reported in the literature for the fabrication of CdS thin films using SILAR.

Table 1: List of conditions reported in the literature for CdS thin film formation using SILAR.

	Cd (M)	**S (M)**	**Dip (s)**	**Rinse (s)**	**No. cycles and thickness**	**Temp**	**Characterization**	**ref**
1	0.025 (pH 5)	0.1 M (pH 9)	15	10	20 (280 nm)	80 °C	Annealing, XRD, SEM, Abs, resistivity	[15]
2	0.2	0.1	40	100	Up to 1500	RT	XRD, SEM,	[16]

	(pH 5)	(pH 12)			Up to 120 nm (0.078 nm/cy)		EDX, RBS	
3	0.0125	0.05	20	20	160 (280 nm)	30 °C	XRD, SEM, TEM, RBS, EDX	[17]
4	0.1 (pH 5.8)	0.05 (pH 12.5)	40	150	115 nm 0.23 nm/cy	RT	XRD, AFM, stress	[18]
5	0.2 (pH 5.3)	0.1 (pH 12)	40	100	0.14 nm/cy	RT	XRD, SEM	[19]
6	0.1 (pH 5.9)	0.05 (pH 11.5)	40	50	100	RT	XRD, SEM, Abs, resistivity	[20]
7	0.1	0.1- 0.7	15		50	RT	Thickness, XRD, SEM, Abs	[21]
8	0.1	0.1	15	10	25 to 100 (125 to 295 nm)	85 °C	FTIR, Abs, SEM, AFM, EDX	[22]
9	0.1 (pH 5.0)	0.05 (pH 12.5)	40	150	200 to 1300 (20 to 120 nm)	RT	Thickness, AFM, stress	[23]
10	0.1	0.1 to 0.7	15	10	Between 100 to 50 (450-500 nm)	80 °C	XRD, SEM, EDX	[24]
11	0.02 (pH 4.9)	0.01 (pH 12.3)	60	60	10	RT	Stripping	[25]
12	0.1 M	0.1 M	29.5	29.5	30	30.1°C	RSM, XRD, SEM, ABS	[26]
13	0.1 M	0.5 M	15	20	100	85 °C	XRD, Abs, PL, SEM, AFM, EDX	[27]
14	0.1 M (pH 5.5)	0.1 M (pH 12)	25	50	Not known	RT	I-V, C-V, C-f	[28]
15	0.1 M (pH 4.1)	0.1 M (pH 11.7)	Not known	Not known	100	RT	XRD, TEM, SEM, Abs	[29]
16	0.3	0.3	300	120	12	RT	XRD, Raman, TEM, SEM, Abs, PL, PEC	[30]
17	0.1	0.05	40	150	100 nm	RT	XRD, AFM	[31]
18	0.02 (pH 11)	0.03 (pH 11)	15	40	30	RT	XRD, SEM, I-V, thermo-emf	[32]
19	0.1 (pH 5.9)	0.05 (pH 11.5)	40	50	100 (320 ±15 nm)	RT	XRD, SEM, Abs, PL	[33]

Another low-cost method for the formation of semiconductor, and metallic, nanofilm materials is electrodeposition. The development of the dual damascene process for fabrication of

high quality copper interconnects in microprocessors demonstrated that electrodeposition can meet the ULSI industry's requirements for large-scale production[34]. As might be expected, the quality of electrodeposits is a function of potential, temperature, substrate structure, solution composition, as well as additives.

Electrochemical atomic layer deposition (E-ALD) [35-40] is the condensed phase equivalent of the gas phase atomic layer deposition (ALD). ALD denotes the growth of nanofilms of materials in a layer-by-layer fashion, where surface limited reactions are used achieve atomic layer growth. In general, a cycle is used to form deposits, where each cycle produces one atomic or monolayer of the desired material, and the number of cycles determines the deposit thickness. The vast majority of ALD is performed in the gas or vacuum phase. In E-ALD, however, deposits are performed in solution, where the potential of the substrate and the precursors in solution are used to deposit the surface limited atomic layers[41]. Surface limited reactions in electrochemistry are referred to as underpotential deposition (UPD). UPD is a phenomenon where an atomic layer of a first element is deposited on a second at a potential prior to that (under) that needed to deposit the first element on itself, due to the negative free energy in the formation of a compound or alloy[41-44]. A variety of metals and semiconductor thin films have been made using E-ALD, including CdTe[43] and $CuInSe_2$(CIS)[40].

Studies of the formation of the first few monolayers of CdS on Au by E-ALD were reported by several groups[39, 45-49], but few investigated well-formed CdS E-ALD thin films thick enough for potential applications in solar cell fabrication. The first part of the present report extends the E-ALD growth of CdS films from the first few layers to over 50 nm, and systematically examines the growth parameters. The second part compares deposits made using E-ALD and SILAR, as both involve the growth of materials one atomic layer at a time. The

same automated flowcell system was used for both sets of deposits, with the SILAR process carried out without potential control, though the substrate potential was monitored during SILAR process. The processes are similar, with SILAR based on adsorption and essentially precipitation of the cations and anions near the substrate surface, while electrochemically controlled redox reactions were used to form the deposits in the E-ALD process. The same parameters that can be manipulated in SILAR can be controlled in E-ALD, with the addition of potential control to achieve UPD. In this report, the SILAR deposits were formed using the same solution, flow rate, immersion time as the optimized E-ALD process for comparison purposes. Use of the E-ALD flowcell system should provide greater control over the SILAR process than the manual control used in most previous SILAR studies reported in the literature.

Experimental

The Cd solution was 0.5 mM $CdSO_4$ (Sigma-Aldrich) in 0.5 M $NaClO_4$, pH 3. The sulfide solution was 0.5 mM Na_2S (J.T.Baker) in 0.5 M $NaClO_4$, pH 10.5. The precursor concentrations were mM, given that deposits were limited to a monolayer (ML), or less, each cycle. A monolayer (ML) in this study is defined as one adsorbate atom per Au surface atom. The precursor solutions, as well as the pH 3 acidic and pH 10.5 basic blanks used for rinsing, contained 0.5 M $NaClO_4$ as a supporting electrolyte. The blanks were used to rinse the cell of any precursor left. All solutions were made using 18 MΩ water, filtered through Millipore Advantage 10. The substrates used were 100 nm of Au coated on 5 nm of Ti on glass slides, purchased from Evaporated Metal Films (Ithaca, NY). The Au substrates were cleaned prior to use with Millipore water and acetone, followed by a 30s immersion in concentrated nitric acid, and then rinsed with Millipore water.

All experiments were performed using an automated flowcell system (Electrochemical ALD, L.C., Athens, GA). Solution bottles were connected to a distribution valve, which controlled the species flowing into the cell. The solutions were sucked through the distribution valve into flowcell where the potential was controlled and or measured using a potentiostat. The pump and potentiostat were automated using a program developed in-house, referred to as "Sequencer". The auxiliary electrode was a gold wire embedded in the cell wall and the reference electrode was 3 M Ag/AgCl (BASi, West Lafayette, IN). The exposed electrode area was 2.1 cm^2. During the deposition of CdS, the flow rate during all flow steps was kept at 11 mL/min. Cyclic voltammetry (CV) was performed at a scan rate of 10 mV/s, with the solution flowing at 2 mL/ min. Prior to all experiments, nitrogen gas was used to purge oxygen from bottles and tubes.

Electron probe microanalysis (EPMA) was performed on a JEOL 8600 Superprobe with 10 keV accelerating voltage, 15 nA beam current, and 10 μm beam dimeter. Thickness measurements were made using a spectroscopic ellipsometry (SE), JA Woolam M-200 V. X-ray diffraction (XRD) measurements were performed on a PANanalytical X'PERT Pro with an open Eulerian cradle, using 0.154 nm Cu Kα1 source and a parallel plate collimator. Raman measurements were made using a Renishaw microscope equipped with a CCD detector using a 514 nm Ar-ion laser (Modu-Laser, LLC, Centerville, UT) running at 0.67 mW. Scanning electron microscopy (SEM) was performed on an FEI Inspect F50 FEG SEM (FEI, Hillsboro, OR).

Results and Discussion

Figure 2.1 displays CVs for Au substrates in separate Cd (Figure 2.1a) and S (Figure 2.1b) precursor solutions. In Figure 1a, as the potential was scanned negatively from the open circuit potential (OCP), 400 mV, and shows a broad reduction peak **a** at -200 mV, corresponding to Cd UPD. As the potential was scanned further negative, Cd alloying with the Au surface occurs, leading to bulk Cd deposition (peak **c**). Near peak **c** the hydrogen evolution reaction (HER) becomes important as well. In the subsequent positive scan, peak **c'** corresponds to bulk Cd stripping peak, as it was not evident prior to reaching -800 mV. The broad oxidation peak **b'** corresponds to stripping Cd from the Au surface alloy, and the peak **a'** corresponded to stripping Cd UPD, the most stable form of Cd. From those CV results possible Cd UPD potentials are suggested to be between -200 and -800 mV. The CV of the Au substrate in sulfide is shown in Figure 1(b). When the potential was scanned negative from OCP, -400 mV, peak **a** was observed starting at -720 mV and was attributed to the reduction of the self-absorbed sulfur on the Au surface. Sulfide is known to spontaneously oxidize to sulfur atom and absorb onto Au surfaces[50-51]. The self-absorbed sulfur coverage was 0.3 ML, assuming a two-electron process. On the reverse scan, peak **a'** was the oxidation of sulfide ions to adsorbed sulfur, or sulfur UPD. Peak **a** and **a'** were similar in size and position, suggesting good reversibility of the redox process. Peak **b'** was the oxidation of sulfide to bulk sulfur and polysulfides. The process was limited because sulfur had a tendency to cover and insulate the electrode surface thus impeding further oxidation. This bulk sulfur coverage appears to be about 1.2 ML, again assuming a two-electron process.

Previous studies suggest a sulfur layer, composed of eight-membered polysulfide rings, when exposed to Cd^{2+} ions, converts to CdS[52]. Scanning further positive results in peak **c'**,

which has been associated with oxidation of sulfur to sulfite and sulfate. Those results suggest sulfur deposition between -700 to 0 mV as a range for sulfur electrodeposition.

An example E-ALD cycle is displayed in Figure 2.2. The green-themed colors represent the potentials for each step, on the left Y axis, while the red curve on the right Y axis depicts that current. The cycle began by flowing Cd^{2+} solution at -600 mV for 10 s, followed by quiescent deposition of Cd for 10 s at -775 mV. The Cd^{2+} solution was then rinsed out using by blank, and then introduction of the S^{2-} solution, at -775 mV. S was then deposited at -300 mV in a quiescent solution for 10 s, followed by blank rinses. The two blank solutions were used in sequence, to convert from previous pH, to the next. All flow steps were performed at 11 mL/min. Each cycle resulted in the deposition of a fraction of a ML of each element. The charge under Cd deposition process was significant larger than that for the oxidation of S, due to the HER. The cycle was repeated until a desired film thickness was reached.

Deposits using the same potentials (Cd at -775 mV; S at -300 mV) but different step times were made. The total deposition time was kept constant by varying the number of cycles performed. Figure 2.3 shows pictures of 4 deposits made with step times: 2.5 s (200 cycles), 5 s (100 cycles), 7.5 s (67 cycles), and 10 s (50 cycles). The vertical stripes appearing in the deposits using 2.5 s and 5 s step times, suggest laminar flow between inlet and outlet holes. The cell used was configured with a row of 8 inlet holes at the bottom, and 8 outlet holes on the top, with the solution entering on the left (inlet) and leaving on the right (outlet). As the step time decreased (and the number of cycles increased), the deposits appeared visually thicker and rougher, and displayed a flow pattern. The principle of ALD is that each cycle should result in the deposition of some fraction of a monolayer, and the number of cycles performed should determine the

deposit thickness. However, as the time per cycle decreases, equilibrium is harder to establish and could account for some roughening. The 10 s step length deposit showed no visible evidence of a flow pattern, though the deposits were much thinner, being formed with only 50 cycles, and was chosen for subsequent deposit studies.

The effect of potential on the film stoichiometry was studied using electron probe microanalysis (EPMA) at an acceleration voltage of 10 kV. Each sample was formed using 50 deposition cycles with a step length of 10 s. Each measurement was an average of 6 spots across the film. Figure 2.4(a) shows the atomic percent of Cd and S at different S deposition potentials with the Cd deposition potential at -775mV. The black squares and red dots represented Cd and S atomic percent respectively, on the left Y axis. The green stars mark the elemental Cd/S ratio on the right Y axis. By varying the S deposition potential from -600 mV to -200 mV, the atomic percents of the two elements were kept at around 3.5, and the Cd/S near 1. When the S deposition potential was increased to -100 mV and above, the atomic percent of S increases from 3.5 to 5.6 and Cd/S dropped below 0.9. Those results are consistent with the onset of bulk sulfide oxidation to sulfur (Figure 2.1b) and the formation of S-rich deposits. Those results suggest an optimal potential range for S deposition of between -600 to -200 mV. As a result, -300 mV was chosen for studies of the optimal Cd deposition potential. Figure 2.4(b) displays the Cd/S as a function of the Cd deposition potential, using a S potential of -300 mV. The atomic percent of the two elements increased slowly as the potential was decreased, with an abrupt increase below -800 mV. However, the Cd/S ratio remained nearly constant, even at -900 mV, where bulk Cd was possible. The coverages of both Cd and S quadrupled at -900 mV, indicating that the surface limited region central to ALD had been exceeded for Cd, yet from the ratio of Cd/S it appears that S deposition nearly kept up with the Cd deposition, demonstrating

the high affinity of S for Cd. However, even though the stoichiometry remained nearly constant, the -900 mV deposit displayed strong flow patterns and appeared clearly rougher with optical microscopy, indicating the growth near micron sized particles. From those EPMA results it was concluded that the best deposits were achieved with a S deposition potential between -600 and -200 mV, with a Cd deposition potential between -700 to -300 mV.

Thickness measurements of the deposits were made using spectroscopic ellipsometry. Figure 2.5 shows the relation of film thickness to the number of cycles performed (Cd potential = -775 mV, S potential = -500 mV), displaying the characteristic linear relationship between coverage and the number of cycles performed expected of an ALD process.

Figure 2.6 depicts the Raman measurement made on a 50-cycle CdS deposit (Cd potential = -775 mV; S potential = -500 mV) using a 514 nm laser. The literature suggests a shift of CdS 1LO from 300 cm^{-1} to 305 cm^{-1} when CdS thickness increased from a single layer to bulk-phase[53]. The 1 LO peak in Figure 6 appeared at 303 cm^{-1}, consistent with the literature, given that the film thickness was tens of monolayers. The two peaks at 604 and 904 cm^{-1} corresponded to the second and third order LO of CdS[54]. No feature corresponding to polymeric S, composed of S_8 rings (150, 215, 462 cm^{-1})[52], was observed, suggesting no excess S and good film purity.

Glancing angle XRD was used to characterize the crystallinity of a 400-cycle deposit (Cd potential = -775 mV; S potential = -500 mV), and the pattern is shown in Figure 2.7. No post-deposition annealing was required to obtain this X-ray diffraction pattern. The black and red spectra were the pattern for the Au substrate and the CdS/Au deposit, respectively. The intense sharp peak at 26° corresponded to the planes of the CdS <111> zinc blend structure, which is

known to be more stable than the wurtzite structure at low temperatures[55]. The CdS zinc blend structure is shown in the Figure 7 inset, with the black dots representing Cd atoms and orange dots S atoms. The two red triangles represent two adjacent <111> plane. According to the powder data base, the CdS <111> zinc blend structure has a lattice constant of a=0.5818 nm. Based on the geometry of the cubic structure, the distance between two <111> plane is calculated to be $d=\frac{\sqrt{3}}{3}a=0.336$ nm. Given a thickness 10 nm for a 50-cycle deposit, the calculated deposition rate is 0.6 compound monolayers per cycle. The grain size calculated from Scherrer's equation was 32 nm.

It was reported that the Au substrates exerts a pronounced templating effect on the electrochemically grown CdS, which is attributed to the strong interaction between S and Au[45]. Figure 8 displays the SEM images of a clean Au substrate and the a CdS/Au deposit (Cd potential = -775 mV, S potential = -500 mV, 50 cycles) at different magnifications. The comparison between the higher magnification clean Au substrate (Fig 2.8 (b)) and CdS (Fig 2.8 (d)) showed similar grain sizes and distribution among the two surfaces, indicating that Au did act as a template, with the CdS thin film conformally deposited.

After the conditions for CdS E-ALD formation were optimized, A SILAR deposit was made using the same solutions and setup as the E-ALD process, differing only in the absence of electrochemical potential control. The OCP in the SILAR process was recorded and plotted (the blue-themed colors) which can be compared with those for the applied potentials used in the E-ALD deposits (the green-themed colors), shown in Figure 2.9. The red and lighter red curves correspond to the current during E-ALD and SILAR, respectively. In the SILAR Cd deposition steps, the OCP drifted between -300 to -100 mV, whereas the E-ALD potential was held at -600

and then -775 mV, leading to Cd UPD. In the following S deposition steps, the E-ALD potential was held at -300 mV, close to the equilibrium OCP potentials recorded during the SILAR deposit. No significant overpotential was needed in the SILAR run due to the affinity between the S and Cd. Though the potentials during S deposition were similar for the two methods, it was reported in the literature that S formed an ordered structure on Au under UPD potential control, but not at OCP[45].

Figure 2.10 shows pictures of a) an E-ALD deposit b), an E-ALD-equivalent SILAR deposit, as well as 3 SILAR deposits made with modified rinsing steps, including: c) rinse with each blank solution for 5 s instead of 10 s. d) 10 s rinse with basic blank only. e) no rinse. The number of cycles for all 5 deposits was kept at 50. The E-ALD-equivalent SILAR deposit (b) appeared to be very thin, the lightest color among the 5 deposits. It appears that the low concentration at the surface, together with the dilution from the long rinsing times, has limited the resulting deposit/cycle. Comparing deposits (a) and (b) suggests that under the same conditions, the electrochemical process is much more efficient then adsorption and precipitation. Reducing the rinsing time to half, (c), the SILAR thickness clearly increased, the result of higher adsorbed and near surface precursor concentrations. Deposit (d) has the same total rinsing time as deposit (c), but only rinsing with the basic blank. Cd^{2+} ions exposed to a basic solution, instead of being rinsed away with the acidic blank, should from $Cd(OH)_2$, which when exposed to S^{2-} should formed the thermodynamically more stable CdS, though it is probable that much of the $Cd(OH)_2$ would be present as a precipitate, differentiating it from an adsorbed layer of Cd^{2+} ions. No obvious visible change in appearance was observed when the basic rinse step was further eliminated in deposit (e), indicating that, following Cd^{2+} ion exposure, rinsing with the basic sulfide solution produced the same results as leaving out the acidic rinse.

Figure 2.11 displays SEM images of the deposits made by E-ALD and SILAR with the different rinsing processes. In all SILAR deposits in the present study, CdS clusters were evident, suggesting homogeneous precipitation and at least some powder-like, and poorly adherent components to the films, in contrast to the compact conformal films made using E-ALD. Those results are consistent with previous results which did not how the random precipitation components with the E-ALD growth process[48].

Conclusion

CdS thin films with a thickness of up to 50 nm were successfully formed on Au substrate using E-ALD. A wide range in the deposition potentials for Cd and S, yielding optimal stoichiometry, were observed, due to the high affinity of the two elements. Spectroscopic ellipsometry showed linear growth with increasing cycle numbers, typical for an ALD process. The deposition rate was determined to be 0.6 ML/cycle. XRD indicated a strong zinc blend <111> preferred orientation. SEM showed conformal coating of the substrate, consistent with the layer-by-layer ALD growth mechanism. The comparison between E-ALD and SILAR deposits, grown with the same hardware and program, showed that the potential driven E-ALD process eliminated the homogeneous precipitation component, observe with the various SILAR programs used here. Overall, the E-ALD process yielded compact and crystalline films, whereas open circuit SILAR solution exchange led to slower deposition rates and the formation of porous clusters on the surface. On the other hand, SILAR can be applied to almost all types of substrates and E-ALD is limited to conducting surfaces.

Acknowledgement

Support from the National Science Foundation, DMR 1410109, is gratefully acknowledged. Thanks are extended to Chris Fleisher and the UGA Microprobe lab. Thanks are extended to the Integrated Bioscience and Nanotechnology Cleanroom for the use of their facilities. In addition, the authors would like to thank Dr. Zhengwei Pan for help in obtaining the SEM images.

References

1. Durose, K.; Edwards, P.; Halliday, D., Materials aspects of CdTe/CdS solar cells. *Journal of Crystal Growth* **1999,** *197* (3), 733-742.

2. Mathew, X.; Enriquez, J. P.; Romeo, A.; Tiwari, A. N., CdTe/CdS solar cells on flexible substrates. *Sol. Energy* **2004,** *77* (6), 831-838.

3. Aramoto, T.; Kumazawa, S.; Higuchi, H.; Arita, T.; Shibutani, S.; Nishio, T.; Nakajima, J.; Tsuji, M.; Hanafusa, A.; Hibino, T., 16.0% efficient thin-film CdS/CdTe solar cells. *Japanese Journal of Applied Physics* **1997,** *36* (10R), 6304.

4. Naghavi, N.; Spiering, S.; Powalla, M.; Cavana, B.; Lincot, D., High-efficiency copper indium gallium diselenide (CIGS) solar cells with indium sulfide buffer layers deposited by atomic layer chemical vapor deposition (ALCVD). *Progress in Photovoltaics: Research and Applications* **2003,** *11* (7), 437-443.

5. Chirilă, A.; Reinhard, P.; Pianezzi, F.; Bloesch, P.; Uhl, A. R.; Fella, C.; Kranz, L.; Keller, D.; Gretener, C.; Hagendorfer, H., Potassium-induced surface modification of Cu (In, Ga) Se2 thin films for high-efficiency solar cells. *Nature Materials* **2013,** *12* (12), 1107-1111.

6. Schaffner, J.; Motzko, M.; Tueschen, A.; Swirschuk, A.; Schimper, H.-J.; Klein, A.; Modes, T.; Zywitzki, O.; Jaegermann, W., 12% efficient CdTe/CdS thin film solar cells deposited by low-temperature close space sublimation. *Journal of Applied Physics* **2011,** *110* (6), 064508.

7. Feldmeier, E. M.; Fuchs, A.; Schaffner, J.; Schimper, H. J.; Klein, A.; Jaegermann, W., Comparison between the structural, morphological and optical properties of CdS layers prepared by Close Space Sublimation and RF magnetron sputtering for CdTe solar cells. *Thin Solid Films* **2011,** *519* (21), 7596-7599.

8. Pavaskar, N.; Menezes, C.; Sinha, A., Photoconductive CdS films by a chemical bath deposition process. *J. Electrochem. Soc.* **1977,** *124* (5), 743-748.

9. Wang, W.; Winkler, M. T.; Gunawan, O.; Gokmen, T.; Todorov, T. K.; Zhu, Y.; Mitzi, D. B., Device characteristics of CZTSSe thin-film solar cells with 12.6% efficiency. *Advanced Energy Materials* **2014,** *4* (7).

10. Ortega-Borges, R.; Lincot, D., Mechanism of Chemical Bath Deposition of Cadmium Sulfide Thin Films in the Ammonia-Thiourea System In Situ Kinetic Study and Modelization. *J. Electrochem. Soc.* **1993,** *140* (12), 3464-3473.

11. Khallaf, H.; Oladeji, I. O.; Chai, G.; Chow, L., Characterization of CdS thin films grown by chemical bath deposition using four different cadmium sources. *Thin Solid Films* **2008,** *516* (21), 7306-7312.

12. Nishino, J.; Chatani, S.; Uotani, Y.; Nosaka, Y., Electrodeposition method for controlled formation of CdS films from aqueous solutions. *J Electroanal Chem* **1999,** *473* (1–2), 217-222.

13. Nicolau, Y., Solution deposition of thin solid compound films by a successive ionic-layer adsorption and reaction process. *Applications of Surface Science* **1985,** *22*, 1061-1074.

14. Li, J. J.; Wang, Y. A.; Guo, W.; Keay, J. C.; Mishima, T. D.; Johnson, M. B.; Peng, X., Large-scale synthesis of nearly monodisperse CdSe/CdS core/shell nanocrystals using air-stable reagents via successive ion layer adsorption and reaction. *Journal of the American Chemical Society* **2003,** *125* (41), 12567-12575.

15. Sankapal, B. R.; Mane, R. S.; Lokhande, C. D., Deposition of CdS thin films by the successive ionic layer adsorption and reaction (SILAR) method. *Materials Research Bulletin* **2000,** *35* (2), 177-184.

16. Valkonen, M. P.; Kanniainen, T.; Lindroos, S.; Leskelä, M.; Rauhala, E., Growth of ZnS, CdS and multilayer ZnS/CdS thin films by SILAR technique. *Applied Surface Science* **1997,** *115* (4), 386-392.

17. Lokhande, C. D.; Sankapal, B. R.; Pathan, H. M.; Muller, M.; Giersig, M.; Tributsch, H., Some structural studies on successive ionic layer adsorption and reaction (SILAR)-deposited CdS thin films. *Applied Surface Science* **2001,** *181* (3), 277-282.

18. Laukaitis, G.; Lindroos, S.; Tamulevičius, S.; Leskelä, M., Stress and morphological development of CdS and ZnS thin films during the SILAR growth on (1 0 0)GaAs. *Applied Surface Science* **2001,** *185* (1), 134-139.

19. Valkonen, M. P.; Lindroos, S.; Kanniainen, T.; Leskelä, M.; Tapper, U.; Kauppinen, E., Thin multilayer CdS/ZnS films grown by SILAR technique. *Applied Surface Science* **1997,** *120* (1), 58-64.

20. Kundakci, M.; Ateş, A.; Astam, A.; Yildirim, M., Structural, optical and electrical properties of CdS, Cd0.5In0.5S and In2S3 thin films grown by SILAR method. *Physica E: Low-dimensional Systems and Nanostructures* **2008,** *40* (3), 600-605.

21. Senthamilselvi, V.; Saravanakumar, K.; Jabena Begum, N.; Anandhi, R.; Ravichandran, A. T.; Sakthivel, B.; Ravichandran, K., Photovoltaic properties of nanocrystalline CdS films deposited by SILAR and CBD techniques—a comparative study. *Journal of Materials Science: Materials in Electronics* **2012,** *23* (1), 302-308.

22. Senthamilselvi, V.; Ravichandran, K.; Saravanakumar, K., Influence of immersion cycles on the stoichiometry of CdS films deposited by SILAR technique. *Journal of Physics and Chemistry of Solids* **2013,** *74* (1), 65-69.

23. Tamulevičius, S.; Valkonen, M. P.; Laukaitis, G.; Lindroos, S.; Leskelä, M., Stress and surface studies of SILAR grown CdS thin films on GaAs(100). *Thin Solid Films* **1999,** *355* (Supplement C), 430-434.

24. Senthamilselvi, V.; K, S.; Anandhi, R.; A.T, R.; Ravichandran, K., *Effect of annealing on the stoichiometry of CdS films deposited by SILAR technique*. 2011; Vol. 5, p 1072-1077.

25. Sasagawa, M.; Nosaka, Y., The effect of chelating reagents on the layer-by-layer formation of CdS films in the electroless and electrochemical deposition processes. *Electrochimica Acta* **2003,** *48* (5), 483-488.

26. Yücel, E.; Yücel, Y.; Durak, M., Process optimization for window material CdS thin films grown by a successive ionic layer adsorption and reaction method using response surface methodology. *Journal of Alloys and Compounds* **2016,** *664* (Supplement C), 530-537.

27. Ravichandran, K.; Senthamilselvi, V., Effect of indium doping level on certain physical properties of CdS films deposited using an improved SILAR technique. *Applied Surface Science* **2013,** *270* (Supplement C), 439-444.

28. Güzeldir, B.; Sağlam, M.; Ateş, A.; Türüt, A., Effects of ageing on the electrical characteristics of Cd/CdS/n-Si/Au–Sb structure deposited by SILAR method. *Journal of Physics and Chemistry of Solids* **2011,** *72* (12), 1506-1514.

29. Patra, S.; Mitra, P.; Pradhan, S. K., Preparation of nanodimensional CdS by chemical dipping technique and their characterization. *Materials Research* **2011,** *14*, 17-20.

30. Jostar. T, S.; Devadason, S.; Suthagar, J., Effect of CdS layers on opto-electrical properties of chemically prepared ZnS/CdS/TiO2 photoanodes. *Mater. Sci. Semicond. Process* **2015,** *34* (Supplement C), 65-73.

31. Lindroos, S.; Puišo, J.; Tamulevičius, S.; Leskelä, M. In *CdS-PbS multilayer thin films grown by the SILAR method*, Solid State Phenom., Trans Tech Publ: 2004; pp 243-246.

32. Desale, D. J.; Shaikh, S.; Ghosh, A.; Birajadar, R.; Siddiqui, F.; Ghule, A.; Sharma, R. B., Preparation and characterization of CdS–Bi2S3 nanocomposite thin film by successive ionic layer adsorption and reaction (SILAR) method. *Composites Part B: Engineering* **2012,** *43* (3), 1095-1100.

33. Rajendra, B. V.; Fuchs, B.; Dhananjaya, K., Characterization of cadmium sulphide thin films prepared by successive ionic layers adsorption and reaction method. *Journal of Materials Science: Materials in Electronics* **2013,** *24* (2), 567-571.

34. Carlà, F.; Loglio, F.; Resta, A.; Felici, R.; Lastraioli, E.; Innocenti, M.; Foresti, M. L., Electrochemical atomic layer deposition of CdS on Ag single crystals: effects of substrate orientation on film structure. *The Journal of Physical Chemistry C* **2014,** *118* (12), 6132-6139.

35. Stickney, J. L., Electrochemical atomic layer epitaxy (EC-ALE): Nanoscale control in the electrodeposition of compound semiconductors. *Advances in Electrochemical Science and Engineering* **2002,** *7*, 1-106.

36. Gregory, B. W.; Suggs, D. W.; Stickney, J. L., Conditions for the deposition of CdTe by electrochemical atomic layer epitaxy. *J. Electrochem. Soc.* **1991,** *138* (5), 1279-1284.

37. Villegas, I.; Stickney, J. L., Preliminary studies of GaAs deposition on Au (100),(110), and (111) surfaces by electrochemical atomic layer epitaxy. *J. Electrochem. Soc.* **1992,** *139* (3), 686-694.

38. Vaidyanathan, R.; Cox, S. M.; Happek, U.; Banga, D.; Mathe, M. K.; Stickney, J. L., Preliminary studies in the electrodeposition of PbSe/PbTe superlattice thin films via electrochemical atomic layer deposition (ALD). *Langmuir* **2006,** *22* (25), 10590-10595.

39. Colletti, L. P.; Flowers, B. H.; Stickney, J. L., Formation of thin films of CdTe, CdSe, and CdS by electrochemical atomic layer epitaxy. *J. Electrochem. Soc.* **1998,** *145* (5), 1442-1449.

40. Banga, D.; Jarayaju, N.; Sheridan, L.; Kim, Y.-G.; Perdue, B.; Zhang, X.; Zhang, Q.; Stickney, J., Electrodeposition of CuInSe2 (CIS) via electrochemical atomic layer deposition (E-ALD). *Langmuir* **2012,** *28* (5), 3024-3031.

41. Gregory, B. W.; Stickney, J. L., Electrochemical atomic layer epitaxy (ECALE). *Journal of electroanalytical chemistry and interfacial electrochemistry* **1991,** *300* (1-2), 543-561.

42. Gregory, B. W.; Norton, M. L.; Stickney, J. L., Thin-layer electrochemical studies of the underpotential deposition of cadmium and tellurium on polycrystalline Au, Pt and Cu electrodes. *Journal of Electroanalytical Chemistry and Interfacial Electrochemistry* **1990,** *293* (1), 85-101.

43. Perdue, B.; Czerniawski, J.; Anthony, J.; Stickney, J., Optimization of Te Solution Chemistry in the Electrochemical Atomic Layer Deposition Growth of CdTe. *J. Electrochem. Soc.* **2014,** *161* (7), D3087-D3092.

44. Czerniawski, J. M.; Perdue, B. R.; Stickney, J. L., Potential Pulse Atomic Layer Deposition of Cu2Se. *Chemistry of Materials* **2016,** *28* (2), 583-591.

45. Demir, U.; Shannon, C., A scanning tunneling microscopy study of electrochemically grown cadmium sulfide monolayers on Au (111). *Langmuir* **1994,** *10* (8), 2794-2799.

46. Gichuhi, A.; Boone, B. E.; Demir, U.; Shannon, C., Electrochemistry of S Adlayers at underpotentially deposited Cd on Au (111): Implications for the electrosynthesis of high-quality CdS thin films. *The Journal of Physical Chemistry B* **1998,** *102* (34), 6499-6506.

47. Demir, U.; Shannon, C., Electrochemistry of Cd at ($\sqrt{3}\times\sqrt{3}$) R30-S/Au (111): Kinetics of structural changes in CdS monolayers. *Langmuir* **1996,** *12* (25), 6091-6097.

48. Boone, B. E.; Shannon, C., Optical properties of ultrathin electrodeposited CdS films probed by resonance Raman spectroscopy and photoluminescence. *The Journal of Physical Chemistry* **1996,** *100* (22), 9480-9484.

49. Torimoto, T.; Nagakubo, S.; Nishizawa, M.; Yoneyama, H., Photoelectrochemical properties of size-quantized CdS thin films prepared by an electrochemical method. *Langmuir* **1998,** *14* (25), 7077-7081.

50. Hamilton, I. C.; Woods, R., An investigation of the deposition and reactions of sulphur on gold electrodes. *J. Appl. Electrochem.* **1983,** *13* (6), 783-794.

51. Lay, M. D.; Varazo, K.; Stickney, J. L., Formation of Sulfur Atomic Layers on Gold from Aqueous Solutions of Sulfide and Thiosulfate: Studies Using EC-STM, UHV-EC, and TLEC. *Langmuir* **2003,** *19* (20), 8416-8427.

52. Gu, J.; Fahrenkrug, E.; Maldonado, S., Analysis of the Electrodeposition and Surface Chemistry of CdTe, CdSe, and CdS Thin Films through Substrate-Overlayer Surface-Enhanced Raman Spectroscopy. *Langmuir* **2014,** *30* (34), 10344-10353.

53. Zou, S.; Weaver, M. J., Surface-Enhanced Raman Scattering of Ultrathin Cadmium Chalcogenide Films on Gold Formed by Electrochemical Atomic-Layer Epitaxy: Thickness-Dependent Phonon Characteristics. *The Journal of Physical Chemistry B* **1999,** *103* (13), 2323-2326.

54. Chuu, D. S.; Dai, C. M.; Hsieh, W. F.; Tsai, C. T., Raman investigations of the surface modes of the crystallites in CdS thin films grown by pulsed laser and thermal evaporation. *Journal of Applied Physics* **1991,** *69* (12), 8402-8404.

55. Nan, W.; Niu, Y.; Qin, H.; Cui, F.; Yang, Y.; Lai, R.; Lin, W.; Peng, X., Crystal Structure Control of Zinc-Blende CdSe/CdS Core/Shell Nanocrystals: Synthesis and Structure-Dependent Optical Properties. *Journal of the American Chemical Society* **2012,** *134* (48), 19685-19693.

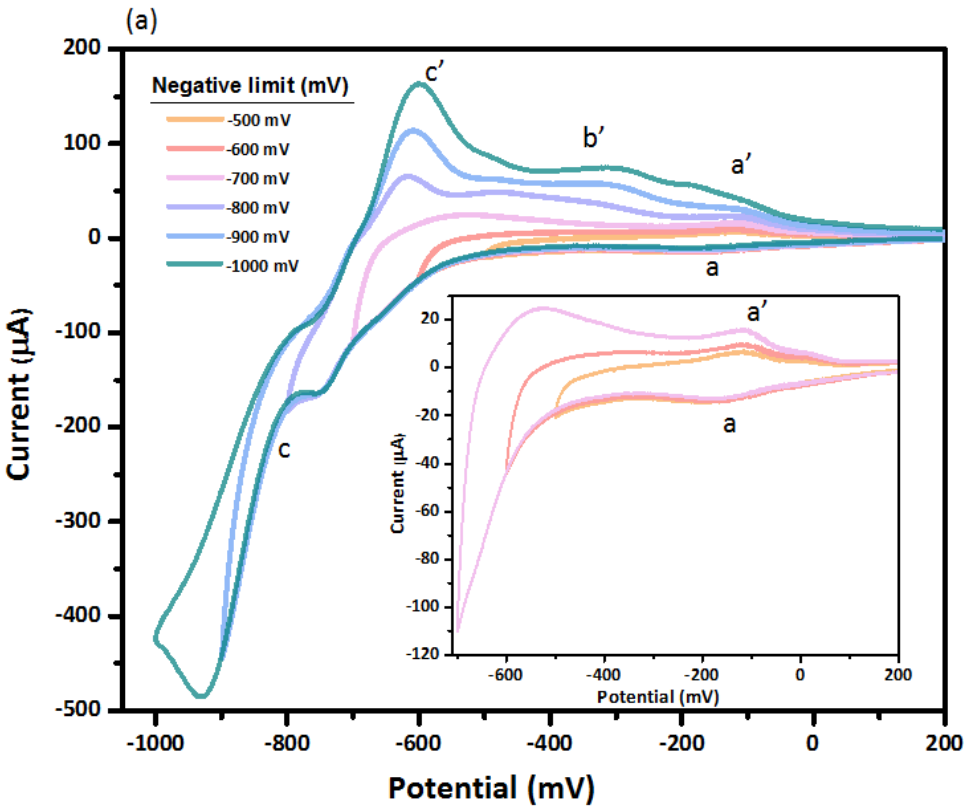

Figure 2.1(a): Cyclic voltammogram of Au in 0.5 mM $CdSO_4$, pH 3. Inset is the zoomed-in of the first 3 scans. Potential was measured vs. Ag/AgCl (3 M KCl) reference electrode with a scan rate of 10 mV/s. The flow rate was 2 mL/min. The electrode area was 2.1 cm^2.

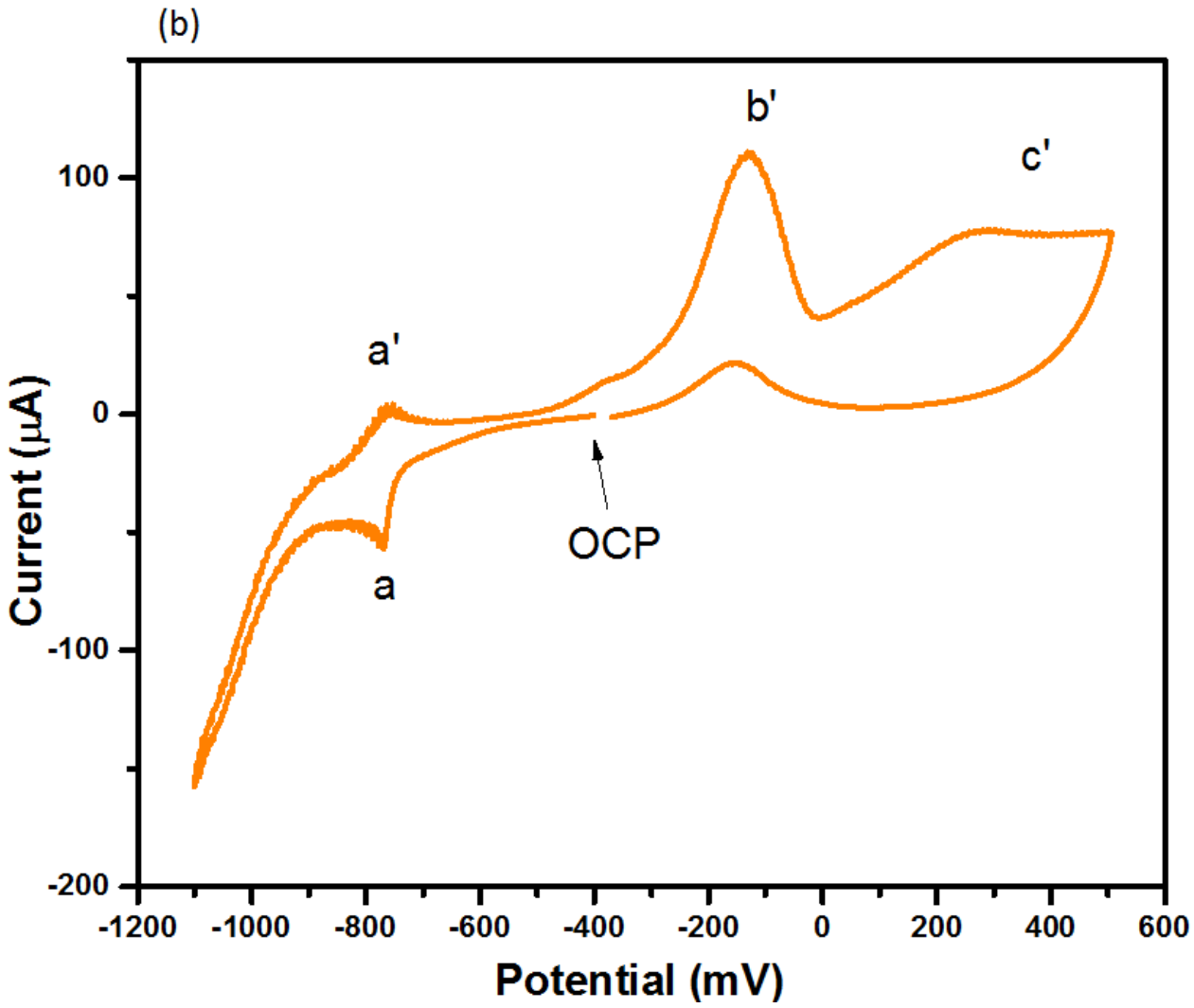

Figure 2.1(b): Cyclic voltammogram of Au in 0.5 mM Na_2S, pH 10.5. Potential was measured vs. Ag/AgCl (3 M KCl) referecne electrode with a scan rate of 10 mV/s. The flow rate was 2 mL/min. The electrode area was 2.1 cm^2.

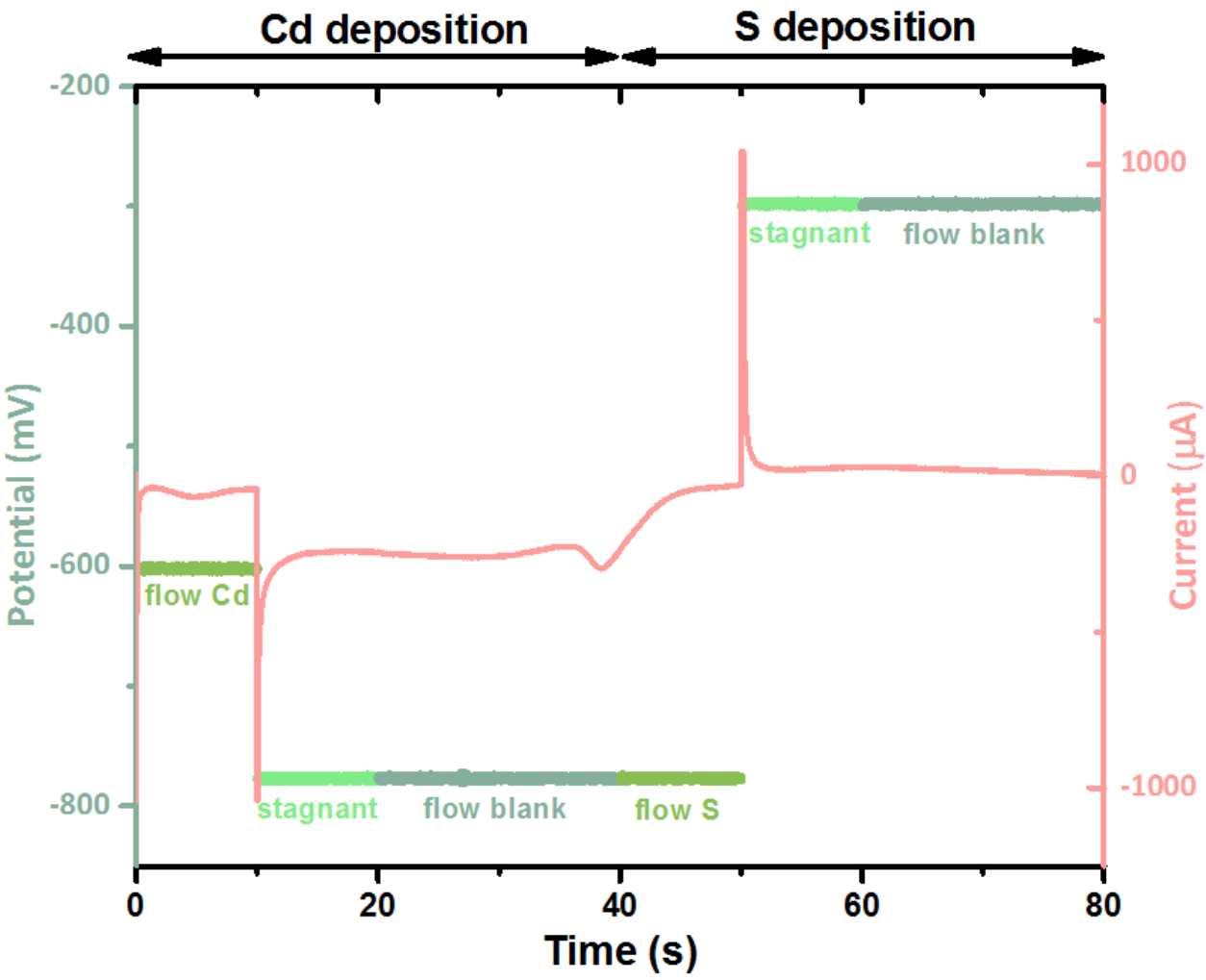

Figure 2.2: Illustration of one complete CdS E-ALD cycle. Straight lines in green indicate the potential for each step. The red curve describes the current corresponding to the potential steps.

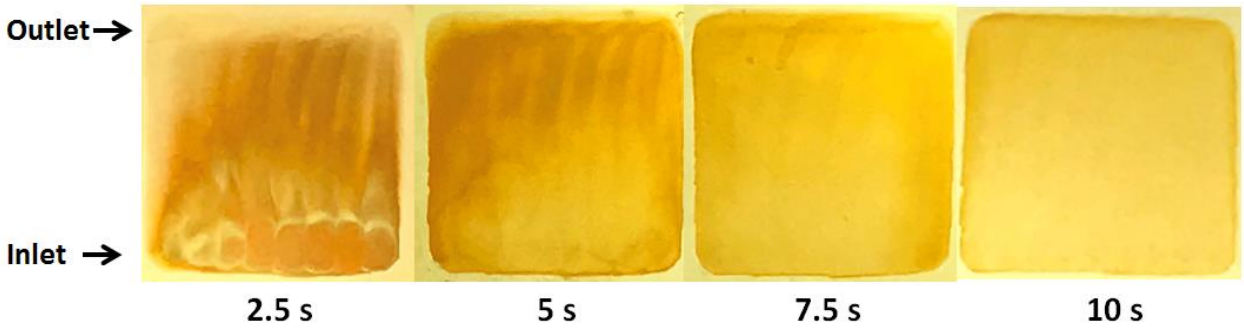

Figure 2.3：From left to right: pictures of deposit made (Cd potential = -775 mV; S potential = -300 mV) using 2.5 s (200 cycles), 5 s (100 cycles), 7.5 s (67 cycles), and 10 s (50 cycles) step lengths.

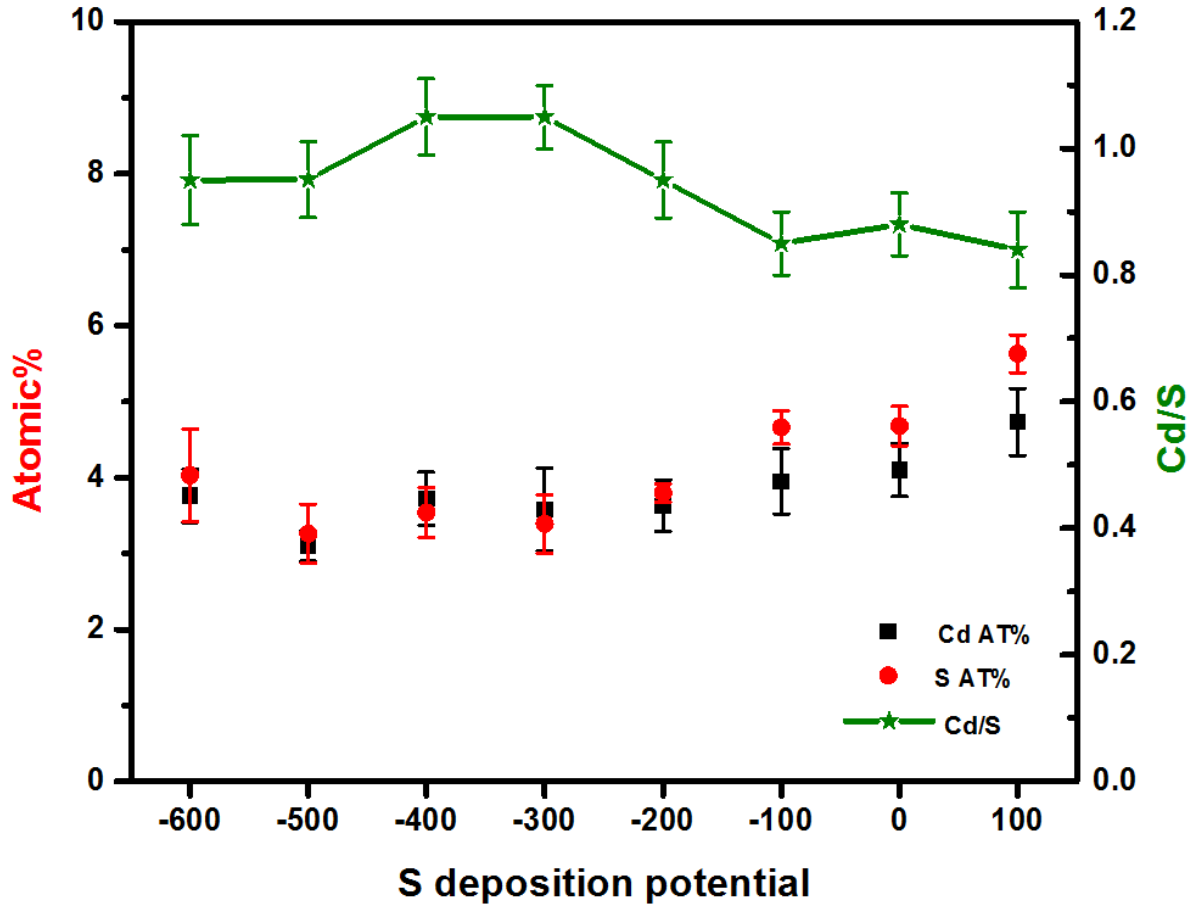

Figure 2.4(a): Dependence of CdS film composition on S potential when Cd potential was held constant at -775 mV.

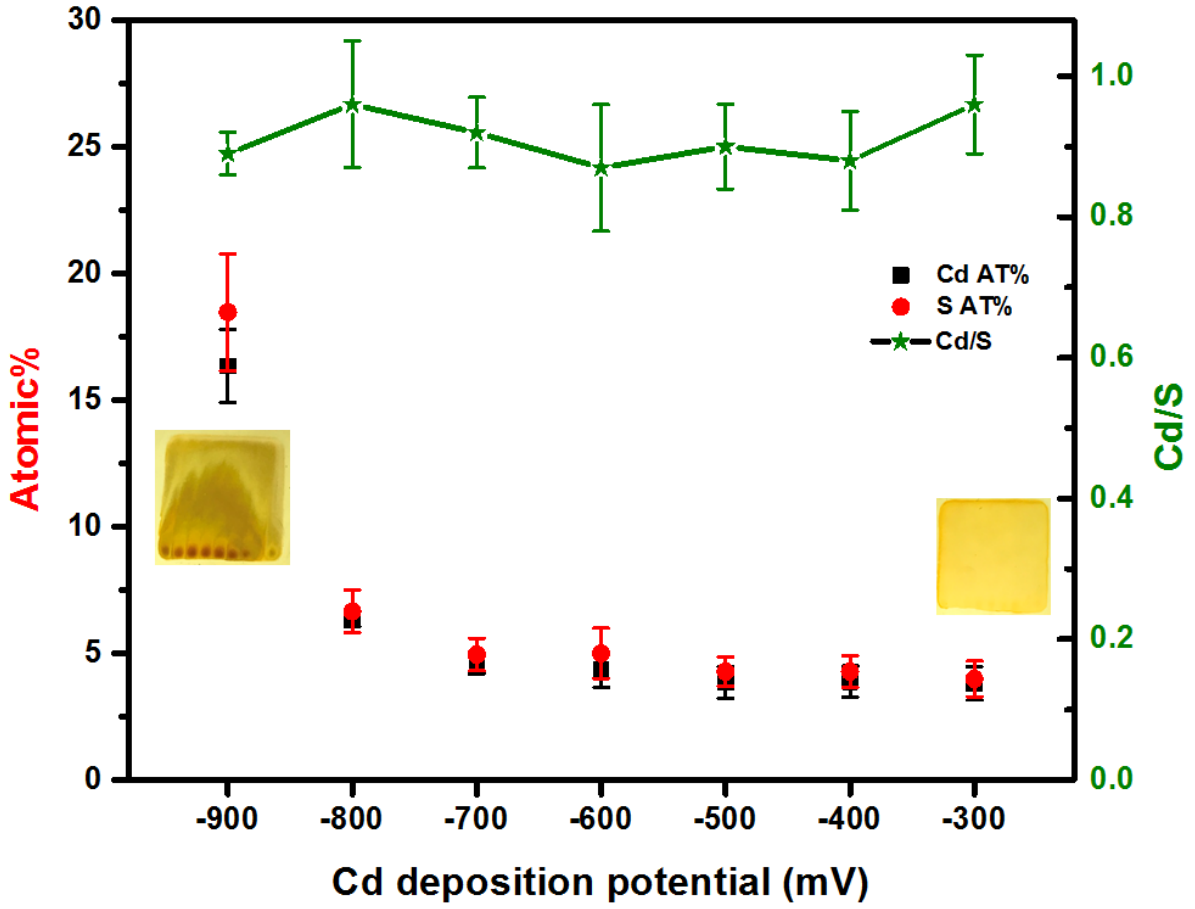

Figure 2.4(b): Dependence of CdS film composition on Cd potential when S potential was held constant at -300 mV.

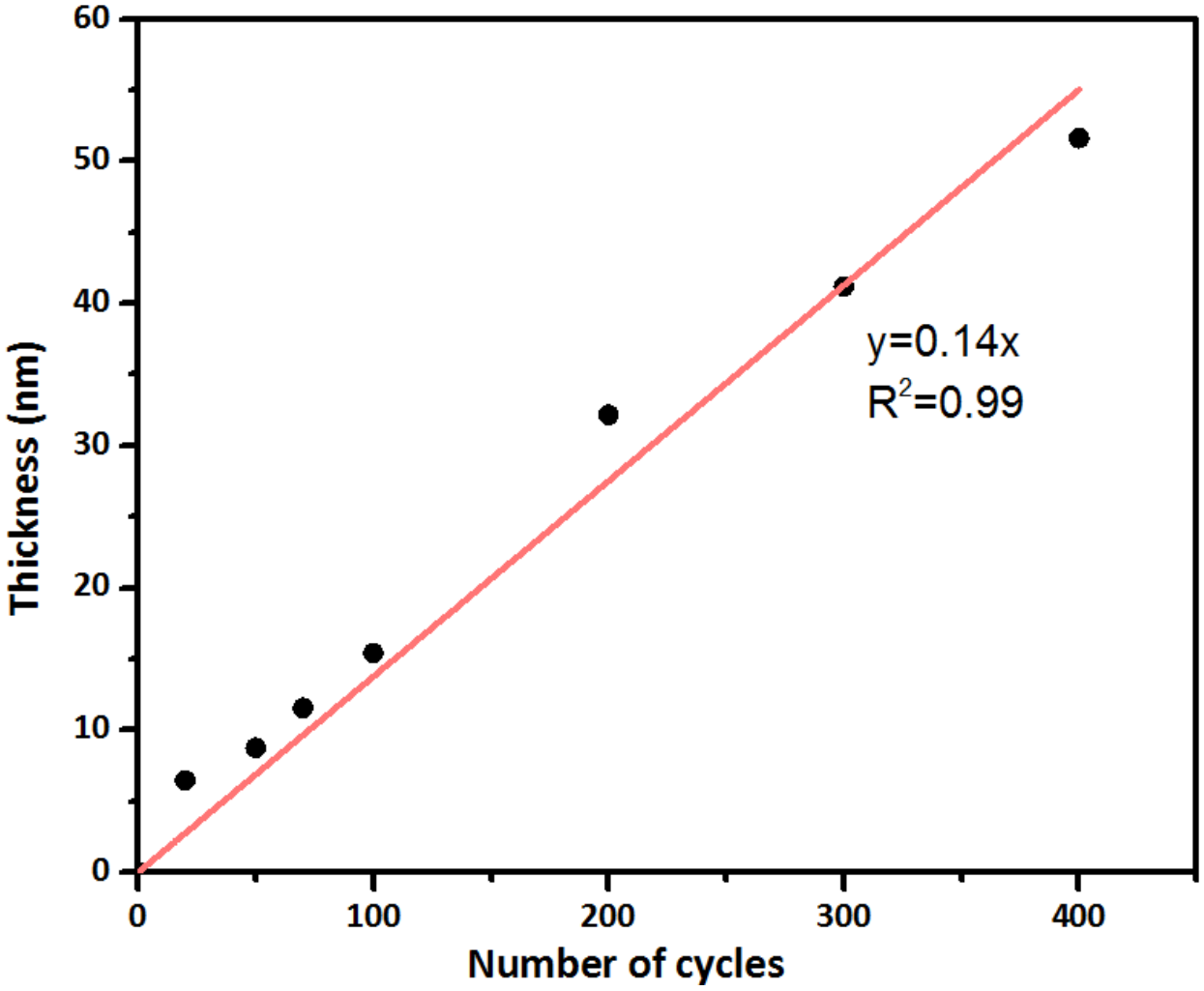

Figure 2.5: CdS thin film thickness as a linear function of the deposition cycle number (Cd potential = -775 mV; S potential = -500 mV).

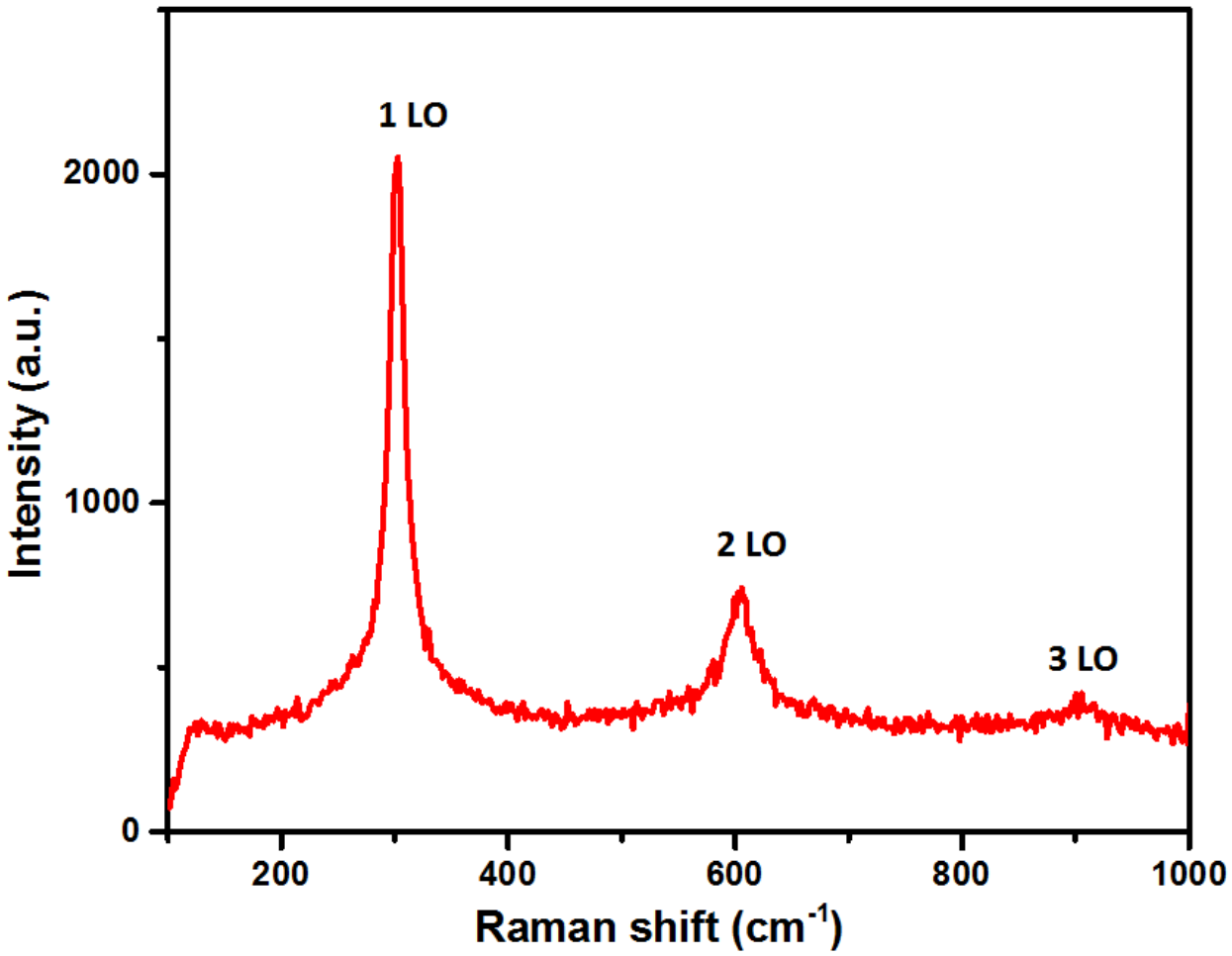

Figure 2.6: Raman spectrum on a 50 cycle CdS deposit (Cd potential = -775 mV; S potential = -500 mV) using a 514nm laser.

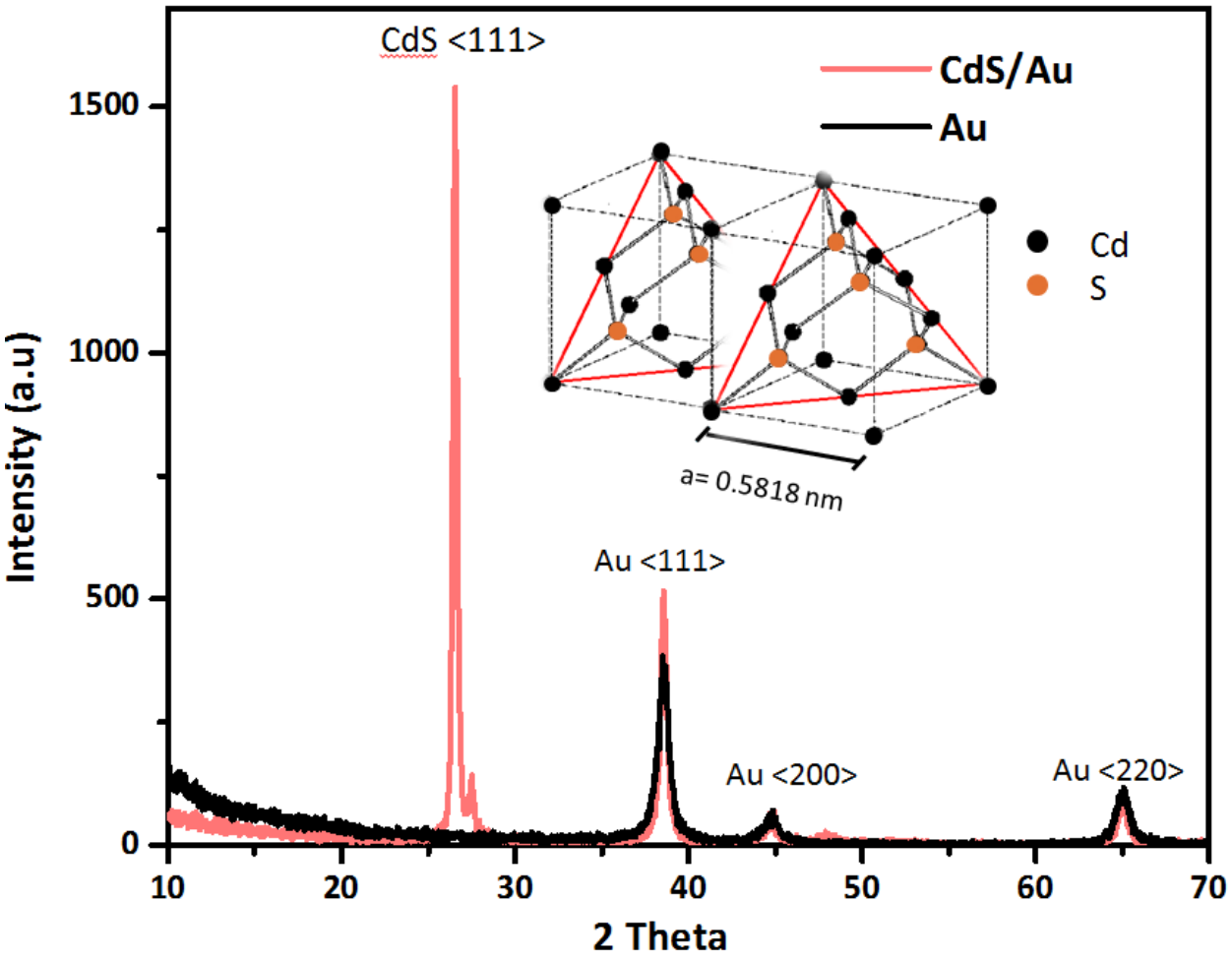

Figure 2.7: XRD patterns of Au substrate (black) and a 400-cycle CdS thin film (Cd potential = -775 mV; S potential = -500 mV) on Au. The inset represents the CdS zinc blend structure, with the red triangle marking the <111> plane.

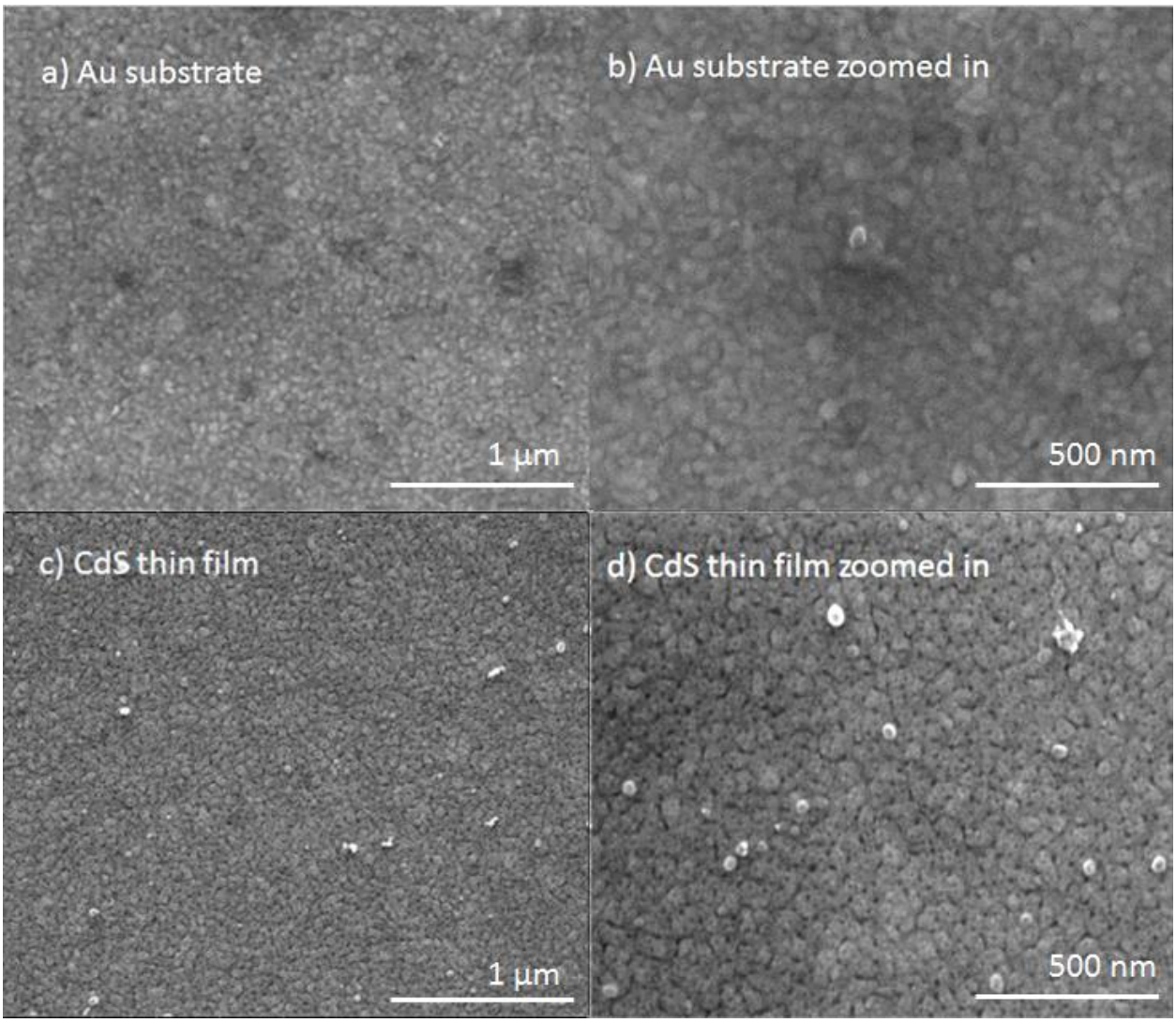

Figure 2.8: SEM images of cleaning Au substrate and the CdS thin film (Cd potential = -775mV, S potential = -500 mV, 50 cycles) on Au substrate. The comparison between the higher magnification clean Au substrate (b) and CdS (d) showed similar grain size and distribution among the two surfaces, indicating that CdS was deposited conformally on the Au substrate.

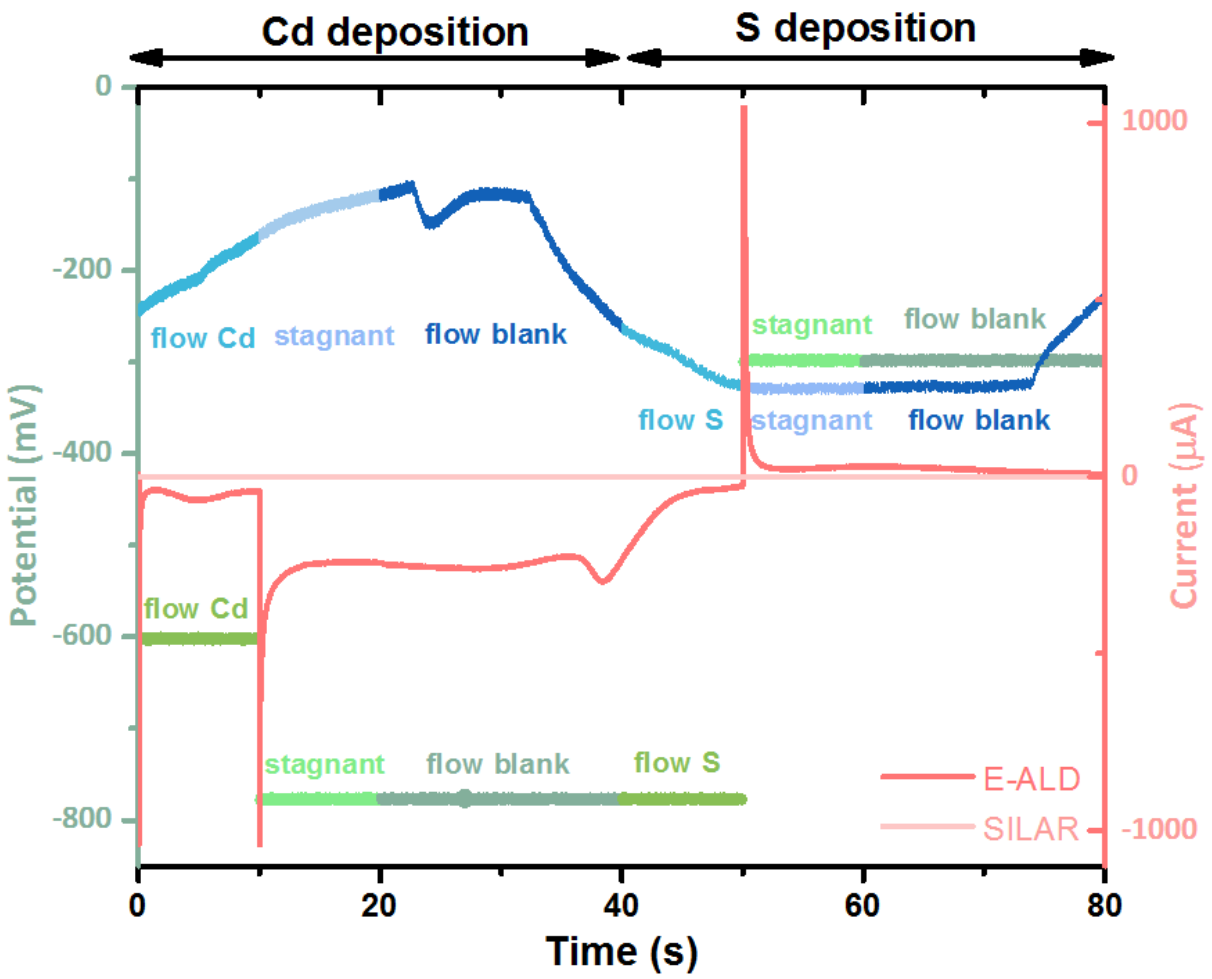

Figure 2.9: Comparison of the cycle potentials for both E-ALD (the green-themed colors) and SILAR (the blue-themed colors).

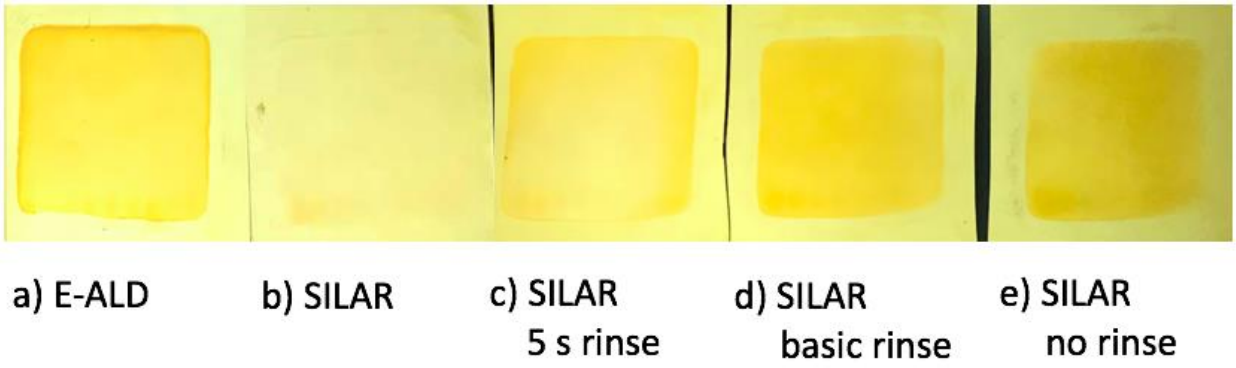

Figure 2.10: pictures of CdS on Au formed with (a) E-ALD, b) E-ALD-equivalent SILAR, c) SILAR with 5 s rinse with each blank. d) SILAR with 10 s rinse with basic blank only. e) SILAR with no rinse. The cycle number for all 5 deposits was kept 50.

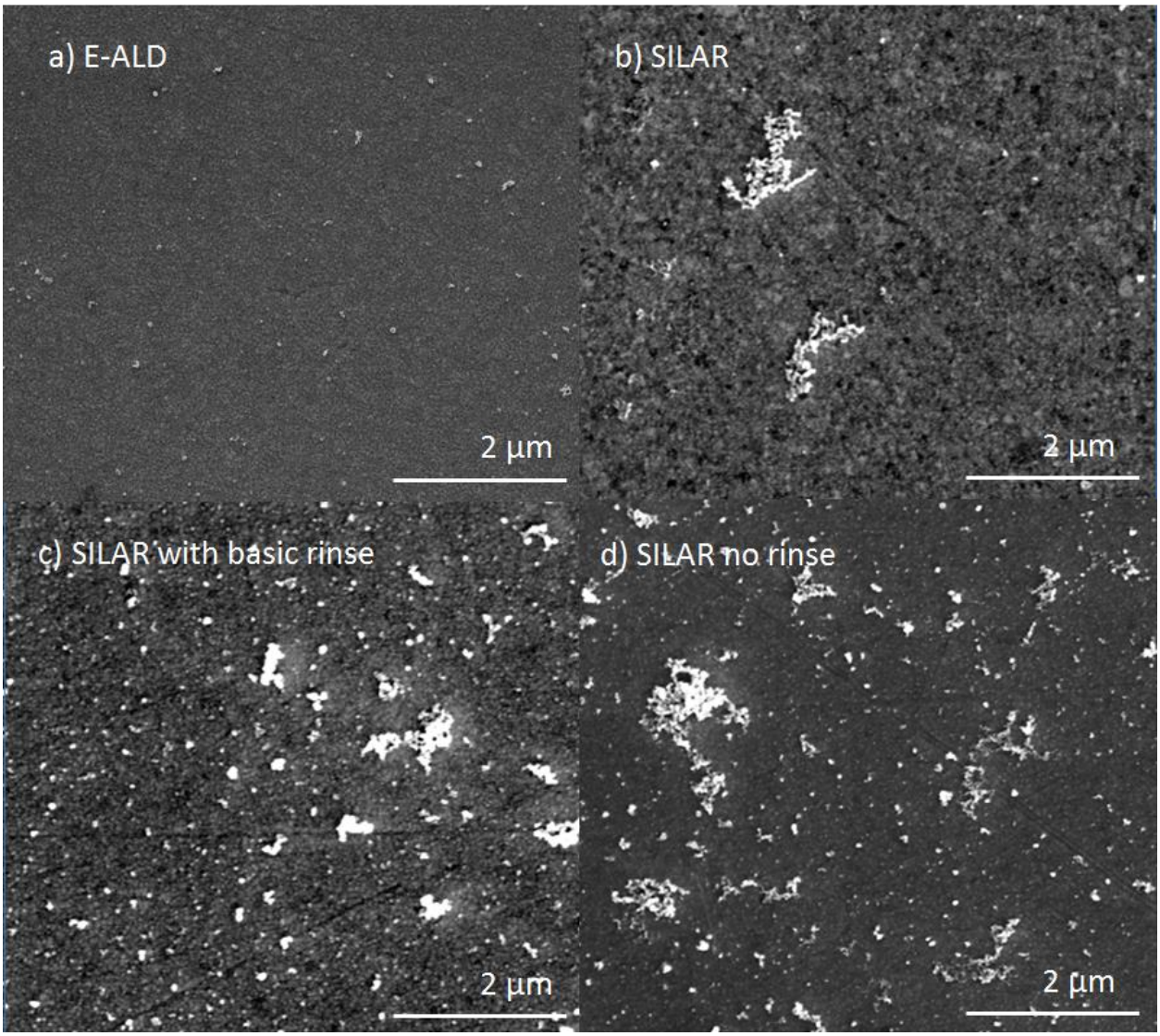

Figure 2.11: SEM images of CdS on Au formed with (a) E-ALD, b) E-ALD equivalent SILAR, c) SILAR with 10 s rinse with basic blank only. d) SILAR with no rinse.

CHAPTER 3

FORMATION OF CADMIUM SULFIDE USING ELECTROCHEMICAL LAYER DEPOSITION (E-ALD) ON PLANAR AG SUBSTRATES AND AG NANORODS[2]

[2]S. Shen, X. Zhang, B. Perdue, J. Stickney, To be submitted to *Journal of the electrochemical society*

Abstract

Silver is one of the most important materials in plasmonics. It has an excellent electricity and heat conductivity, and is able to support surface plasmons across the spectrum from 300 to 1200 nm[1]. To test the photoresponse enhancement of the Ag nanorods, a thin layer of CdS was deposited as a photocatalyst using electrochemical atomic layer deposition (ALD). Cyclic voltammetry (CV) was used to estimate the deposition potentials for Cd and S, which were then examined to systematically optimize the cycle. EPMA was used to measure the Cd/S ratios as a function of S deposition potential. The experiment conditions on Ag planar films were then transferred to Ag nanorods. SEM suggested the deposits were uniformly covering both types of Ag substrates.

Introduction

The ability of coinage metal nanostructures to manipulate light at the nanoscale has resulted in an emerging research field called plasmonics. Applications such as chemical and biological sensing[2-9], thermal therapeutics[10-17], and solar energy[18-27] has benefitted from the development of plasmonics. Plasmonics is the art of guiding and manipulating electronmagnetive waves down to the nanometer length scale[28-29]. Nanostructures with many different sizes (tens to hundreds of manometers) can be used to generate surface plasmons, thus bridging the gap between the micrometer and nanometer levels[30]. In localized surface plasmons, the electric field associated with the light exerts a force on the electrons in the conduction band of the metal nanostructure, causing them to oscillate at the same frequency. With a certain incident light frequency, the oscillation of the electrons will be in resonance with the incident light, resulting in an amplified strong oscillation of the surface electrons, known as the localized surface plasmon resonance mode[19]. By tailoring the size, shape, orientation of the nanostructures, light can be

manipulated in unique ways[31].Among all nanostructures, ordered nanorods are desirable for photo-electrochemical catalysis, because of the anisotropy in their collective responses of optical and electrical properties[32]. By controlling the length, diameter, packing density, and shape of the nanorod structure, the photoresponse enhancement magnitude can be tuned[33].

Silver is one of the most important materials in plasmonics. It has an excellent electricity and heat conductivity, and is able to support surface plasmons across the spectrum from 300 to 1200 nm[34]. Silver is relatively cheap (~13.4 USD/ounce compared with ~1207 USD/ ounce for Pt) among the metals that support plasmons.

The Ag nanorod substrates were provided by Dr. Shanlin Pan from the University of Alabama. A template-free electrodeposition technique was used to fabricate the vertically standing Ag nanorods on Indium-Tin-Oxide (ITO) by applying a constant voltage in the absence of a supporting electrolyte onto the cathode using a two-electrode system[35].To test the photoresponse enhancement of the Ag nanorods, a thin layer of CdS was deposited as a photocatalyst.

CdS thin layer can be fabricated using a number of methods, such as successive ionic layer adsorption reaction (SILAR)[36-37], close-spaced sublimation (CSS)[38-40], chemical bath deposition (CBD)[41-45] and electrodeposition[46]. Electrodeposition is a low-cost, highly controllable method of forming metal and semiconductor materials. Since the dual damascene method was developed to fabricate high quality copper interconnects in microprocessors, electrodeposition has been proven to meet the industry requirements for large-scale production[47]. In this experiment, CdS thin film was prepared using electrochemical atomic layer deposition (E-ALD)[48-53], developed by John Stickney. Similar to gas phase atomic layer deposition, surface

limited reaction is utilized to form one atomic layer of deposit on the surface at a time in E-ALD. In electrochemistry, this surface limited reaction is called underpotential deposition (UPD), which describes the formation of one atomic layer of the element on the substrate atoms before it starts to deposit on itself. This is driven by the negative free energy of surface compound formation. By alternating the solution exposed to the surface, a second element can be deposited on top of the first element, forming a compound bilayer. By varying the number of cycles applied, the thickness of the resulting thin film can be carefully tuned. pH, solution concentrations, and potential can also be varied to controlled the morphology and composition of the film. Various semiconductor thin films have been made using E-ALD, such as CdTe[50], $MoSe_2$[54], and $CuInSe_2$(CIS)[53]. To simplify the study, E-ALD of CdS on planar Ag substrate was investigated as a starting point. After the deposition conditions on planar Ag substrate were optimized, the treatment was transferred to Ag nanorods for CdS thin film deposition.

Experimental

The Ag nanorod substrates were prepared by Dr. Pan's group from the University of Alabama. For detailed synthesis procedure, please see reference[32].

For the electrodeposition of CdS, All potentials are reported vs. an Ag/AgCl (3 M KCl) reference electrode (Bioanalytical Systems, Inc). The Cd solution was pH 3, contained 0.5 mM $CdSO_4$ (Sigma-Aldrich) in 0.5 M $NaClO_4$. The sulfide solution was pH 10.5, contained 0.5 mM Na_2S (J.T.Baker) in 0.5 M $NaClO_4$. The acidic and basic blank rinse solution was 0.5 M $NaClO_4$ with pH 3 and 10.5, respectively. All solutions were made using 18 MΩ nanopure water filtered through Millipore Advantage 10.

All electrochemistry was carried out in a flowcell system (Electrochemical ALD, L.C., Athens, GA) consisting of a distributing valve, a flowcell, a pump, and a potentiostat. The auxiliary used was an Au wire embedded in the cell wall facing the ITO working electrode. The exposed electrode area was 2.1 cm^2. The whole system was automated by an in-house written LabVIEW-based program named Sequencer. The flow rate for CdS deposition was kept at 11 mL/min for the entire process. CVs were performed with a scan rate of 10 mV/s. All solutions were purged with N_2 prior to and during the experiment.

Scanning electron microscopy and energy dispersive X-ray spectroscopy (SEM-EDX) was performed on an FEI Teneo SEM (FEI, Hillsboro, OR) with an acceleration voltage of 10 keV.

Results and Discussion

Figure 3.1 is the cyclic voltammetry of planar Ag substrate in blank solution (pH 10.5) after exposed to Na_2S solution for 1 min. The scan started from open circuit, as the potential was scanned negative, a large reduction peak showed up at -720 mV that corresponded to the reduction of Ag_2S. Ag is a more reactive metal than Au. The formation of Ag_2S will occur as Ag metal is exposed to S^{2-}. Unlike with Au, where there is only a fraction of a monolayer of self-absorbed S, the reaction between Ag and S^{2-} goes deeper than the surface layer. The reduction peak integrated to be 3.76 ML, assuming a two-electron process.

In order to find out the detailed potential for where Ag_2S starts to form, a positive Ag window opening in Na_2S was carried out, shown in Figure 3.2. The reversible redox peaks at -850 mV appeared to have some UPD characteristic to them, but the integration showed the peak area to be ca. 0.02 ML, which is too small to be utilized for deposition. As the oxidation potential was

reversed more and more positive, a reduction peak appeared at ca. -770 mV, which should correspond to the formation of UPD Ag_2S. As the potential was reversed positive of -675 mV, the same peak as the bulk Ag_2S stripping peak in Figure 3.1 appeared at -720 mV. The window opening suggests that if the potential goes positive of -675 mV, the formation of bulk Ag_2S would occur. If the potential goes negative of -750, the UPD layer of Ag_2S would be reduced off. This gave a rough range of potential where S can be deposited.

Figure 3.3 depicts the negative window opening of Ag planer substrates in $CdSO_4$ solution. As the potential was scanned negative and reversed at -700 mV, no UPD stripping peak was observed. When the negative scan was reversed at -800 mV, a bulk Cd stripping peak was observed, and the peak grew as the potential was reversed at -1000 mV. A broad shoulder peak was also observed that corresponded to Ag-Cd alloy formation. The black cross marks where the bulk deposition started to happen. As long as bulk deposition is avoided, the affinity of Cd to S may be exploited for the UPD deposition of CdS.

Figure 3.4 depicts the potential-current time trace for an example cycle of CdS E-ALD on planar Ag substrate. The cycle begins with a basic environment to prepare for the entering of the S^{2-} solution. The potential was kept at -600 mV for S deposition. After the deposition, the S^{2-} solution was rinsed out with the basic blank and acidic blank was flown in at open circuit to prepare for the entering of Cd solution and to avoid any unnecessary reactions during the solution exchange. The deposition potential for Cd was kept at -600 mV to avoid bulk Cd formation. The integration of the oxidation current for S deposition is 1.25 ML, roughly in equivalent with the Cd reduction charge, which integrated to be to 1.55 ML. Considering the charging current and hydrogen evolution involved in the Cd deposition step, it is reasonable to have the Cd reduction charge slightly higher than S oxidation charge.

Three S deposition potential (-675 mV, -625 mV, -600 mV) were studied to investigate the effect of potential on the compound stoichiometry. The Cd deposition potential was kept at -600 mV. Figure 3.5 shows the atomic percent of Cd and S on a 50-cycle deposit measured by EPMA. The black blocks and red dots represent the atomic percent of Cd and S, respectively. The green stars mark the Cd/S ratio on the right axis. As the S deposition potential increased to more positive potential, the Cd to S atomic percent difference decreased, and the Cd/S ratio decreased from 1.4 to 1, which is the optimum ratio for CdS compound. This is expected because positive potentials favor S deposition, thus alters the compound from S-deficient to a 1:1 ratio deposit.

The same deposition cycle was repeated 50 times on the Ag nanorods substrate. Figure 3.6 depicts the SEM of the CdS thin film on planar Ag substrate and on Ag nanorods. The CdS on planar Ag (a) covered the surface uniformly and followed the morphology of the plain Ag substrate (b). The Ag nanorods before any treatment (d) had a smooth surface, and after coated with the CdS layer (c), the surface was clearly roughened. The CdS seem to cover not only the top surface of the rods, but also the valleys and ridges.

The EDX spectrum gave distinct Cd and S peaks, as shown in Figure 3.7. However EDX gave a Cd/S ratio of 1.9. This could be due to the closeness of the Cd peak and substrate Ag peak causing interference. Element peak overlap may lead to inaccurate quantifications in EDX more than in EPMA.

Conclusion

In this study, the E-ALD of CdS on both planar Ag films and Ag nanorods on ITO was investigated. The difference between CdS E-ALD on Au substrates and Ag substrate is that Ag is

a much more reactive metal than Au. Ag oxidizes easily and can form bulk Ag_2S at open circuit when exposed to sulfide solution. Thus the potential for CdS E-ALD on Ag must be carefully tuned. Cyclic voltammetry (CV) was used to study the electrochemical behavior of Cd and S individually on planar Ag substrate. No Cd UPD behavior was found on Ag substrate other than Cd-Ag alloy formation. The UPD formation of S on Ag substrate was limited to a small range from -750 mV to -675 mV. In the actual E-ALD process, Cd deposition potential was kept at -600 mV, and S deposition potential was varied from -675 mV to -600 mV. EPMA measured sulfur-deficient deposit until the potential was pushed to -600 mV. Stoichiometric deposits were formed at a potential of -600 mV for both Cd and S. SEM images showed conformal coating of CdS on planar Ag substrates. The deposition condition was transferred to the Ag nanorods, and under SEM the CdS thin film followed the morphology of the nanorods can coated the points and ridges conformally.

Acknowledgement

Support from the National Science Foundation, DMR 1410109, is gratefully acknowledged. Thanks are extended to Chris Fleisher and the UGA Microprobe lab. Thanks to Dr. Shanlin Pan and Dr. Jue Wang from the University of Alabama for making the Ag nanorods substrates. Thanks are extended to the Integrated Bioscience and Nanotechnology Cleanroom for the use of their facilities. Dr. Zhengwei Pan is also appreciated for the use of his SEM.

References

1. Rycenga, M.; Cobley, C. M.; Zeng, J.; Li, W.; Moran, C. H.; Zhang, Q.; Qin, D.; Xia, Y., Controlling the synthesis and assembly of silver nanostructures for plasmonic applications. *Chemical reviews* **2011,** *111* (6), 3669-3712.

2. Liu, N.; Mesch, M.; Weiss, T.; Hentschel, M.; Giessen, H., Infrared perfect absorber and its application as plasmonic sensor. *Nano letters* **2010,** *10* (7), 2342-2348.

3. Stewart, M. E.; Anderton, C. R.; Thompson, L. B.; Maria, J.; Gray, S. K.; Rogers, J. A.; Nuzzo, R. G., Nanostructured plasmonic sensors. *Chemical reviews* **2008,** *108* (2), 494-521.

4. Liu, N.; Weiss, T.; Mesch, M.; Langguth, L.; Eigenthaler, U.; Hirscher, M.; Sonnichsen, C.; Giessen, H., Planar metamaterial analogue of electromagnetically induced transparency for plasmonic sensing. *Nano letters* **2009,** *10* (4), 1103-1107.

5. Kabashin, A.; Evans, P.; Pastkovsky, S.; Hendren, W.; Wurtz, G.; Atkinson, R.; Pollard, R.; Podolskiy, V.; Zayats, A., Plasmonic nanorod metamaterials for biosensing. *Nature materials* **2009,** *8* (11), 867-871.

6. Becker, J.; Trügler, A.; Jakab, A.; Hohenester, U.; Sönnichsen, C., The optimal aspect ratio of gold nanorods for plasmonic bio-sensing. *Plasmonics* **2010,** *5* (2), 161-167.

7. Camden, J. P.; Dieringer, J. A.; Zhao, J.; Van Duyne, R. P., Controlled plasmonic nanostructures for surface-enhanced spectroscopy and sensing. *Accounts of chemical research* **2008,** *41* (12), 1653-1661.

8. Cobley, C. M.; Skrabalak, S. E.; Campbell, D. J.; Xia, Y., Shape-controlled synthesis of silver nanoparticles for plasmonic and sensing applications. *Plasmonics* **2009,** *4* (2), 171-179.

9. Tittl, A.; Mai, P.; Taubert, R.; Dregely, D.; Liu, N.; Giessen, H., Palladium-based plasmonic perfect absorber in the visible wavelength range and its application to hydrogen sensing. *Nano letters* **2011,** *11* (10), 4366-4369.

10. Huang, X.; Jain, P. K.; El-Sayed, I. H.; El-Sayed, M. A., Plasmonic photothermal therapy (PPTT) using gold nanoparticles. *Lasers in medical science* **2008,** *23* (3), 217-228.

11. Huang, P.; Lin, J.; Li, W.; Rong, P.; Wang, Z.; Wang, S.; Wang, X.; Sun, X.; Aronova, M.; Niu, G., Biodegradable gold nanovesicles with an ultrastrong plasmonic coupling effect for photoacoustic imaging and photothermal therapy. *Angewandte Chemie* **2013,** *125* (52), 14208-14214.

12. Huang, P.; Bao, L.; Zhang, C.; Lin, J.; Luo, T.; Yang, D.; He, M.; Li, Z.; Gao, G.; Gao, B., Folic acid-conjugated silica-modified gold nanorods for X-ray/CT imaging-guided dual-mode radiation and photo-thermal therapy. *Biomaterials* **2011,** *32* (36), 9796-9809.

13. Zhang, J. Z., Biomedical applications of shape-controlled plasmonic nanostructures: a case study of hollow gold nanospheres for photothermal ablation therapy of cancer. *The Journal of Physical Chemistry Letters* **2010,** *1* (4), 686-695.

14. Larson, T. A.; Bankson, J.; Aaron, J.; Sokolov, K., Hybrid plasmonic magnetic nanoparticles as molecular specific agents for MRI/optical imaging and photothermal therapy of cancer cells. *Nanotechnology* **2007,** *18* (32), 325101.

15. Mackey, M. A.; Ali, M. R.; Austin, L. A.; Near, R. D.; El-Sayed, M. A., The most effective gold nanorod size for plasmonic photothermal therapy: theory and in vitro experiments. *The Journal of Physical Chemistry B* **2014,** *118* (5), 1319-1326.

16. Huang, P.; Rong, P.; Lin, J.; Li, W.; Yan, X.; Zhang, M. G.; Nie, L.; Niu, G.; Lu, J.; Wang, W., Triphase interface synthesis of plasmonic gold bellflowers as near-infrared light mediated

acoustic and thermal theranostics. *Journal of the American Chemical Society* **2014,** *136* (23), 8307-8313.

17. Huang, X.; Tang, S.; Liu, B.; Ren, B.; Zheng, N., Enhancing the Photothermal Stability of Plasmonic Metal Nanoplates by a Core‐Shell Architecture. *Advanced Materials* **2011,** *23* (30), 3420-3425.

18. Odom, T. W.; Schatz, G. C., Introduction to Plasmonics. *Chemical Reviews* **2011,** *111* (6), 3667-3668.

19. Maier, S. A., *Plasmonics: fundamentals and applications*. Springer Science & Business Media: 2007.

20. Pillai, S.; Green, M., Plasmonics for photovoltaic applications. *Solar Energy Materials and Solar Cells* **2010,** *94* (9), 1481-1486.

21. Ozbay, E., Plasmonics: merging photonics and electronics at nanoscale dimensions. *science* **2006,** *311* (5758), 189-193.

22. Ferry, V. E.; Munday, J. N.; Atwater, H. A., Design considerations for plasmonic photovoltaics. *Advanced materials* **2010,** *22* (43), 4794-4808.

23. Gan, Q.; Bartoli, F. J.; Kafafi, Z. H., Plasmonic‐enhanced organic photovoltaics: Breaking the 10% efficiency barrier. *Advanced materials* **2013,** *25* (17), 2385-2396.

24. Munday, J. N.; Atwater, H. A., Large integrated absorption enhancement in plasmonic solar cells by combining metallic gratings and antireflection coatings. *Nano letters* **2010,** *11* (6), 2195-2201.

25. Wu, C.; Neuner III, B.; John, J.; Milder, A.; Zollars, B.; Savoy, S.; Shvets, G., Metamaterial-based integrated plasmonic absorber/emitter for solar thermo-photovoltaic systems. *Journal of Optics* **2012,** *14* (2), 024005.

26. Chen, F.-C.; Wu, J.-L.; Lee, C.-L.; Hong, Y.; Kuo, C.-H.; Huang, M. H., Plasmonic-enhanced polymer photovoltaic devices incorporating solution-processable metal nanoparticles. *Applied Physics Letters* **2009,** *95* (1), 182.

27. Cushing, S. K.; Li, J.; Meng, F.; Senty, T. R.; Suri, S.; Zhi, M.; Li, M.; Bristow, A. D.; Wu, N., Photocatalytic activity enhanced by plasmonic resonant energy transfer from metal to semiconductor. *Journal of the American Chemical Society* **2012,** *134* (36), 15033-15041.

28. Zouhdi, S.; Sihvola, A.; Vinogradov, A. P., *Metamaterials and plasmonics: fundamentals, modelling, applications*. Springer Science & Business Media: 2008.

29. Maier, S. A.; Atwater, H. A., Plasmonics: Localization and guiding of electromagnetic energy in metal/dielectric structures. *Journal of applied physics* **2005,** *98* (1), 10.

30. Marinica, D. C.; Kazansky, A. K.; Nordlander, P.; Aizpurua, J.; Borisov, A., Quantum plasmonics: nonlinear effects in the field enhancement of a plasmonic nanoparticle dimer. *Nano letters* **2012,** *12* (3), 1333-1339.

31. Lal, S.; Link, S.; Halas, N. J., Nano-optics from sensing to waveguiding. *Nature photonics* **2007,** *1* (11), 641-648.

32. Wang, J.; Gupta, A.; Pan, S., A facile template-free electrodeposition method for vertically standing nanorods on conductive substrates and their applications for photoelectrochemical catalysis. *International Journal of Hydrogen Energy* **2017,** *42* (12), 8462-8474.

33. Atwater, H. A.; Polman, A., Plasmonics for improved photovoltaic devices. *Nature materials* **2010,** *9* (3), 205-213.

34. Sankapal, B.; Mane, R.; Lokhande, C., Deposition of CdS thin films by the successive ionic layer adsorption and reaction (SILAR) method. *Materials research bulletin* **2000,** *35* (2), 177-184.

35. Pathan, H.; Lokhande, C., Deposition of metal chalcogenide thin films by successive ionic layer adsorption and reaction (SILAR) method. *Bulletin of Materials Science* **2004,** *27* (2), 85-111.

36. Schaffner, J.; Motzko, M.; Tueschen, A.; Swirschuk, A.; Schimper, H.-J.; Klein, A.; Modes, T.; Zywitzki, O.; Jaegermann, W., 12% efficient CdTe/CdS thin film solar cells deposited by low-temperature close space sublimation. *Journal of Applied Physics* **2011,** *110* (6), 064508.

37. Aramoto, T.; Kumazawa, S.; Higuchi, H.; Arita, T.; Shibutani, S.; Nishio, T.; Nakajima, J.; Tsuji, M.; Hanafusa, A.; Hibino, T., 16.0% efficient thin-film CdS/CdTe solar cells. *Japanese Journal of Applied Physics* **1997,** *36* (10R), 6304.

38. Feldmeier, E. M.; Fuchs, A.; Schaffner, J.; Schimper, H. J.; Klein, A.; Jaegermann, W., Comparison between the structural, morphological and optical properties of CdS layers prepared by Close Space Sublimation and RF magnetron sputtering for CdTe solar cells. *Thin Solid Films* **2011,** *519* (21), 7596-7599.

39. Pavaskar, N.; Menezes, C.; Sinha, A., Photoconductive CdS films by a chemical bath deposition process. *J. Electrochem. Soc.* **1977,** *124* (5), 743-748.

40. Wang, W.; Winkler, M. T.; Gunawan, O.; Gokmen, T.; Todorov, T. K.; Zhu, Y.; Mitzi, D. B., Device characteristics of CZTSSe thin‐film solar cells with 12.6% efficiency. *Advanced Energy Materials* **2014,** *4* (7).

41. Chirilă, A.; Reinhard, P.; Pianezzi, F.; Bloesch, P.; Uhl, A. R.; Fella, C.; Kranz, L.; Keller, D.; Gretener, C.; Hagendorfer, H., Potassium-induced surface modification of Cu (In, Ga) Se2 thin films for high-efficiency solar cells. *Nature Materials* **2013,** *12* (12), 1107-1111.

42. Ortega‐Borges, R.; Lincot, D., Mechanism of Chemical Bath Deposition of Cadmium Sulfide Thin Films in the Ammonia‐Thiourea System In Situ Kinetic Study and Modelization. *J. Electrochem. Soc.* **1993,** *140* (12), 3464-3473.

43. Khallaf, H.; Oladeji, I. O.; Chai, G.; Chow, L., Characterization of CdS thin films grown by chemical bath deposition using four different cadmium sources. *Thin Solid Films* **2008,** *516* (21), 7306-7312.

44. Nishino, J.; Chatani, S.; Uotani, Y.; Nosaka, Y., Electrodeposition method for controlled formation of CdS films from aqueous solutions. *J Electroanal Chem* **1999,** *473* (1–2), 217-222.

45. Carlà, F.; Loglio, F.; Resta, A.; Felici, R.; Lastraioli, E.; Innocenti, M.; Foresti, M. L., Electrochemical atomic layer deposition of CdS on Ag single crystals: effects of substrate orientation on film structure. *The Journal of Physical Chemistry C* **2014,** *118* (12), 6132-6139.

46. Stickney, J. L., Electrochemical atomic layer epitaxy (EC-ALE): Nanoscale control in the electrodeposition of compound semiconductors. *Advances in Electrochemical Science and Engineering* **2002,** *7*, 1-106.

47. Gregory, B. W.; Suggs, D. W.; Stickney, J. L., Conditions for the deposition of CdTe by electrochemical atomic layer epitaxy. *J. Electrochem. Soc.* **1991,** *138* (5), 1279-1284.

48. Villegas, I.; Stickney, J. L., Preliminary studies of GaAs deposition on Au (100),(110), and (111) surfaces by electrochemical atomic layer epitaxy. *J. Electrochem. Soc.* **1992,** *139* (3), 686-694.

49. Vaidyanathan, R.; Cox, S. M.; Happek, U.; Banga, D.; Mathe, M. K.; Stickney, J. L., Preliminary studies in the electrodeposition of PbSe/PbTe superlattice thin films via electrochemical atomic layer deposition (ALD). *Langmuir* **2006,** *22* (25), 10590-10595.

50. Colletti, L. P.; Flowers, B. H.; Stickney, J. L., Formation of thin films of CdTe, CdSe, and CdS by electrochemical atomic layer epitaxy. *J. Electrochem. Soc.* **1998,** *145* (5), 1442-1449.

51. Banga, D.; Jarayaju, N.; Sheridan, L.; Kim, Y.-G.; Perdue, B.; Zhang, X.; Zhang, Q.; Stickney, J., Electrodeposition of CuInSe2 (CIS) via electrochemical atomic layer deposition (E-ALD). *Langmuir* **2012,** *28* (5), 3024-3031.

52. Gregory, B. W.; Norton, M. L.; Stickney, J. L., Thin-layer electrochemical studies of the underpotential deposition of cadmium and tellurium on polycrystalline Au, Pt and Cu electrodes. *Journal of Electroanalytical Chemistry and Interfacial Electrochemistry* **1990,** *293* (1), 85-101.

53. Perdue, B.; Czerniawski, J.; Anthony, J.; Stickney, J., Optimization of Te Solution Chemistry in the Electrochemical Atomic Layer Deposition Growth of CdTe. *J. Electrochem. Soc.* **2014,** *161* (7), D3087-D3092.

54. Tsang, C. F.; Ledina, M. A.; Stickney, J. L., Molybdenum diselenide formation using electrochemical atomic layer deposition (E-ALD). *J Electroanal Chem* **2017**.

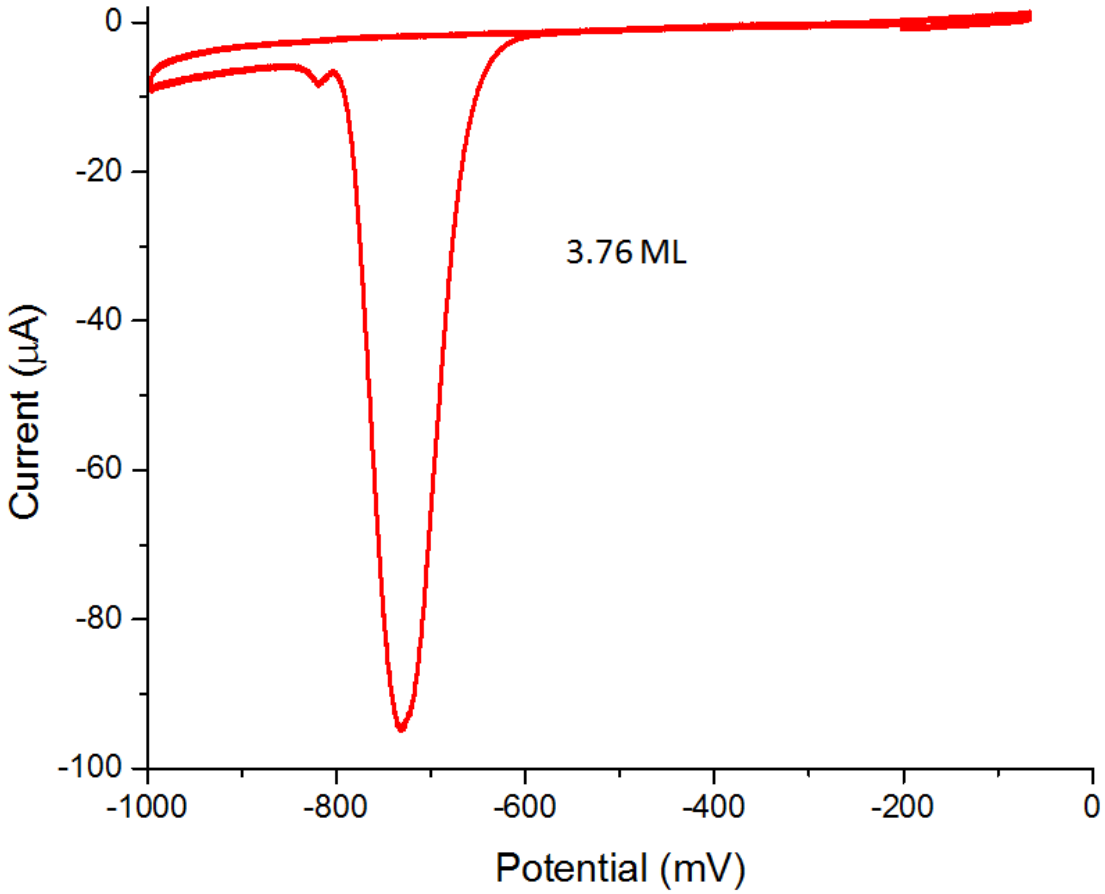

Figure 3.1: Cyclic voltammetry of planar Ag substrate in blank solution (pH 10.5) after exposed to Na_2S solution for 1 min. The scan rate was 10 mV/s.

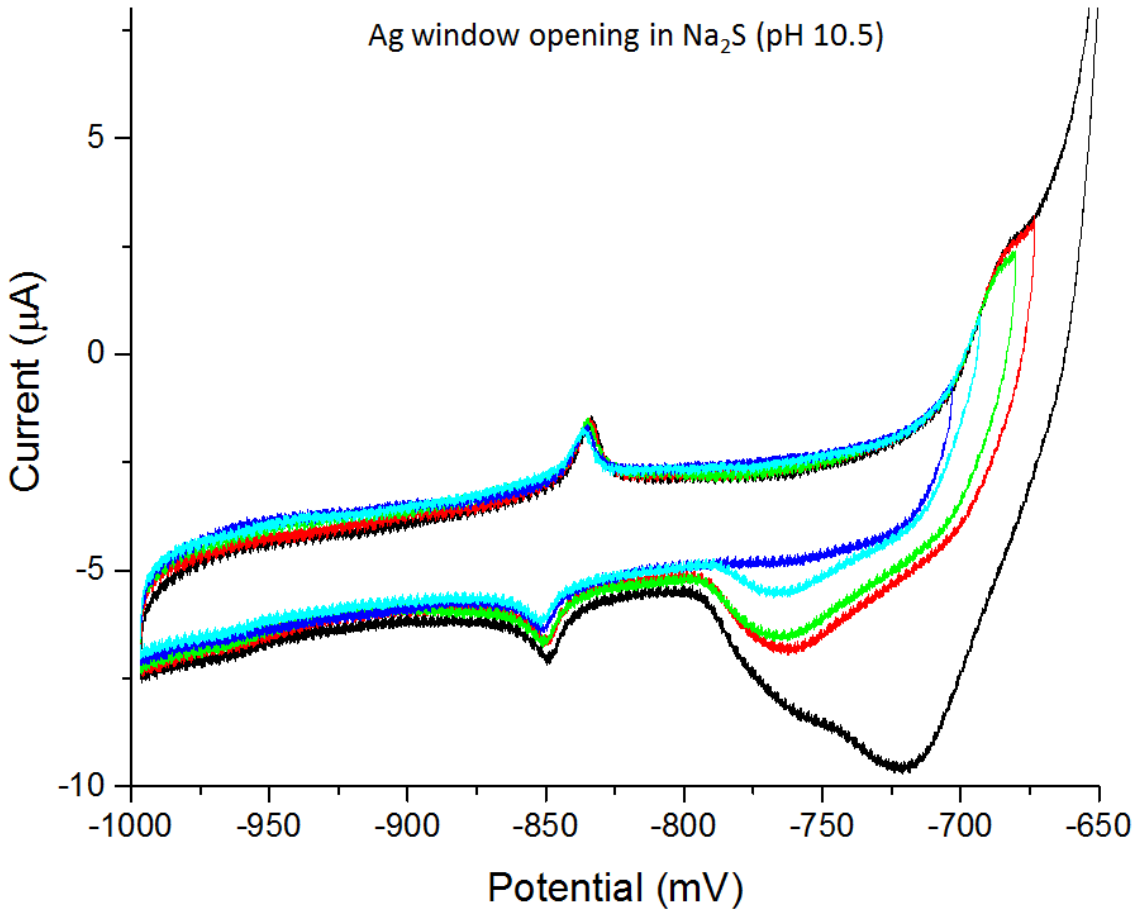

Figure 3.2: Positive window opening of Ag in Na_2S at 10 mV/s.

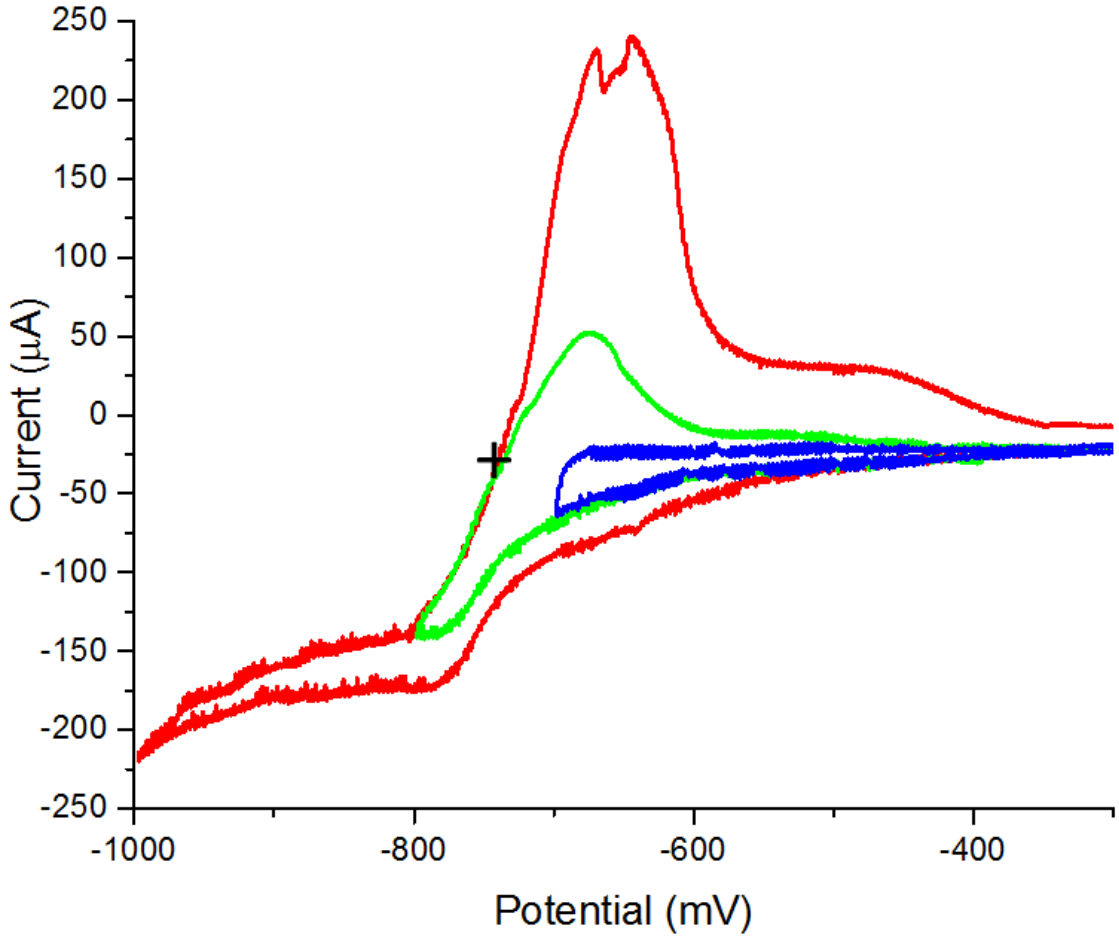

Figure 3.3: Negative window opening of Ag planer substrates in $CdSO_4$ solution. The black cross indicates the formal potential of Cd^{2+} in the given environment.

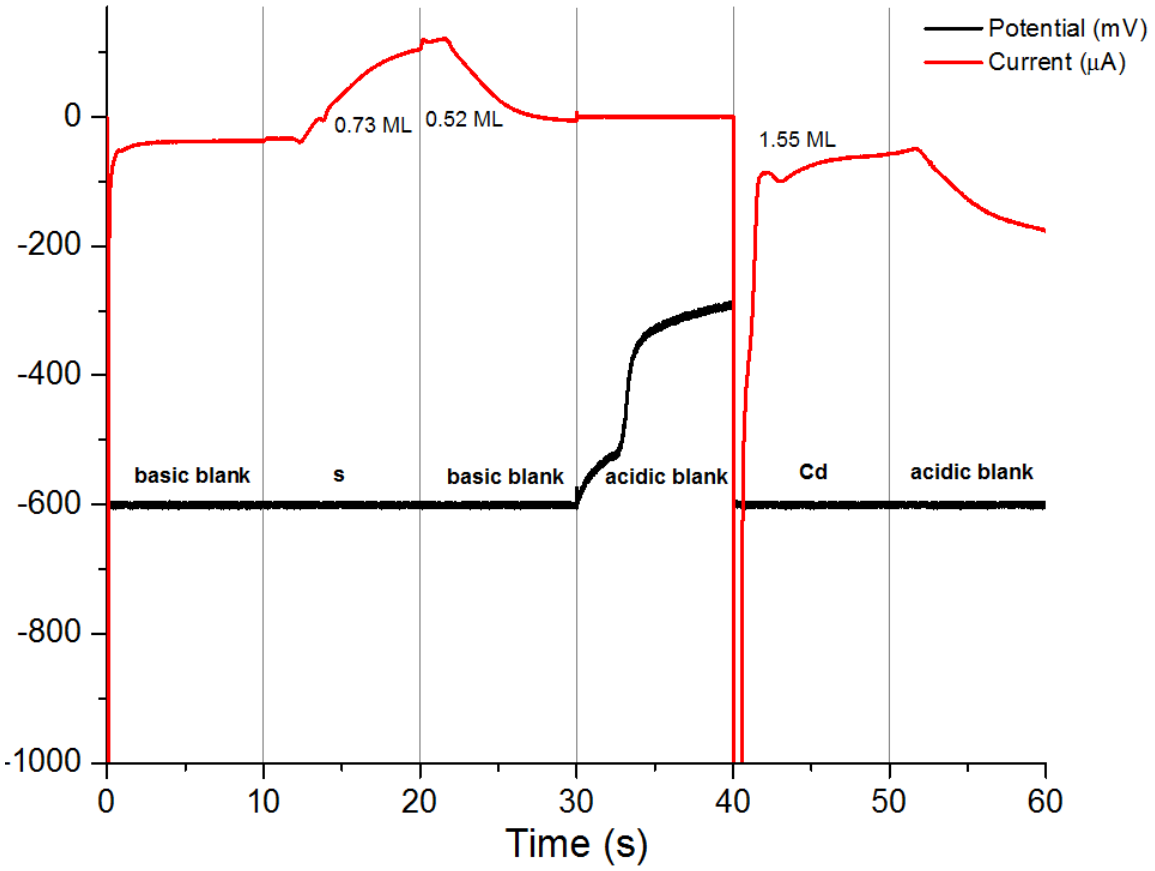

Figure 3.4 Potential (black)-current (red) time trace for an example cycle of CdS E-ALD on planar Ag substrate.

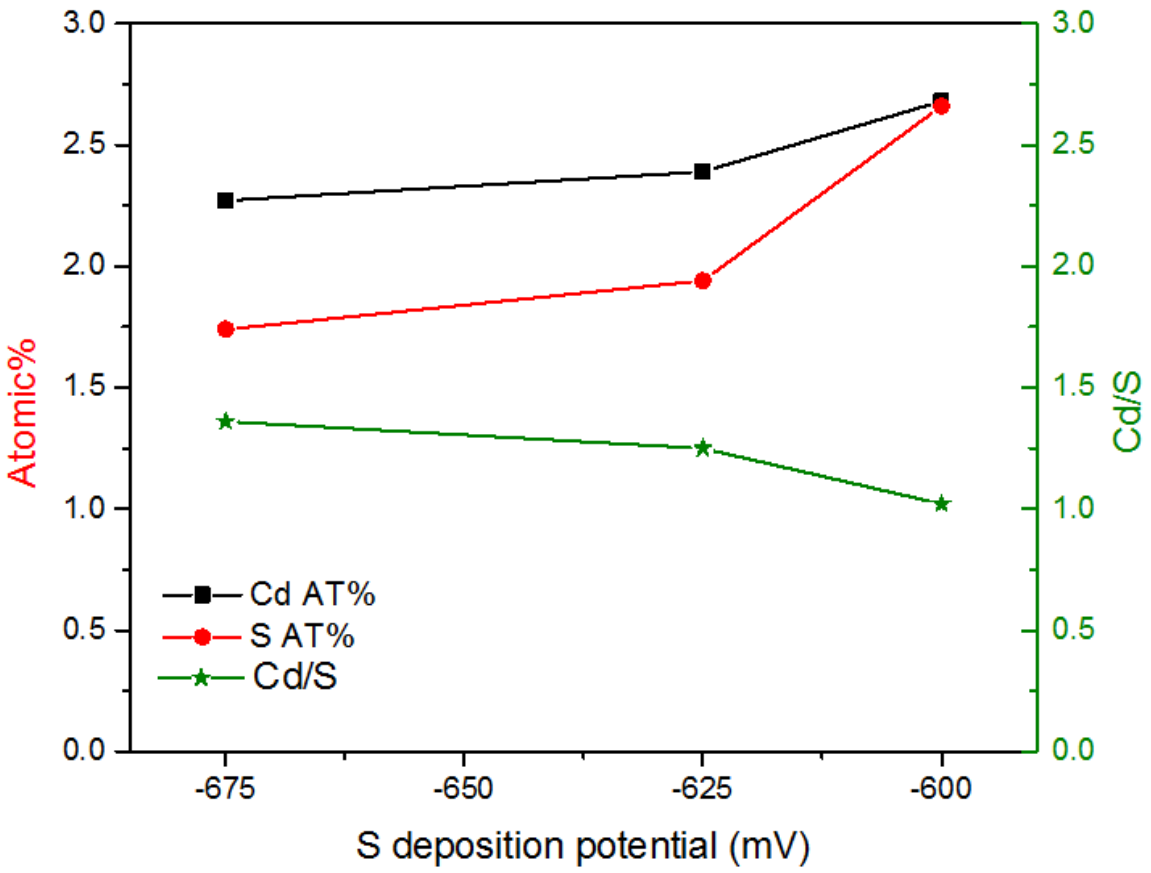

Figure 3.5: Atomic percents of Cd and S on a 50-cycle deposit measured by EPMA. S deposition potential were varied while Cd deposition potential was kept at -600 mV.

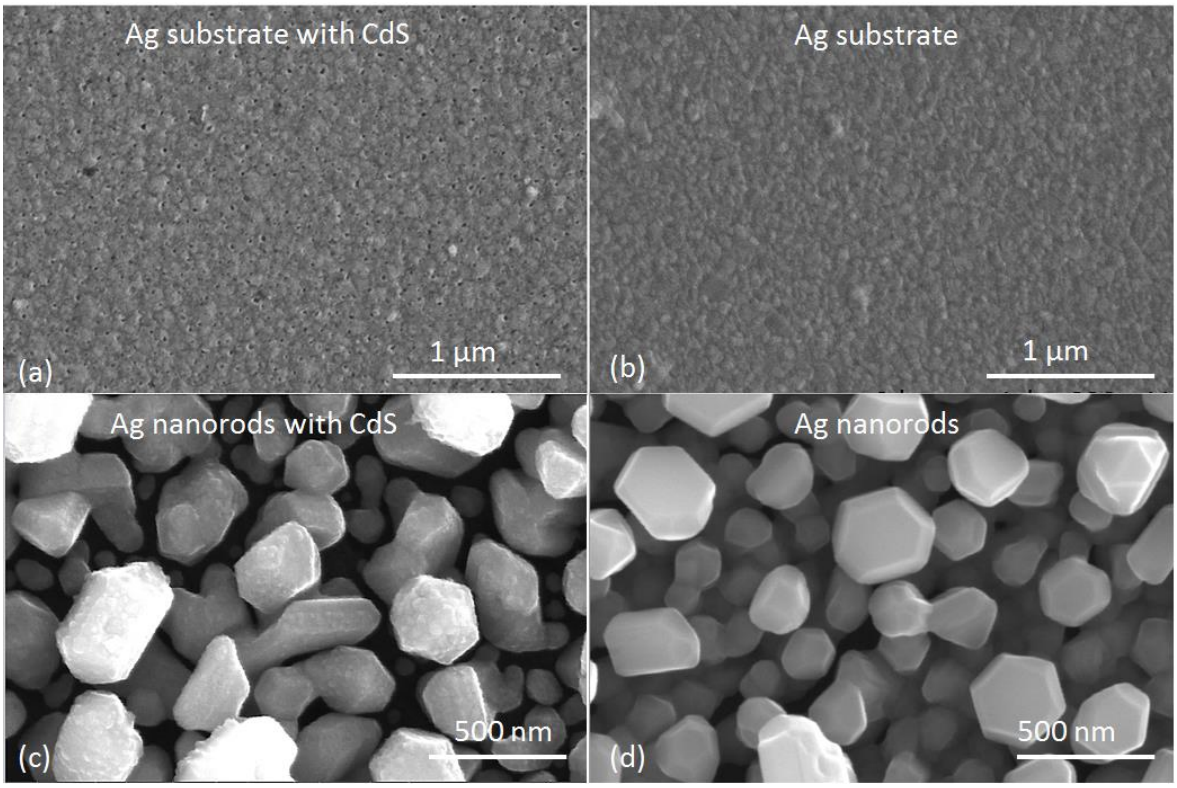

Figure 3.6: SEM of the (a) CdS thin film on planar Ag substrate (b) untreated planar Ag substrate (c) CdS on Ag nanorods (d) untreated Ag nanorods.

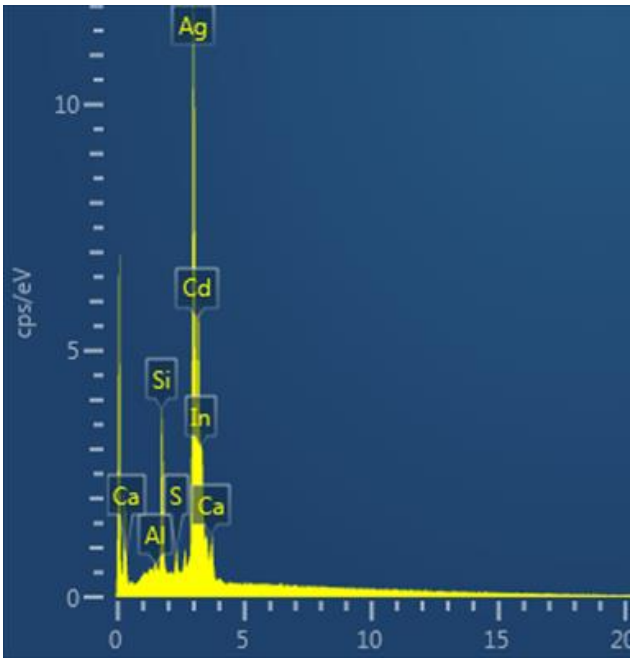

Figure 3.7: EDX spectrum of CdS on Ag nanorods. Distinct S and Cd peaks can be observed, but the difficulty to separate the Cd peak and the Ag substrate peak can lead to inaccurate Cd/S ratio.

CHAPTER 4

MAXIMIZATION OF NUCLEATION AND GROWTH FOR CADMIUM SULFIDE ELECTRODEPOSITION ON INDIUM-TIN-OXIDE[3]

[3]S. Shen, J. Stickney, To be submitted to *ACS Applied Materials &Interfaces*

Abstract

CdS deposition on Indium-Tin-Oxide (ITO) is an important step in most thin film photovoltaic synthesis process. CdS deposits on ITO through nucleation and growth mechanism, thus it is key to maximize the number of nucleation sites on ITO surface. In this report, an electrochemical process was developed by reducing a tiny amount of ITO to In metal and then exchanging the In with Cu^{2+}, leaving small amounts of stable Cu on the ITO surface as nucleation anchor points for CdS electrodeposition. This method effectively increased the number of nucleation sites on ITO by over 10 times compared with that on pristine ITO, and made the electrochemical atomic layer deposition of CdS on ITO possible. Film adhesion to substrates was also significantly improved after the treatment.

Introduction

Electrodeposition has been successfully applied to form photovoltaics since the 1970s[1]. Over the years, many photovoltaic materials, such as CdTe[2-4], Cu(In,Ga)Se (CIGS)[5-8], and Cu_2ZnSnS_4 (CZTS)[9-12] have been formed using electrodeposition. The advantage of electrodeposition over other physical and chemical deposition techniques is that everything can be done in a beaker or flow cell under ambient conditions. The stoichiometry, doping, bandgap, and conduction type can be controlled with a reasonable accuracy, by varying the deposition potential, time, precursor concentration and pH, etc. Low temperature deposition techniques such as electrodeposition are not only more energy-saving, but also avoid material interdiffusion, which is typical in high-temperature process, thus yielding a sharper junction[13].

In a typical superstrate thin film solar cell configuration, n-type semiconductor CdS is deposited on a transparent conducting oxide (TCO), usually indium-tin oxide (ITO), followed by

the deposition of the p-type absorber material and a metal back contact. A thin CdS layer will lead to a higher J_{sc} compared with a thicker layer due to enhanced blue response. But making CdS too thin often leads to pinholes results in the reduction of V_{oc} and Fill Factor[14]. Thus a uniform coverage of CdS thin film on the TCO is of significant importance to the overall performance of the solar cell.

ITO is an n-type semiconductor with a bandgap between 3.5–4.3 eV. It usually consists of In_2O_3 with 10 wt% SnO_2[15]. There may be up to 4 different forms of oxygen on the surface of ITO, as well as at least two forms of In and Sn[16]. Due to the oxide nature of ITO, the different degree of hydrolysis of the lattice, along with the density and orientation of the oxide grains, can all lead to a fairly high level of heterogeneity on the surface. The high carrier concentration of ITO comes from the various defects sites including oxygen vacancies, interstitial indium, substitutional Sn^{4+} preplaced at In^{3+} sites[17]. Chemical reactions are expected to take place preferentially on the chemically active defect sites. The heterogeneity nature of the ITO surface poses difficulties to a uniform electrodeposition of thin films on ITO surface,

The author's group has been working on the electrodeposition of semiconductors for many years, and has developed an electrochemical version of atomic layer deposition (E-ALD) [18-25]. Similar to gas phase atomic layer deposition, E-ALD takes advantage of surface-limited reaction to deposit one atomic layer at a time. The surface limited reaction in E-ALD is referred to as underpotential deposition (UPD), where one element deposits on a second element before it deposits on itself due to the free energy decrease associated with the surface compound formation[26-27]. Atomic layers of elements can be deposited on the substrate, and by alternating the elements exposed to the surface, bilayers of compound can be deposited uniformly to form

thin film semiconductors. UPD is observed with Cd and S on metal elements such as Au[28-29] and Ag[30-32], but not with oxides like ITO, since no single potential can realize the atomic deposition of elements on a surface with such variations.

Attempts of successive ionic layer adsorption and reaction (SILAR) have been done by the author to form CdS on ITO. However, every time CdTe was deposited onto the CdS/ITO, delamination of CdS/CdTe from the ITO substrate was observed. Figure 4.1 is the SEM showing the delamination of the CdS/CdTe layer. A possible explanation is that the weak adhesion between the SILAR-made CdS and the ITO substrate was not enough to overcome the stress exerted by the CdTe layer, causing buckling of the film. Other approaches to solve this problem must be explored.

Ever since the first paper[33] that provided direct evidence of the electrochemical polarization on the composition of Indium oxide was published, Electrochemical reduction of ITO has been studied under different pHs with different electrolytes[17, 34-42]. Most of the studies focus on the electrochemical stability of ITO, rather than surface modification. In 2014, Switzer et. al has successfully deposited Ge wires by reducing ITO to form In metal that acted as reduction sites for Ge (IV)[43]. This work has pointed to the direction that if In is used as the metallic nucleation site, UPD growth of Cd and S on ITO could be made possible. The In nucleation sites created by ITO reduction can provide starting points for CdS spherical layer-by-layer growth, without the need to step into bulk potential deposition regime. As the coverage grows, the film will coalesce and eventually cover the whole surface. The In atoms can also act as anchor points for better adhesion between the film and the substrate. However, according to Pourbaix diagram of Cd and In, metallic In is on the verge of being oxidized at the condition

where Cd can deposit. A more stable metal should be used to replace In as the nucleation site. The idea proposed in this study is that Cu^{2+} can be introduced to the system after ITO reduction to trigger the redox displacement reaction between Cu and In: $3\ Cu^{2+} + 2\ In \rightarrow 3\ Cu + 2\ In^{3+}$, and replace In as the nucleation site for CdS UPD growth. Moreover, doping in CdS thin film with metal such as Sn[44-45], Ga[46], Ag[47-48], Cu has been investigated. Literature reports that the use of Cu as a dopant of CdS allows for the reduction of CdS thickness from 70 nm to 30 nm, keeping the same high efficiency level[49]. An increase in transmittance with Cu-Doped CdS was reported[50]. Thus Cu can be chosen as a promising candidate for replacing In after ITO reduction.

Experimental

All potentials are reported vs. an Ag/AgCl (3 M KCl) reference electrode (Bioanalytical Systems, Inc). The ITO substrates (Delta Technologies) have Rs = 70-100 Ω/square, and were cleaned prior to use by three 15 min rounds of sonication in fresh aliquots of acetone and then three aliquots of Nanopure water. The Cd solution was pH 3, containing 0.5 mM $CdSO_4$ (Sigma-Aldrich) in 0.5 M $NaClO_4$. The sulfide solution was pH 10.5, containing 0.5 mM Na_2S (J.T.Baker) in 0.5 M $NaClO_4$. The Cu solution was pH 3, containing 0.5 mM $CuSO_4$ (Baker Analyzed, 99.8%) in 0.5 M $NaClO_4$. The acidic and basic blank rinse solution was 0.5 M $NaClO_4$ with pH 3 and 10.5, respectively. All solutions were made using 18 MΩ nanopure water filtered through Millipore Advantage 10.

All electrochemistry was carried out in a flow cell system (Electrochemical ALD, L.C., Athens, GA) consisting of a distributing valve, a flow cell, a pump, and a potentiostat. The whole system was automated by an in-house written LabVIEW-based program named Sequencer. The auxiliary used was an Au wire embedded in the cell wall facing the ITO working electrode. The

exposed electrode area was 2.1 cm^2. The flow rate for CdS deposition was kept at 11 mL/min for the entire process. The flow rate for ITO treatment and all cyclic voltammetry (CV) was kept 2 mL/min. CVs were performed at a scan rate of 10 mV/s. All solutions were purged with N_2 prior to and during the experiment.

Scanning electron microscopy and energy dispersive X-ray spectroscopy (SEM-EDX) was performed on an FEI Teneo SEM (FEI, Hillsboro, OR) with an acceleration voltage of 10 keV.

Results and Discussion

Figure 4.2 depicts the window opening of ITO in acidic blank from OCP scanning negative. No sign of reduction was observed when the potential was reversed at -800 mV. When the negative limit was pushed to -900 mV (Figure 4.2 inset), in the reverse scan a small oxidation peak was observed at -650 mV that corresponded to In re-oxidation. But because of the existence of hydrogen evolution reaction (HER), the total current was still in the reduction territory. As the negative limit was pushed to -1000 mV, an obvious In re-oxidation peak showed up at -570 mV, a slight positive shift from the peak in the purple curve, due to the higher amount of In metal formed. No reduction and re-oxidation peak of Sn was observed, which is consistent with the literature[36]. This could be explained by the passivation of SnO_2 and the difficulty for its reduction. Since the purpose of this study was the surface modification of ITO rather than altering the nature of the oxide, a minimum reduction potential was desired, thus -900 mV was chosen as the potential for ITO reduction.

Figure 4.3 is the anodic scan of ITO after being reduced at -900 mV for 10 s, 30 s, 90 s to correlate the amount of In metal created with the time stayed at -900 mV. The oxidation current

increased as the reduction time increased. The oxidation charge was plotted against the reduction time (Figure 3 inset) and a linear relationship was observed, suggesting the amount of In metal formed can be controlled by varying the reducing time at -900 mV.

To study the effect of reduction on surface morphology, SEM images were taken of the reduced ITOs. Figure 4.4 is the SEM of 3 pieces of ITO reduced at -900 mV for 60 s, 90 s, and 180 s, compared with the untreated ITO. An increase in the number of pits and clusters was observed as the reduction time increased. The clusters were identified using EDX to be high in In percentage compared with the background. The In clusters appeared to form right next to the pits. A possible explanation is that the reduction started at the grain boundaries[35, 42, 51], where In^{3+} was slowly dissolved from the ITO lattice, creating valleys in the surface. The reduced In aggregated in to In metal droplets and resided next to the valleys created by reduction. The resulting In clusters were found to be not stable and would eventually dissolve away if left in the blank. Figure 4.5 is the comparison of (a) ITO reduced at -900 mV for 90 s and taken out right away with (b) ITO reduced at -900 mV for 90 s and leaving in blank solution for 5 min. As can be seen from image (b) the In clusters had already dissolved away, leaving only pits on the surface.

To overcome the poor stability issue of the In nucleation sites, a more stable metal Cu was utilized to replace the In metal as the nucleus. The Cu was introduced into the surface as Cu^{2+} at open circuit, a redox displacement reaction occurred that reduced the Cu^{2+} to Cu, taken the place of In as nucleation sites.

To quantify the amount of Cu metal on ITO after the displacement reaction, CV was done to strip off the Cu. Figure 4.6 is the stripping of Cu after 5 min of redox replacement with In

created by 90 s of ITO reduction at -900 mV. The scan started from OCP at ca. 10 mV, and immediately an oxidation current was observed peaking at 100 mV that corresponded to bulk Cu stripping. The current stabilized at a low level yet still above 0 when potential was scanned positive of 200 mV. This current is interesting because it implied the existence of a more stable form of Cu on the surface. The effect of Cu on the interface between ITO and CdS is still unclear. The existence of a more stable form of Cu suggests that the majority of the Cu can be stripped off by scanning positive to 200 mV, leaving only a minimum amount as the nucleation sites.

To visualize if this treatment can increase the nucleation sites on ITO, 90 s of Cd deposition was applied at -800 mV, which is the onset potential for Cd bulk formation. The reason why bulk potential was chosen rather than UPD potentials is that UPD is self-terminating after one atomic layer, making it impossible to resolve under the microscope. Figure 4.7 is the SEM of (a) ITO reduced at -900 mV for 90 s followed by 5 min of Cu^{2+} redox displacement at OCP, (b) same treatment with (a) plus scanning anodically to 200 mV to strip off bulk Cu, (d) same treatment with (b) plus 90 s of Cd deposition at -800 mV, whereas (c) is 90 s of Cd deposition at -800 mV on untreated ITO. The comparison between (a) and (b) suggests that most of the metallic Cu has been stripped, leaving only a minimum amount on the surface as nucleation anchor sites. In (c), large and sparse Cd clusters can be seen whereas in (d) the Cd particles are smaller and much denser in population. In a 3x3 μm^2 area, the number of clusters in (c) were counted to be less than 10% of the ones in the same area in (d) (33 versus 424), which indicated the treatment had significantly increased the number of nucleation sites for Cd deposited under equivalent conditions.

As described above, the pretreatment of ITO substrate includes 90 s of ITO reduction at -900 mV, followed by 5 min of $CuSO_4$ solution exposure at open circuit, and end with an anodic scan in $CuSO_4$ from the OCP to 200 mV. This leaves the surface with a minimum yet essential Cu nucleation sites for CdS electrodeposition. A CdS thin film was deposited on the Cu-treated ITO substrate. Figure 4.8 is an illustration of one complete cycle. The black straight lines and red curves describe the potential on the left axis and current on the right axis, respectively. The solution in the cell corresponding to each step is marked in green. Each potential change was 2 seconds behind the solution change to give time for the solution to reach the cell from the distribution valve so that the solution change and potential change was synced.

Figure 4.9 is the SEM of (a) 50 cycles of CdS deposited on a Cu-treated ITO using the method described above, compared with 50 cycles of CdS deposited on ITO reduced at -900 for 90 s without any Cu displacement. The whole surface of deposit (a) was covered, with the top layer being round uniform CdS particles, whereas in (b) most of the area is exposed ITO surface with a low deposit coverage density, suggesting the Cu displacement step is essential in increasing the nucleation sites. To shed more light into the growth process, images of (c) 5 cycles, (d) 15 cycles and (e) 25 cycles of CdS deposited on the Cu-treated ITO was taken. As can be seen from the images, the initial stage of growth (c) started at the right next to the valleys, where the nucleation sites created by reduction were formed, indicating the metal particles were the preferred nucleation sites for CdS growth. As the deposit started to grow, nucleation sites in the smooth area started to form. In image (e) not only did the deposit form on almost all the nucleation sites next to the valleys, but also on the planer smooth areas, suggesting a progressive growth. The Cd/S atomic ratio was determined by EDX to be 0.7, consistent with the S-deficient n-type CdS.

To see if this treatment improved the film adhesion to the substrate, CdTe was electrodeposited onto the CdS/Cu-ITO in the same fashion as the ones that delaminated from untreated ITO. On the CdTe/CdS/Cu-ITO structure, no film delamination was observed. Even when the thickness of CdTe quadrupled, both CdTe and CdS stayed on the substrate nicely, proving that the metal nucleation sites did act as anchor points and created a strong binding between the film and the substrate.

Conclusion

By reducing a small amount of ITO to In and allowing Cu^{2+} to exchange with the In, ITO with tiny Cu particles on the surface were made and used as substrate for CdS electrodeposition. This treatment of the ITO surface has proven to increase the nucleation density for electrodeposition, and promoted better adhesion between the film and the substrate. Future studies should be done on how and to what degree the ITO reduction would affect the photovoltaic performance, as well as the role of the Cu between the CdS and ITO interface.

Acknowledgements

Support from the National Science Foundation, DMR 1410109, is gratefully acknowledged. Thanks are extended to the Georgia Electron Microscopy for use of their SEM.

References

1. Kröger, F. A., Cathodic Deposition and Characterization of Metallic or Semiconducting Binary Alloys or Compounds. *J. Electrochem. Soc.* **1978,** *125* (12), 2028-2034.

2. Sella, C.; Boncorps, P.; Vedel, J., The electrodeposition mechanism of CdTe from acidic aqueous solutions. *J. Electrochem. Soc.* **1986,** *133* (10), 2043-2047.

3. Barker, J.; Binns, S.; Johnson, D.; Marshall, R.; Oktik, S.; Özsan, M.; Patterson, M.; Ransome, S.; Roberts, S.; Sadeghi, M., Electrodeposited CdTe for thin film solar cells. *International journal of solar energy* **1992,** *12* (1-4), 79-94.

4. Diso, D.; Fauzi, F.; Echendu, O.; Olusola, O.; Dharmadasa, I., Optimisation of CdTe electrodeposition voltage for development of CdS/CdTe solar cells. *Journal of Materials Science: Materials in Electronics* **2016,** *27* (12), 12464-12472.

5. Saji, V. S.; Choi, I.-H.; Lee, C.-W., Progress in electrodeposited absorber layer for CuIn (1− x) GaxSe 2 (CIGS) solar cells. *Sol. Energy* **2011,** *85* (11), 2666-2678.

6. Calixto, M.; Sebastian, P.; Bhattacharya, R.; Noufi, R., Compositional and optoelectronic properties of CIS and CIGS thin films formed by electrodeposition. *Solar energy materials and solar cells* **1999,** *59* (1), 75-84.

7. Bhattacharya, R. N.; Oh, M.-K.; Kim, Y., CIGS-based solar cells prepared from electrodeposited precursor films. *Solar Energy Materials and Solar Cells* **2012,** *98*, 198-202.

8. Lincot, D.; Guillemoles, J.-F.; Taunier, S.; Guimard, D.; Sicx-Kurdi, J.; Chaumont, A.; Roussel, O.; Ramdani, O.; Hubert, C.; Fauvarque, J., Chalcopyrite thin film solar cells by electrodeposition. *Sol. Energy* **2004,** *77* (6), 725-737.

9. Pawar, S.; Pawar, B.; Moholkar, A.; Choi, D.; Yun, J.; Moon, J.; Kolekar, S.; Kim, J., Single step electrosynthesis of Cu 2 ZnSnS 4 (CZTS) thin films for solar cell application. *Electrochimica Acta* **2010,** *55* (12), 4057-4061.

10. Ahmed, S.; Reuter, K. B.; Gunawan, O.; Guo, L.; Romankiw, L. T.; Deligianni, H., A high efficiency electrodeposited Cu2ZnSnS4 solar cell. *Advanced Energy Materials* **2012,** *2* (2), 253-259.

11. Scragg, J. J.; Dale, P.; Peter, L. M., Synthesis and characterization of Cu 2 ZnSnS 4 absorber layers by an electrodeposition-annealing route. *Thin Solid Films* **2009,** *517* (7), 2481-2484.

12. Gurav, K.; Yun, J.; Pawar, S.; Shin, S.; Suryawanshi, M.; Kim, Y.; Agawane, G.; Patil, P.; Kim, J., Pulsed electrodeposited CZTS thin films: Effect of duty cycle. *Materials Letters* **2013,** *108*, 316-319.

13. Lokhande, C.; Pawar, S., Electrodeposition of thin film semiconductors. *physica status solidi (a)* **1989,** *111* (1), 17-40.

14. Nakamura, K.; Gotoh, M.; Fujihara, T.; Toyama, T.; Okamoto, H., Influence of CdS window layer on 2-μm thick CdS/CdTe thin film solar cells. *Solar Energy Materials and Solar Cells* **2003,** *75* (1), 185-192.

15. Kim, H.; Gilmore, C.; Pique, A.; Horwitz, J.; Mattoussi, H.; Murata, H.; Kafafi, Z.; Chrisey, D., Electrical, optical, and structural properties of indium–tin–oxide thin films for organic light-emitting devices. *Journal of Applied Physics* **1999,** *86* (11), 6451-6461.

16. Donley, C.; Dunphy, D.; Paine, D.; Carter, C.; Nebesny, K.; Lee, P.; Alloway, D.; Armstrong, N. R., Characterization of Indium−Tin Oxide Interfaces Using X-ray Photoelectron

Spectroscopy and Redox Processes of a Chemisorbed Probe Molecule: Effect of Surface Pretreatment Conditions. *Langmuir* **2002,** *18* (2), 450-457.

17. Bejitual, T. S.; Ramji, K.; Kessman, A. J.; Sierros, K. A.; Cairns, D. R., Corrosion of an amorphous indium tin oxide film on polyethylene terephthalate at low concentrations of acrylic acid. *Materials Chemistry and Physics* **2012,** *132* (2–3), 395-401.

18. Gregory, B. W.; Stickney, J. L., Electrochemical atomic layer epitaxy (ECALE). *Journal of electroanalytical chemistry and interfacial electrochemistry* **1991,** *300* (1-2), 543-561.

19. Tsang, C. F.; Ledina, M. A.; Stickney, J. L., Molybdenum diselenide formation using electrochemical atomic layer deposition (E-ALD). *J Electroanal Chem* **2017**.

20. Perdue, B.; Czerniawski, J.; Anthony, J.; Stickney, J., Optimization of Te Solution Chemistry in the Electrochemical Atomic Layer Deposition Growth of CdTe. *J. Electrochem. Soc.* **2014,** *161* (7), D3087-D3092.

21. Banga, D.; Perdue, B.; Stickney, J., Formation of CuIn(1-x)GaxSe2 (CIGS) by Electrochemical Atomic Layer Deposition (ALD). *J. Electrochem. Soc.* **2014,** *161* (4), D141-D146.

22. Thambidurai, C.; Kim, Y. G.; Jayaraju, N.; Venkatasamy, V.; Stickney, J. L., Copper Nanofilm Formation by Electrochemical ALD. *J. Electrochem. Soc.* **2009,** *156* (8), D261-D268.

23. Venkatasamy, V.; Stickney, J. L., Formation of HgCdTe by Electrochemical Atomic Layer Epitaxy (EC-ALE). *ECS Transactions* **2006,** *3* (accepted).

24. Venkatasamy, V.; Jayaraju, N.; Thambidurai, C.; Cox, C.; Happek, U.; Stickney, J. L., Optimization studies of CdTe nanofilm formation by electrochemical atomic layer epitaxy (EC-ALE). *J. Appl. Electrochem.* **2006,** *36*, 1223.

25. Mathe, M. K.; Cox, S. M.; Flowers, B. H.; Vaidyanathan, R.; Pham, L.; Srisook, N.; Happek, U.; Stickney, J. L., Deposition of CdSe by EC-ALE. *Journal of Crystal Growth* **2004,** *271* (1-2), 55-64.

26. Gregory, B. W.; Norton, M. L.; Stickney, J. L., Thin-layer electrochemical studies of the underpotential deposition of cadmium and tellurium on polycrystalline Au, Pt and Cu electrodes. *J Electroanal Chem* **1990,** *293* (1-2), 85-101.

27. Gregory, B. W.; Stickney, J. L., Electrochemical atomic layer epitaxy (ECALE). *J Electroanal Chem* **1991,** *300* (1-2), 543-561.

28. Colletti, L. P.; Flowers, B. H.; Stickney, J. L., Formation of thin films of CdTe, CdSe, and CdS by electrochemical atomic layer epitaxy. *J. Electrochem. Soc.* **1998,** *145* (5), 1442-1449.

29. Lay, M. D.; Varazo, K.; Stickney, J. L., Formation of Sulfur Atomic Layers on Gold from Aqueous Solutions of Sulfide and Thiosulfate: Studies Using EC-STM, UHV-EC, and TLEC. *Langmuir* **2003,** *19* (20), 8416-8427.

30. Foresti, M. L.; Milani, S.; Loglio, F.; Innocenti, M.; Pezzatini, G.; Cattarin, S., Ternary CdSxSe1-x deposited on Ag(111) by ECALE. Synthesis and characterization. *Langmuir* **2005,** *21* (15), 6900-6907.

31. Foresti, M. L.; Pezzatini, G.; Cavallini, M.; Aloisi, G.; Innocenti, M.; Guidelli, R., Electrochemical atomic layer epitaxy deposition of CdS on Ag (111): An electrochemical and STM investigation. *J. Phys. Chem. B* **1998,** *102* (38), 7413-7420.

32. Forni, F.; Innocenti, M.; Pezzatini, G.; Foresti, M. L., Electrochemical aspects of CdTe growth on the face of (111) of silver by EC-ALE. *Electrochemica Acta* **2000,** *45* (20), 3225-3231.

33. Armstrong, N. R.; Lin, A. W.; Fujihira, M.; Kuwana, T., Electrochemical and surface characteristics of tin oxide and indium oxide electrodes. *Analytical Chemistry* **1976,** *48* (4), 741-750.

34. Senthilkumar, M.; Mathiyarasu, J.; Joseph, J.; Phani, K. L. N.; Yegnaraman, V., Electrochemical instability of indium tin oxide (ITO) glass in acidic pH range during cathodic polarization. *Materials Chemistry and Physics* **2008,** *108* (2–3), 403-407.

35. Gao, W.; Cao, S.; Yang, Y.; Wang, H.; Li, J.; Jiang, Y., Electrochemical impedance spectroscopy investigation on indium tin oxide films under cathodic polarization in NaOH solution. *Thin Solid Films* **2012,** *520* (23), 6916-6921.

36. Liu, L.; Yellinek, S.; Valdinger, I.; Donval, A.; Mandler, D., Important Implications of the Electrochemical Reduction of ITO. *Electrochimica Acta* **2015,** *176*, 1374-1381.

37. Spada, E. R.; de Paula, F. R.; Plá Cid, C. C.; Candiotto, G.; Faria, R. M.; Sartorelli, M. L., Role of acidic and basic electrolytes on the structure and morphology of cathodically reduced indium tin oxide (ITO) substrates. *Electrochimica Acta* **2013,** *108*, 520-524.

38. Bouden, S.; Dahi, A.; Hauquier, F.; Randriamahazaka, H.; Ghilane, J., Multifunctional Indium Tin Oxide Electrode Generated by Unusual Surface Modification. *Scientific Reports* **2016,** *6*.

39. Matveeva, E., Electrochemistry of the Indium-Tin Oxide Electrode in 1 M NaOH Electrolyte. *J. Electrochem. Soc.* **2005,** *152* (9), H138-H145.

40. Huang, C. A.; Li, K. C.; Tu, G. C.; Wang, W. S., The electrochemical behavior of tin-doped indium oxide during reduction in 0.3 M hydrochloric acid. *Electrochimica Acta* **2003,** *48* (24), 3599-3605.

41. van den Meerakker, J. E. A. M.; Baarslag, P. C.; Scholten, M., On the Mechanism of ITO Etching in Halogen Acids: The Influence of Oxidizing Agents. *J. Electrochem. Soc.* **1995,** *142* (7), 2321-2325.

42. Huang, C.; Li, K.; Tu, G.; Wang, W., The electrochemical behavior of tin-doped indium oxide during reduction in 0.3 M hydrochloric acid. *Electrochimica Acta* **2003,** *48* (24), 3599-3605.

43. Mahenderkar, N. K.; Liu, Y.-C.; Koza, J. A.; Switzer, J. A., Electrodeposited Germanium Nanowires. *ACS Nano* **2014,** *8* (9), 9524-9530.

44. Roy, P.; Srivastava, S. K., In situ deposition of Sn-doped CdS thin films by chemical bath deposition and their characterization. *Journal of Physics D: Applied Physics* **2006,** *39* (22), 4771.

45. Jafari, A.; Zakaria, A.; Rizwan, Z.; Ghazali, M. S. M., Effect of low concentration Sn doping on optical properties of CdS films grown by CBD technique. *International journal of molecular sciences* **2011,** *12* (9), 6320-6328.

46. Khallaf, H.; Chai, G.; Lupan, O.; Chow, L.; Park, S.; Schulte, A., Characterization of gallium-doped CdS thin films grown by chemical bath deposition. *Applied surface science* **2009,** *255* (7), 4129-4134.

47. Shah, N.; Nazir, A.; Mahmood, W.; Syed, W.; Butt, S.; Ali, Z.; Maqsood, A., Physical properties and characterization of Ag doped CdS thin films. *Journal of Alloys and Compounds* **2012,** *512* (1), 27-32.

48. Ristova, M.; Ristov, M., Silver-doped CdS films for PV application. *Solar energy materials and solar cells* **1998,** *53* (1), 95-102.

49. Sánchez, Y.; Espíndola-Rodríguez, M.; Xie, H.; López-Marino, S.; Neuschitzer, M.; Giraldo, S.; Dimitrievska, M.; Placidi, M.; Izquierdo-Roca, V.; Pulgarín-Agudelo, F. A.; Vigil-

Galán, O.; Saucedo, E., Ultra-thin CdS for highly performing chalcogenides thin film based solar cells. *Solar Energy Materials and Solar Cells* **2016,** *158*, 138-146.

50. Shah, N. A.; Sagar, R. R.; Mahmood, W.; Syed, W. A. A., Cu-doping effects on the physical properties of cadmium sulfide thin films. *Journal of Alloys and Compounds* **2012,** *512* (1), 185-189.

51. Choi, J.-H.; Kim, S.-O.; Hilton, D. L.; Cho, N.-J., Acid-catalyzed kinetics of indium tin oxide etching. *Thin Solid Films* **2014,** *565*, 179-185.

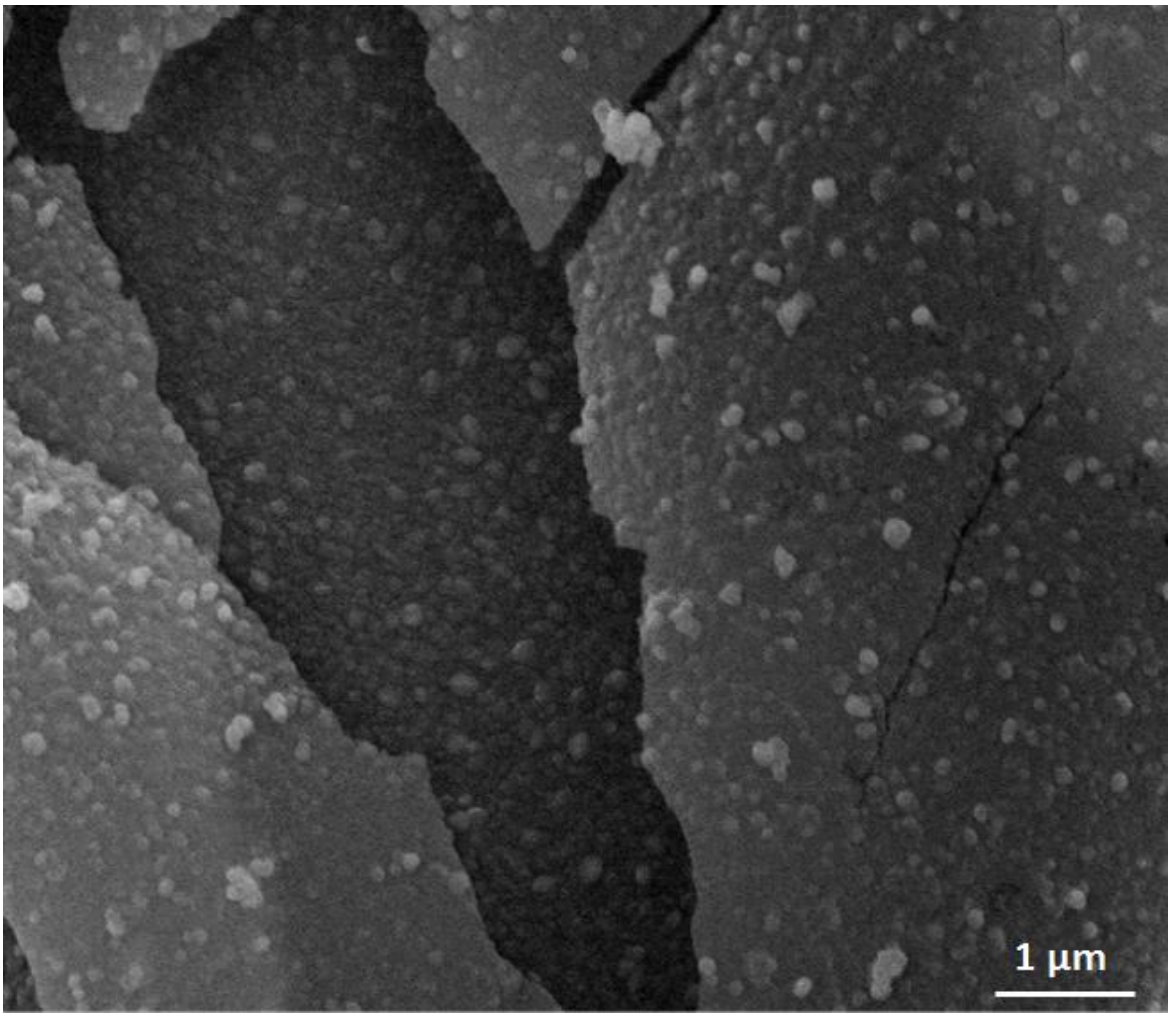

Figure 4.1: SEM of CdTe/CdS delaminated from the ITO surface.

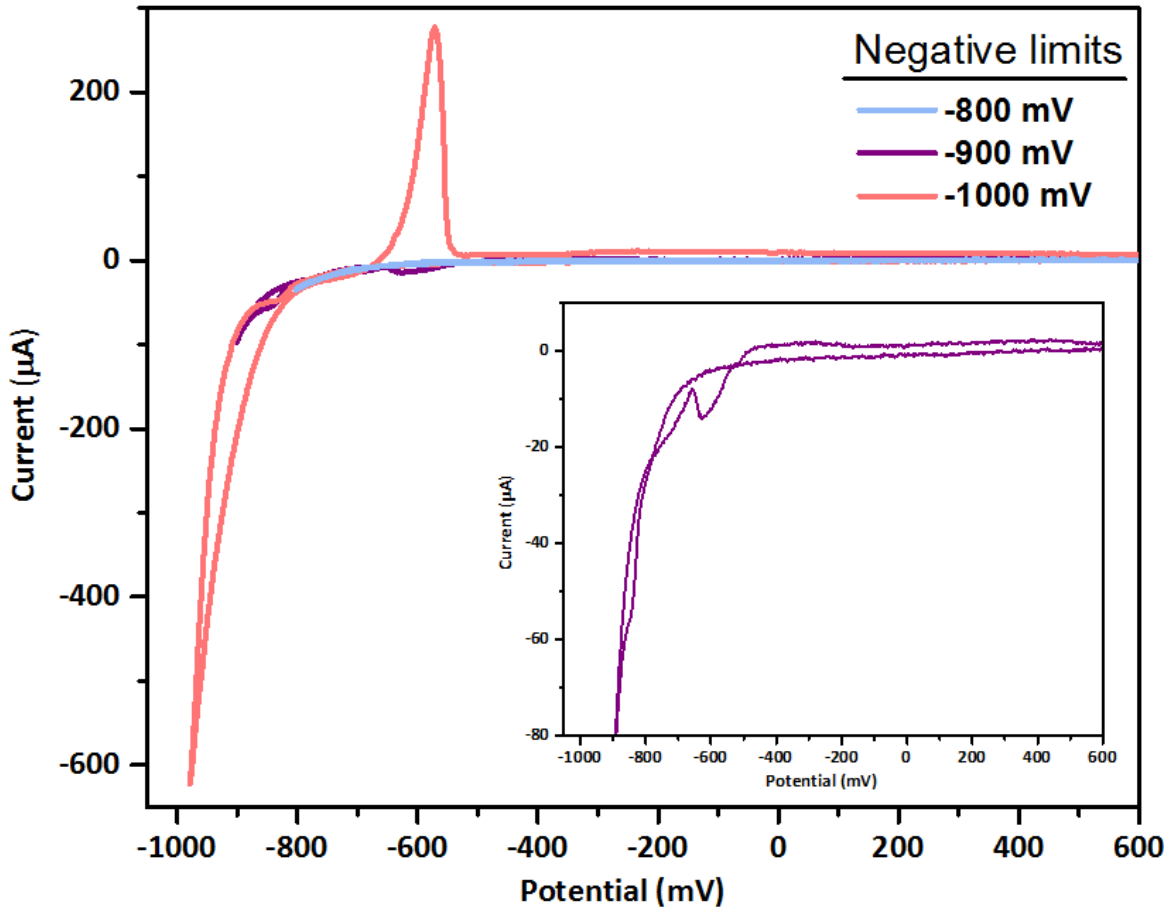

Figure 4.2: Window-opening of ITO in pH 3 blank solution. Potentials were reversed at -800 mV (blue), -900 mV (purple), and -1000 mV (red). The inset is the zoomed-in of the purple scan. Potential was measured versus the Ag/AgCl reference electrode with a scan rate of 10 mV/s

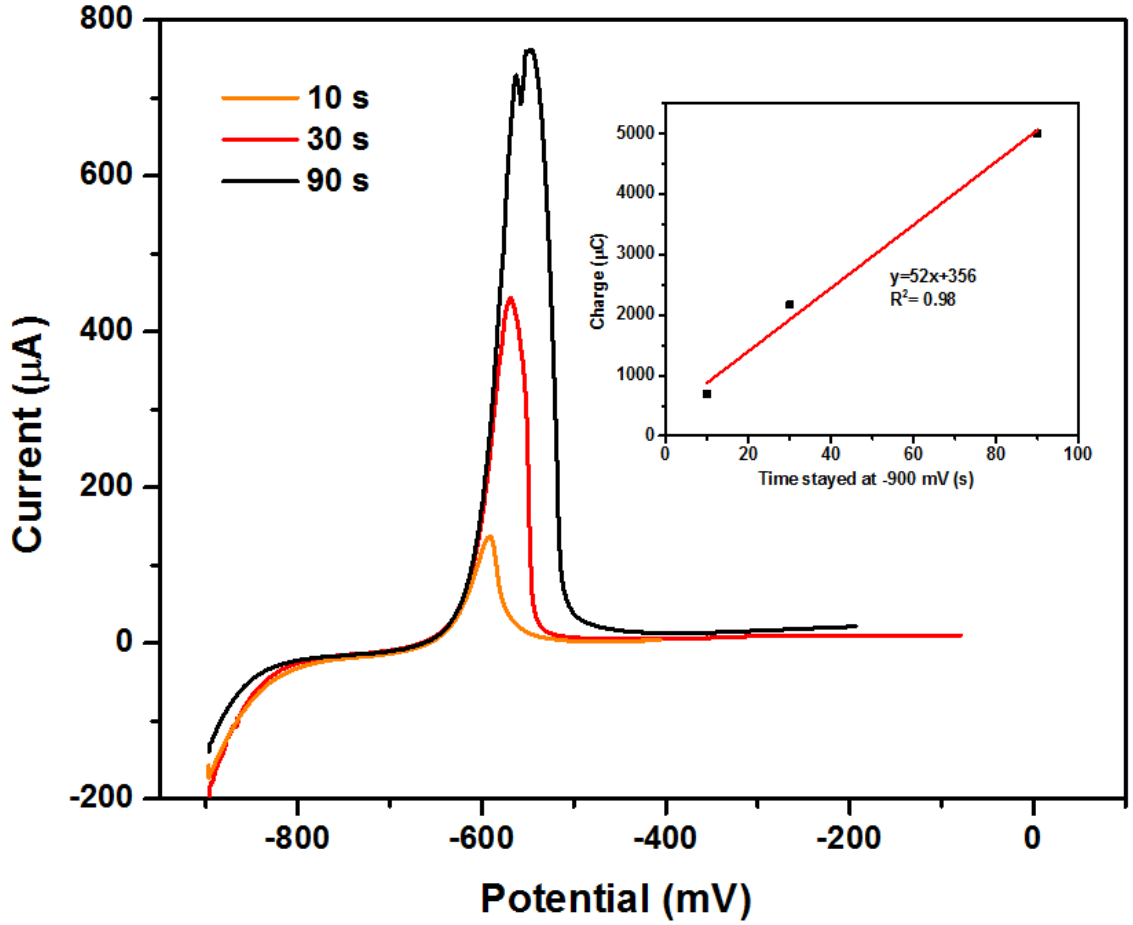

Figure 4.3: Cyclic voltammogram of the anodic scan after ITO was reduced at -900 mV for 10 s (orange), 30 s (red), and 90 s (black). The inset is the linear fit of the oxidation charge versus the reduction time. Potential was measured versus the Ag/AgCl reference electrode with a scan rate of 10 mV/s.

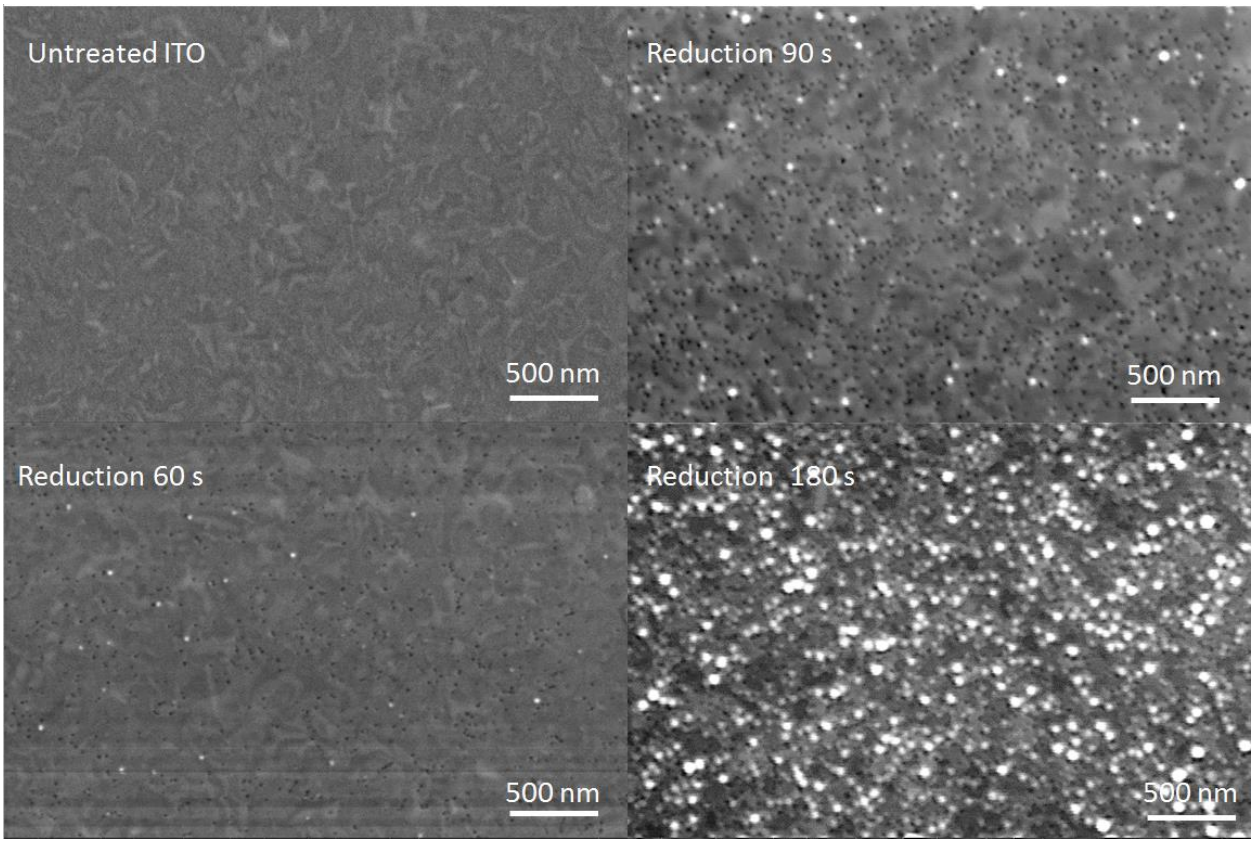

Figure 4.4: SEM of untreated ITO, compared with ITO reduced at -900 mV for 60 s, 90 s, and 180s. The acceleration voltage used was 10 kV.

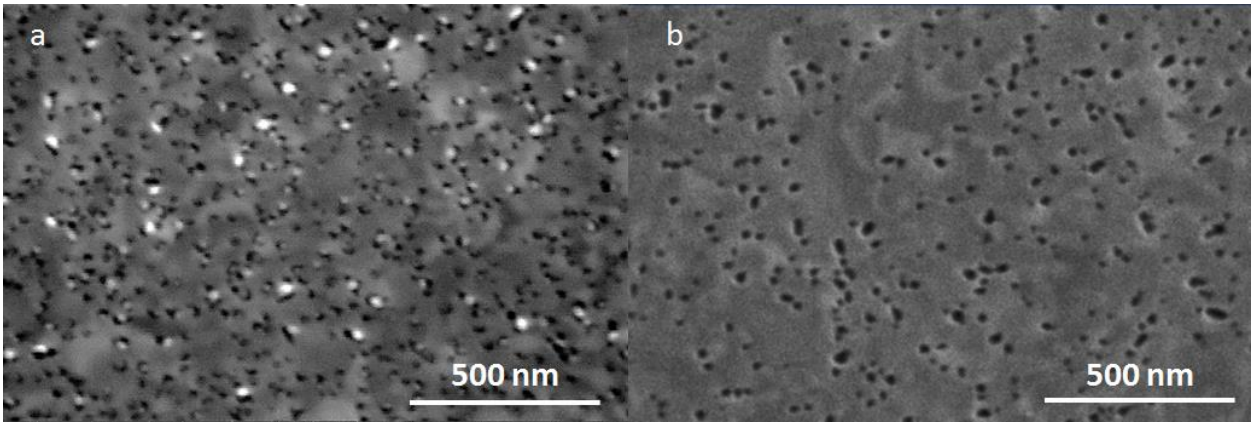

Figure 4.5: SEM of (a) ITO reduced at -900 mV for 90 s and taken out right away, (b) ITO reduced at -900 mV for 90 s and leaving in blank solution for 5 min.

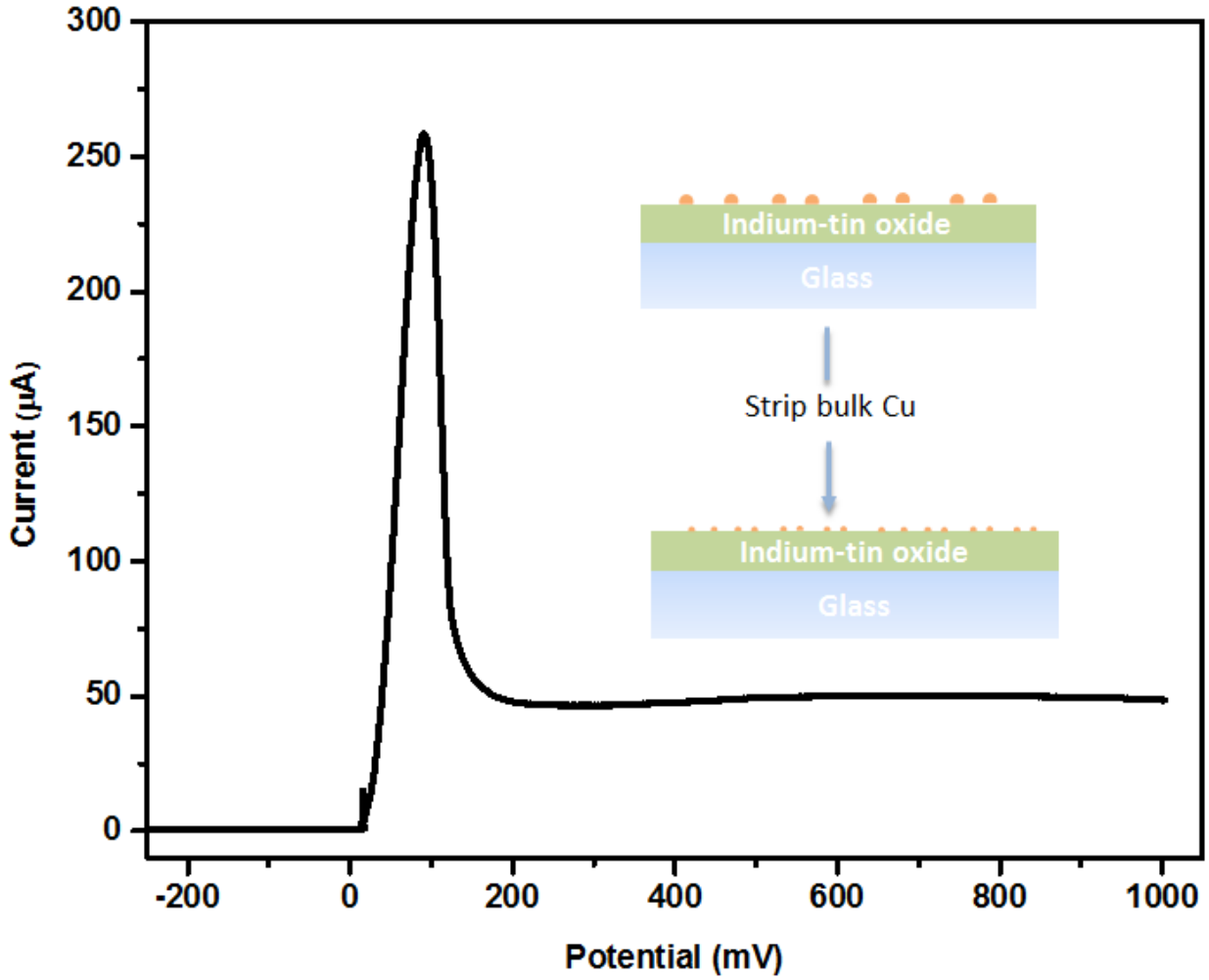

Figure 4.6: Stripping of Cu from OCP after 5 min of redox replacement with In created by 90 s of ITO reduction at -900 mV. The cartoon is the illustration of stripping bulk Cu by scanning to 200 mV, thus removing extra Cu, exposing smaller nucleation sites.

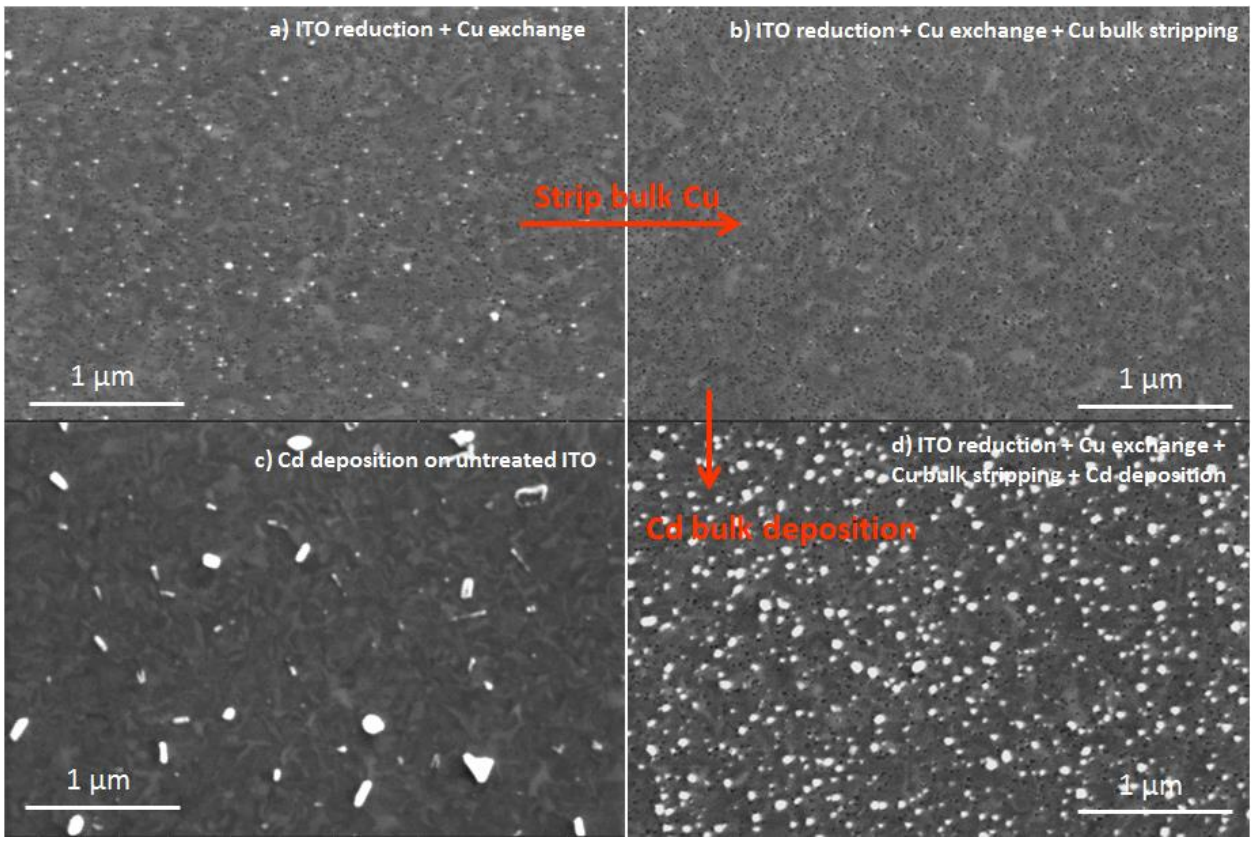

Figure 4.7: SEM of (a) ITO reduced at -900 mV for 90 s followed by 5 min of Cu^{2+} redox displacement at OCP, (b) same treatment with (a) plus scanning anodically to 200 mV to strip off bulk Cu, (d) same treatment with (b) plus 90 s of Cd deposition at -800 mV. (c) 90 s of Cd deposition at -800 mV on untreated ITO.

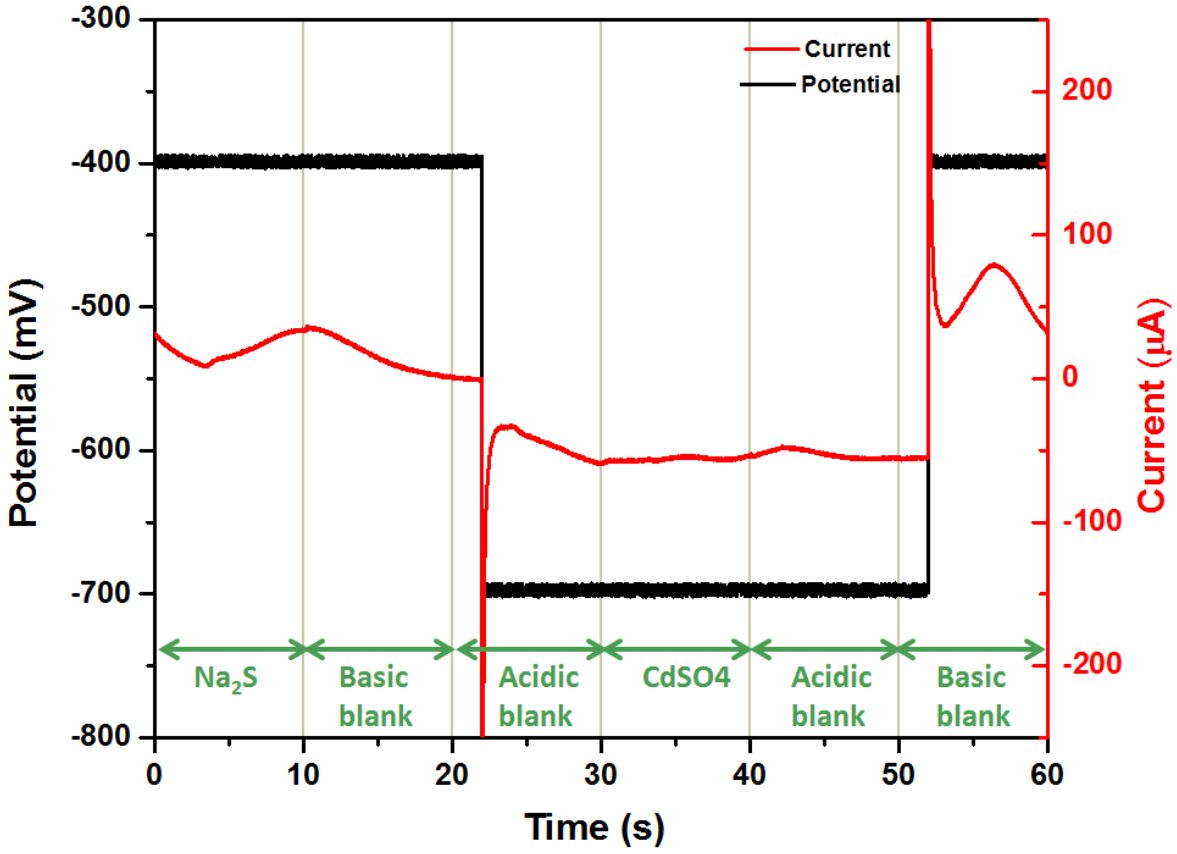

Figure 4.8: Potential-current-time trace of one complete CdS E-ALD cycle. The straight black lines represent the programmed potential, and the red curves are the corresponding current. The solution in the cell corresponding to each step is marked in green.

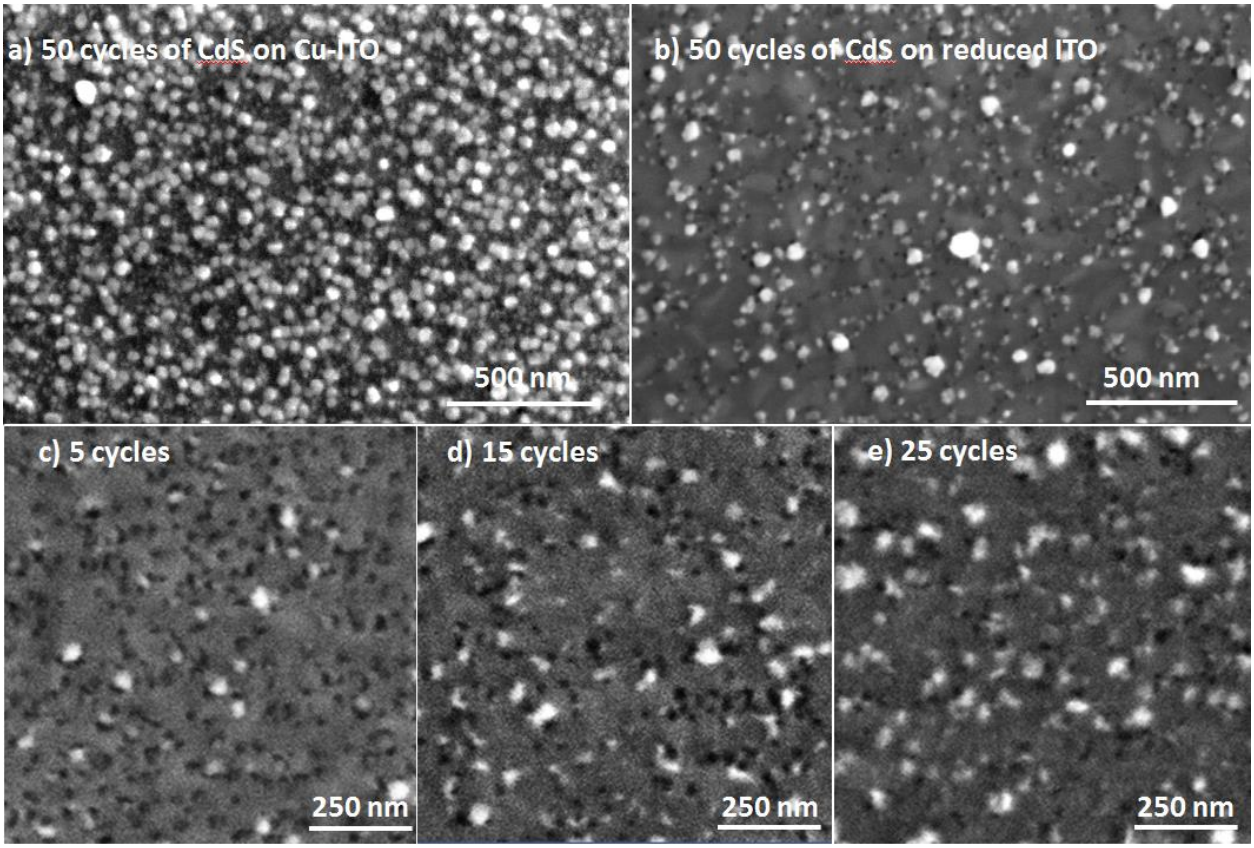

Figure 4.9: SEM of (a) 50 cycles of CdS deposited on a Cu-treated ITO, (b) 50 cycles of CdS deposited on ITO reduced at -900 for 90 s without any Cu displacement.

CHAPTER 5

PRELIMINARY STUDIES OF THE FORMATION OF A PHOTOVOLTAIC (PV) USING ELECTRODEPOSITION[4]

[4]S. Shen, X. Zhang, B. Perdue, J. Stickney, To be submitted to *Journal of the electrochemical society*

Abstract

CdTe/CdS p-n junctions in both substrate and superstrate configurations were made. In the substrate configuration, CdTe was first deposited onto Au substrates using 15 minutes of codeposition at -700 mV, followed by electrochemical atomic layer deposition (E-ALD) of CdS on CdTe/Au. In the superstrate configuration, the ITO substrate was first patterned with 1x1 mm^2 squares using photolithography, and then treated with electrochemical methods to form Cu nucleation sites on the ITO surface. CdS E-ALD was then performed on the treated ITO substrate. CdTe thin films were deposited onto CdS/ITO using pulse plating atomic layer deposition (PP-ALD). A layer of Au was deposited electrochemically on CdTe/CdS/ITO as the back contact. Photoelectrochemical measurements on the substrate configuration showed good p-type response and clean dark current. XRD showed CdTe zinc blend <111> and CdS zinc blend <111> structure. SEM images of the CdTe/CdS/ITO showed compact deposits covering the whole surface. Work on collecting more information on cell performance is on the way.

Introduction

With the energy crisis the world is faced with today, researcher all over the world are looking for renewable alternative energy sources, and solar energy is the most promising solution to solving our energy shortage problem for the future. Solar photovoltaic industry is one of the fastest growing businesses in the world, with a compound annual growth rate over 40%.[2]

Photovoltaic describes a group of device that converts solar energy to electricity. It usually consists of an electron-rich n-type semiconductor and a hole- rich p-type semiconductor. It was first observed by Alexandre-Edmund Becquerel in 1893 that "electrical current arose from certain light induced chemical reactions"[3]. The real development of photovoltaics started in the

late 1940s when the first solid state device was developed with an efficiency of 6%[3]. A typical photovoltaic device usually consists of an electron-rich n-type semiconductor and a hole-rich p-type semiconductor. When the semiconductors are brought together and in contact with each other, the electrons in the n-type semiconductor are going to diffuse across the semiconductor interface and the same situation will occur for the hole in the p-type semiconductor. As the electrons and hole diffuse and neutralize, the fixed ion cores left behind at the interface is going to set up an electric field called the depletion region. When the equilibrium is re-established, a p-n junction is formed, and the Fermi levels of the two semiconductors are going to align, causing bending of the valence band and the conduction band. This band bending sets up a potential barrier. When the p-n junction is illuminated by light, energy from photons is going to be absorbed, exciting the electrons, and electron-hole pairs are generated. Because of the potential barrier, the electrons and holes can only go a certain direction, and this movement of electrons and holes creates current. Only photons with energy higher than the bandgap will be absorbed.

The first generation solar cells are based on Si wafers, including both Sin single crystals and bulk polycrystalline Si wafers[4-10]. In today's solar cell market, 80-90% of the technology is dominated by silicon-based materials[11]. As an indirect bandgap material, in order for an electron to absorb a photon to be excited to the conduction band, the assistance of a phonon needed. This has led to the low absorption coefficient of Si wafers, which require the material thickness to be a few hundred um to absorb most of the incident light. In the last 10 years, the efficiency of average commercial wafer-based silicon modules increased from about 12 % to 17 %[12]. High-efficiency research Si solar cells have advantages in performance but are often unsuitable for low-cost production due to their complex structures and the lengthy manufacturing process required for fabrication[10]. Efforts have been made to reduce the thickness of Si wafers in order to

reduce Si consumption[13-14], but the reduction in process yield caused by problems such as crack propagation comes along. Material usage for silicon cells has been reduced significantly during the last 10 years from around 16 g/Wp to less than 6 g/Wp due to increased efficiencies and thinner wafers[2]. The high manufacturing cost associated with the large amount of materials needed is the major factor hindering the development of Si solar cells.

To reduce the cost and achieve high efficiency, researchers have developed 2nd generation of solar cells that are based on thin film materials such as CdTe[15-20], CZTS[21-29], CIGS[30-35], etc. These semiconductors are possible candidates for solar cells because they have bandgaps near the optimal 1.5 eV and have theoretical efficiency limit of 30%[36-37]. The cost of thin solar cell can be kept relatively low by the use of inexpensive substrates, effective use of raw materials, high throughput and large area deposition at low temperatures[38]. In 2015, the market share of all thin film technologies amounted to about 8 % of the total annual production[2]. In structure of a typical thin film solar cell, the p-type absorber material is usually partnered with the n-type semiconductor CdS to form a p-n junction. The light comes in from the front transparent conducting oxide (TCO) and passes through semi-transparent CdS layer and eventually be absorbed by the p-type absorber layer. Electron-hole pairs are generated at the p-n junction and are conducted out to the external circuit by the back contact.

CdTe is one of the most prevailing absorber material used in thin film solar cells. It was introduced as first as CdTe/CdS cell in 1972 by Bonnet and Rabenhorst with an efficiency of 6%[40]. CdTe has a large absorption coefficient ($>1x10^4$ cm^{-1})[41-42], and only a few micron is sufficient to absorb 90% of the light with energy above CdTe's bandgap (1.4 eV). The reduced thickness gives rise to an intense electric field, which facilitates carrier generation and collection.

Cadmium telluride is the only stable Cd–Te compound in the Cd–Te phase diagram, and this lead to the relatively simple fabrication of near stoichiometric CdTe films with various deposition technologies. On the other hand, the occurrence of native defects renders the precise control of the doping density difficult.

Another critical component of CdTe solar cell is CdS. CdS is the most widely used n-type material in thin film solar cell. The major function of CdS layer is to allow the maximum amount of light to pass through and to form p-n junction with the absorber layer. For high optical throughput, an ideal candidate for the n-type material should have a bandgap as high as possible and thickness as low as possible thus to absorb the minimum amount of light and to maintain low series resistance. The CdS layer should also be compact so as to avoid shunts between the absorber and the front contact. CdS also facilitates the formation of large bandgap $CdTe_{1-x}S_x$ mixed crystal layer near the CdS-CdTe interface. When annealing at high temperature is needed, interdiffusion between CdS and CdTe takes place. In such cases the CdS layer should be thick enough so as not to be completely consumed.

A popular method for fabricating CdS thin film is chemical bath deposition (CBD), where the growth of CdS is realized by ion-by-ion condensation of Cd^{2+} and S^{2-} on the surface of the substrate. A Cd source in the form of a salt is dissolved in the solution and slowly releases Cd^{2+}. The S^{2-} in the solution generated by thiosulfate will precipitate with the Cd^{2+}, forming CdS on the substrate surface. The entire process can be done with a beaker on a hotplate. Thin, compact CdS thin films have been fabricated using chemical bath deposition.

Another low cost method for forming CdS thin film at ambient condition is electrodeposition. The film quality and composition can be controlled by varying the precursor

concentration, pH, deposition potential, and temperature. The problem of conventional electrodeposition is that bulk deposition usually results in rough surface morphology and limited control of thickness.

Electrochemical atomic layer deposition (E-ALD) was devoloped by this group and is the electrochemical equivalent of gas phase ALD. Similar to ALD, E-ALD uses surface limited reaction, which is referred to as underpotential deposition (UPD). UPD allows for atomically thick layers of materials to be deposited on a second material at a potential before the potential needed for the element to deposit on itself. In a typical E-ALD cycle, a solution containing the ionic form of the element of interest is introduced to the cell, and is deposited at a potential where only less than a monolayer of deposit should form. A monolayer is defined as one adsorbate atom per surface atom. After the reaction is completed, a blank solution is introduced to cell to rinse away any excess precursor ions, and a new solution containing the second element is introduced at its UPD and forms an atomic layer on the surface of the first element. After the reaction is completed, the solution is rinse away with a blank solution, and a bilayer of the compound of interest is formed on the substrate. This cycle can be repeated many times until the desired film thickness is reached. This method significantly increases the deposit morphology and prevents 3D growth, at the same time gives precise control of the deposit composition and thickness.

Another essential component in a CdS/CdTe is the front contact, which transmit light to the absorber layer. This layer is usually made with transparent conducting oxides (TCO). In the older cell no TCO was used, and CdS was used to draw the current laterally to the contact. In this case, the sheet resistance of CdS layer should be within a few tens of Ohms, which can only be

realized with a rather thick CdS layer doped with In or Ga. When TCO is used as the front contact, the requirement for CdS layer thickness is essentially eliminated. Thus, the TCO/CdS/CdTe structure is now generally adopted. The thickness of the TCO layer should be thick enough to give a low sheet resistance (lower than 10 Ohm/square), but not too thick the trasparency is comprised. TCOs are transparent in the $0.4<\lambda<0.7$ μm wavelength range. In the infrared (IR) their metallic properties leads to reflectance, and in the ultraviolet (UV) range, the electrons can absorb sufficient energy to be excited depending on the bandgap of the TCO. Indium-tin-oxide is the most widely used TCO for making thin film solar cells. ITO films retain the cubic bixbyte structure of bulk In_2O_3, but with a slight increase in the lattice constant depending on the deposition condictions.

Experimental

For superstrate configuration, the mask used for ITO photolithography was purchased from CAD/Art Services, Inc, with 1x1 mm^2 transparent squares 0.1 mm apart. The ITO substrates (Delta Technologies) have Rs = 70-100 Ω/square, and were cleaned prior to use by three 15 min rounds of sonication in fresh aliquots of acetone and then three aliquots of Nanopure water. The photoresist used was S1818 (Fisher scientific). The spin coating speed was 500 rpm for the initial 15 s, and 3500 rpm for the next 60 s. After spin coating, the substrate was baked 60 s at 110 °C. The exposure was done with an MA6 mask aligner (SUSS MicroTec) for 30 s. After exposure, the substrate was developed in 319 developer for 60 s, and then rinsed with copious amounts of water. After drying with nitrogen, the patterned ITO was post-baked at 110 °C for 60 s.

All potentials are reported vs. an Ag/AgCl (3 M KCl) reference electrode (Bioanalytical Systems, Inc). The substrate used was the pattern ITO described above. The Cd solution was pH 3, containing 0.5 mM $CdSO_4$ (Sigma-Aldrich) in 0.5 M $NaClO_4$. The sulfide solution was pH 10.5, containing 0.5 mM Na_2S (J.T.Baker) in 0.5 M $NaClO_4$. The Cu solution was pH 3, containing 0.5 mM $CuSO_4$ (Baker Analyzed, 99.8%) in 0.5 M $NaClO_4$. The acidic and basic blank rinse solution was 0.5 M $NaClO_4$ with pH 3 and 10.5, respectively. All solutions were made using 18 MΩ nanopure water filtered through Millipore Advantage 10.

All electrochemistry was carried out in a flow cell system (Electrochemical ALD, L.C., Athens, GA) consisting of a distributing valve, a flow cell, a pump, and a potentiostat. The whole system was automated by an in-house written LabVIEW-based program named Sequencer. The auxiliary used was an Au wire embedded in the cell wall facing the ITO working electrode. The exposed electrode area was 2.1 cm^2. The flow rate for CdS deposition was kept at 11 mL/min for the entire process. The flow rate for ITO treatment and all cyclic voltammetry (CV) was kept 2 mL/min. CVs were performed at a scan rate of 10 mV/s. All solutions were purged with N_2 prior to and during the experiment.

Before CdS E-ALD, patterned ITO substrate was pretreated with 90 s of reduction at -900 mV in acidic blank, followed by 5 min of $CuSO_4$ solution exposure at open circuit, and end with an anodic scan in $CuSO_4$ from the OCP to 200 mV. This leaves the surface with a minimum yet essential Cu nucleation sites for CdS electrodeposition.

The deposition cycle used for the E-ALD of CdS was as follows. The S solution was pumped into the cell for 10 s at a potential of -400 mV. The excess S was rinsed from the cell by pumping in the pH 10.5 blank solution for 10 s while maintaining at the same potential. Next the

pH 3 solution was pumped into the cell at a potential of -700 mV to prepare the pH for Cd entering. The Cd solution was pumped in at the same potential for 10 s. The excess Cd solution was removed from the cell by pumping in the pH 3 blank solution while maintaining the potential at -700 mV. The cycle was completed with pumping in 10 s of the pH 10.5 solution at -400 mV to prepare the environment for the S entering at beginning of the next cycle.

All potentials are reported vs. an Ag/AgCl (3 M KCl) reference electrode (Bioanalytical Systems, Inc). The substrate used was the CdS/ITO prepared using methods described above. The CdTe codeposition solution contained mM $CdSO_4$ and mM TeO_2 in 0.1 M $NaClO_4$, pH 2. The electrochemistry setup was the same as ones used for the CdS deposition. The flow rate for CdS deposition was kept at 2 mL/min for the entire process.

The Au solution used for electrodeposition was ELEVATED® GOLD 7990 from TECHNIC INC. The deposition was done in a beaker with the aforementioned CdTe/CdS/ITO as the working electrode, a gold wire as the counter electrode, and Ag/AgCl (3 M KCl) as the reference electrode. A potential of -735 mV as applied for 1 min. The electrode was then taken out and rinsed with copious amounts of water.

The substrate configuration CdS/CdTe/Au was prepared in a similar fashion with Au as the substrate instead of ITO. The substrates used were 100 nm of Au coated on 5 nm of Ti on glass, purchased from Evaporated Metal Films (Ithaca, NY). The Au substrates were cleaned prior to use with nanopure water and acetone, followed by a 30s immersion in concentrated nitric acid, and then rinsed with nanopure water. CdTe was deposited onto the Au substrate first at a potential of -700 mV for 15 min using the same codeposition solution describe above. The flow rate was kept at 2 mL/min for the entire process. The CdS E-ALD was performed using the

CdTe/Au as the working electrode. There are 8 steps in one defined E-ALD cycle in this experiment. The four steps for Cd deposition includes: Step 1). flow in $CdSO_4$ solution at -600 mV for 10 s. Step 2). quiescent deposition of Cd for 10 s at -775 mV. Step 3). flow in acidic blank solution for 10s to rinse out excess Cd^{2+} ions. Step 4). flow in basic blank solution for 10 s at -775 mV to prepare the pH environment for the entering of sulfide ions. The subsequent 4 steps for S deposition includes: Step 5). flow in Na_2S for 10 s at -775 mV. Step 6). quiescent deposition of Na_2S for 10 s at -300 mV. Step 7). flow in basic blank solution for 10 s at -300 mV to rinse out excess sulfide ions. Step 8). flow in acidic blank solution for 10 s at –300 mV to prepare the pH environment for the entering of Cd^{2+} for the next cycle. The flow rate for all the flowing cycles is kept at 11 mL/min.

Results and Discussion

In the substrate configuration CdS/CdTe/Au, due to the high transparency nature of CdS thin films, there was no obvious change in appearance after CdS was deposited onto CdTe/Au. The stoichiometry of the CdTe film on Au is measured prior to the deposition of Au using EPMA and shows Cd/Te ratio of 0.97. The composition of the resulting film is measured using EPMA. The composition of the resulting CdS/CdTe film is subsequently measured and the results show a Cd/(Te+S) ratio of 0.97, suggesting that both the CdTe and the CdS thin films have an optimal ratio. The thickness of the CdTe layer is measured to be ~50 nm using spectroscopic ellipsometry and CdS layer ~10 nm. X-ray diffraction is also performed on the CdS/CdTe/Au film, as show in Figure 5.1. The pattern shows a single CdTe <111> peak and a single CdS <111> peak. The CdS thin film crystal structure is consistent with the CdS thin film deposited on clean Au. The CdTe film with its <111> structure matches well with the lattice

structure of CdS, and acts as a good substrate for CdS growth. The CdTe peak has a higher intensity compared with CdS due to a higher film thickness and thus larger plane to diffract X-ray. The spectrum shows a good separation of the CdTe and CdS peak and this could give some insight into the level of Cd interlayer diffusion at the interface.

Because no front contact layer was deposited, the photoresponse of the CdS/CdTe p-n junction cannot be measured directly. Thus a solution/CdS/CdTe/Au environment was used to characterize the photoelectrochemical response. Figure 5.2 is the I-V curve of CdS/CdTe/Au in methyl viologen solution under 1 sun illumination with AM 1.5 filter. The illuminated area was 0.283 cm^2. A p-type response was observed in the I-V scan, which is expected for a good p-n junction with a matching redox couple. The minimum dark current suggested low defect density and few trap states. The fact that the photocurrent curved upward instead of downward as the potential was scanned negative was an indication of a low Fill Factor. But in this measurement, the Fill Factor was largely affected by the bandgap alignment between the deposit and the solution interface. The Fill Factor may be improved if a more suitable redox couple was adopted.

In the superstrate configuration, AFM and SEM images of the CdTe/CdS/ITO/Glass structure were taken and shown in Figure 5.3 and Figure 5.4, respectively. Both images showed similar compact grainy structure. The photoelectrochemical performance of the Au/CdTe/CdS/ITO/Glass was yet unable to determine due to instrumentation limitations. More efforts are on the way to build a setup for cell performance characterization.

Conclusion

This study focused on the fabrication of CdS/CdTe photovoltaic device with both superstrate and substrate configuration. In the superstrate configuration, the ITO substrate was

patterned with 1x1 mm^2 squares using photolithography to separate the 2 cm^2 area into many individual cells. CdS thin film was deposited onto the patterned ITO using methods decribed in chapter 4. CdTe thin film was deposited onto CdS/ITO using pulse plating atomic layer deposition. Finally a Au was layer was electrochemically deposited onto the CdTe/CdS/ITO as the back contact. In the substrate configuration, CdTe was deposited onto Au substrate using cdepostion at -700 mV for 15 mimniutes. CdS was deposited onto CdTe/Au using E-ALD with Cd depostion of -775 mV and S potential of -500 mV. The stoiochimetry of CdTe was measured with EPMA to be 1:1, and after CdS deposition, the Cd to (S+Te) was measured again with EPMA with 1:1, suggesting good stoichimetry with both films. XRD diffraction was taken for the CdS/CdTe/Au configuration to show CdTe zinc blend <111> structure and CdS <111> structure. Photoelectrochemistry measurement of the CdS/CdTe/Au configuration in methyl viologen solution under 1 sun with AM 1.5 filter showed p-type response, which is expected for a p-n junction in an appropriate redox couple solution.

Acknowledgements

Support from the National Science Foundation, DMR 1410109, is gratefully acknowledged. Thanks to Dr. Mubeen and Dr. Wei Cheng from the University of Iowa for making the photoelectrochemistry measurements. Thanks are extended to the Georgia Electron Microscopy for use of their SEM.

References

1. El Chaar, L.; El Zein, N., Review of photovoltaic technologies. *Renewable and sustainable energy reviews* **2011,** *15* (5), 2165-2175.

2. Jäger-Waldau, A., PV Status Report 2016. *EUR 28159 EN*.

3. Chapin, D. M.; Fuller, C. S.; Pearson, G. L., A New Silicon p-n Junction Photocell for Converting Solar Radiation into Electrical Power. *Journal of Applied Physics* **1954,** *25* (5), 676-677.

4. Badawy, W. A., A review on solar cells from Si-single crystals to porous materials and quantum dots. *Journal of advanced research* **2015,** *6* (2), 123-132.

5. Petermann, J. H.; Zielke, D.; Schmidt, J.; Haase, F.; Rojas, E. G.; Brendel, R., 19%-efficient and 43 μm-thick crystalline Si solar cell from layer transfer using porous silicon. *Progress in Photovoltaics: Research and Applications* **2012,** *20* (1), 1-5.

6. Masuko, K.; Shigematsu, M.; Hashiguchi, T.; Fujishima, D.; Kai, M.; Yoshimura, N.; Yamaguchi, T.; Ichihashi, Y.; Mishima, T.; Matsubara, N., Achievement of more than 25% conversion efficiency with crystalline silicon heterojunction solar cell. *IEEE Journal of Photovoltaics* **2014,** *4* (6), 1433-1435.

7. Bergmann, R., Crystalline Si thin-film solar cells: a review. *Applied Physics A: Materials Science & Processing* **1999,** *69* (2), 187-194.

8. Nishida, S.; Nakagawa, K.; Iwane, M.; Iwasaki, Y.; Ukiyo, N.; Mizutani, M.; Shoji, T., Si-film growth using liquid phase epitaxy method and its application to thin-film crystalline Si solar cell. *Solar energy materials and solar cells* **2001,** *65* (1), 525-532.

9. Green, M. A.; Basore, P.; Chang, N.; Clugston, D.; Egan, R.; Evans, R.; Hogg, D.; Jarnason, S.; Keevers, M.; Lasswell, P., Crystalline silicon on glass (CSG) thin-film solar cell modules. *Sol. Energy* **2004,** *77* (6), 857-863.

10. Saga, T., Advances in crystalline silicon solar cell technology for industrial mass production. *NPG Asia Materials* **2010,** *2* (3), 96-102.

11. Rahman, M. Z., Advances in surface passivation and emitter optimization techniques of c-Si solar cells. *Renewable and Sustainable Energy Reviews* **2014,** *30*, 734-742.

12. ©Fraunhofer, I., Photovoltaics Report. **updated: 17 November 2016**.

13. Palm, J.; Kruhler, W.; Kusian, W.; Lerchenberger, A.; Endros, A.; Mihalik, G.; Fickett, B.; Jester, T. In *Characterization of tri-crystalline silicon for photovoltaic applications*, Photovoltaic Specialists Conference, 2000. Conference Record of the Twenty-Eighth IEEE, IEEE: 2000; pp 40-45.

14. Mackintosh, B.; Ouellette, M.; Rosenblum, M.; Kalejs, J.; Piwczyk, B. In *100 micron thick multicrystalline Si wafers and cells from large diameter EFG cylinders*, Photovoltaic Specialists Conference, 2000. Conference Record of the Twenty-Eighth IEEE, IEEE: 2000; pp 46-48.

15. Durose, K.; Edwards, P.; Halliday, D., Materials aspects of CdTe/CdS solar cells. *Journal of Crystal Growth* **1999,** *197* (3), 733-742.

16. Mathew, X.; Enriquez, J. P.; Romeo, A.; Tiwari, A. N., CdTe/CdS solar cells on flexible substrates. *Sol. Energy* **2004,** *77* (6), 831-838.

17. Aramoto, T.; Kumazawa, S.; Higuchi, H.; Arita, T.; Shibutani, S.; Nishio, T.; Nakajima, J.; Tsuji, M.; Hanafusa, A.; Hibino, T., 16.0% efficient thin-film CdS/CdTe solar cells. *Japanese Journal of Applied Physics* **1997,** *36* (10R), 6304.

18. Britt, J.; Ferekides, C., Thin-film CdS/CdTe solar cell with 15.8% efficiency. *Applied Physics Letters* **1993,** *62* (22), 2851-2852.

19. Sites, J.; Pan, J., Strategies to increase CdTe solar-cell voltage. *Thin Solid Films* **2007,** *515* (15), 6099-6102.

20. Mitchell, K. W.; Fahrenbruch, A. L.; Bube, R. H., Evaluation of the CdS/CdTe heterojunction solar cell. *Journal of Applied Physics* **1977,** *48* (10), 4365-4371.

21. Katagiri, H.; Jimbo, K.; Maw, W. S.; Oishi, K.; Yamazaki, M.; Araki, H.; Takeuchi, A., Development of CZTS-based thin film solar cells. *Thin Solid Films* **2009,** *517* (7), 2455-2460.

22. Malerba, C.; Biccari, F.; Azanza Ricardo, C. L.; Valentini, M.; Chierchia, R.; Müller, M.; Santoni, A.; Esposito, E.; Mangiapane, P.; Scardi, P.; Mittiga, A., CZTS stoichiometry effects on the band gap energy. *Journal of Alloys and Compounds* **2014,** *582* (0), 528-534.

23. Suryawanshi, M. P.; Agawane, G. L.; Bhosale, S. M.; Shin, S. W.; Patil, P. S.; Kim, J. H.; Moholkar, A. V., CZTS based thin film solar cells: a status review. *Materials Technology* **2013,** *28* (1/2), 98-109.

24. Jiang, M.; Yan, X., *Cu2ZnSnS4 Thin Film Solar Cells: Present Status and Future Prospects*. 2013.

25. Minlin, J.; Dhakal, R.; Yong, L.; Thapaliya, P.; Xingzhong, Y. In *Cu2ZnSnS4 (CZTS) polycrystalline thin films prepared by sol-gel method*, Photovoltaic Specialists Conference (PVSC), 2011 37th IEEE, 19-24 June 2011; 2011; pp 001283-001286.

26. Kask, E.; Raadik, T.; Grossberg, M.; Josepson, R.; Krustok, J., Deep defects in Cu2ZnSnS4 monograin solar cells. *Energy Procedia* **2011,** *10* (0), 261-265.

27. Araki, H.; Kubo, Y.; Jimbo, K.; Maw, W. S.; Katagiri, H.; Yamazaki, M.; Oishi, K.; Takeuchi, A., Preparation of Cu2ZnSnS4 thin films by sulfurization of co-electroplated Cu-Zn-Sn precursors. *physica status solidi (c)* **2009,** *6* (5), 1266-1268.

28. Tatsuo, F.; Shin, T.; Tadayoshi, I., Enhancement of Conversion Efficiency of Cu 2 ZnSnS 4 Thin Film Solar Cells by Improvement of Sulfurization Conditions. *Applied Physics Express* **2013,** *6* (6), 062301.

29. Chen, S.; Walsh, A.; Gong, X.-G.; Wei, S.-H., Classification of Lattice Defects in the Kesterite Cu2ZnSnS4 and Cu2ZnSnSe4 Earth-Abundant Solar Cell Absorbers. *Advanced Materials* **2013,** *25* (11), 1522-1539.

30. Naghavi, N.; Spiering, S.; Powalla, M.; Cavana, B.; Lincot, D., High-efficiency copper indium gallium diselenide (CIGS) solar cells with indium sulfide buffer layers deposited by atomic layer chemical vapor deposition (ALCVD). *Progress in Photovoltaics: Research and Applications* **2003,** *11* (7), 437-443.

31. Chirilă, A.; Reinhard, P.; Pianezzi, F.; Bloesch, P.; Uhl, A. R.; Fella, C.; Kranz, L.; Keller, D.; Gretener, C.; Hagendorfer, H., Potassium-induced surface modification of Cu (In, Ga) Se2 thin films for high-efficiency solar cells. *Nature Materials* **2013,** *12* (12), 1107-1111.

32. Repins, I.; Contreras, M. A.; Egaas, B.; DeHart, C.; Scharf, J.; Perkins, C. L.; To, B.; Noufi, R., 19· 9%-efficient ZnO/CdS/CuInGaSe2 solar cell with 81· 2% fill factor. *Progress in Photovoltaics: Research and applications* **2008,** *16* (3), 235-239.

33. Ramanathan, K.; Contreras, M. A.; Perkins, C. L.; Asher, S.; Hasoon, F. S.; Keane, J.; Young, D.; Romero, M.; Metzger, W.; Noufi, R., Properties of 19.2% efficiency ZnO/CdS/CuInGaSe2 thin-film solar cells. *Progress in Photovoltaics: research and applications* **2003,** *11* (4), 225-230.

34. Nakada, T.; Mizutani, M., 18% efficiency Cd-free Cu (In, Ga) Se2 thin-film solar cells fabricated using chemical bath deposition (CBD)-ZnS buffer layers. *Japanese Journal of Applied Physics* **2002,** *41* (2B), L165.

35. Islam, M. M.; Ishizuka, S.; Yamada, A.; Sakurai, K.; Niki, S.; Sakurai, T.; Akimoto, K., CIGS solar cell with MBE-grown ZnS buffer layer. *Solar Energy Materials and Solar Cells* **2009,** *93* (6), 970-972.

36. Triboulet, R., Progress in Crystal Growth and Characterization of Materials. *Progress in Crystal Growth and Characterization of Materials* **2014,** *60*, 1-14.

37. Shah, A.; Torres, P.; Tscharner, R.; Wyrsch, N.; Keppner, H., Photovoltaic technology: the case for thin-film solar cells. *science* **1999,** *285* (5428), 692-698.

38. Poortmans, J.; Arkhipov, V., *Thin film solar cells: fabrication, characterization and applications*. John Wiley & Sons: 2006; Vol. 5.

39. Shah, A.; Schade, H.; Vanecek, M.; Meier, J.; Vallat-Sauvain, E.; Wyrsch, N.; Kroll, U.; Droz, C.; Bailat, J., Thin-film silicon solar cell technology. *Progress in photovoltaics: Research and applications* **2004,** *12* (2-3), 113-142.

40. Bonnet, D.; Rabenhorst, H. In *New results on the development of a thin-film p-CdTe-n-CdS heterojunction solar cell*, Photovoltaic Specialists Conference, 9 th, Silver Spring, Md, 1972; pp 129-132.

41. Lee, J.; Im, H., Effects of junction formation conditions on the photovoltaic properties of sintered CdS/CdTe solar cells. *Journal of materials science* **1986,** *21* (3), 980-984.

42. Bai, Z.; Yang, J.; Wang, D., Thin film CdTe solar cells with an absorber layer thickness in micro-and sub-micrometer scale. *Applied Physics Letters* **2011,** *99* (14), 143502.

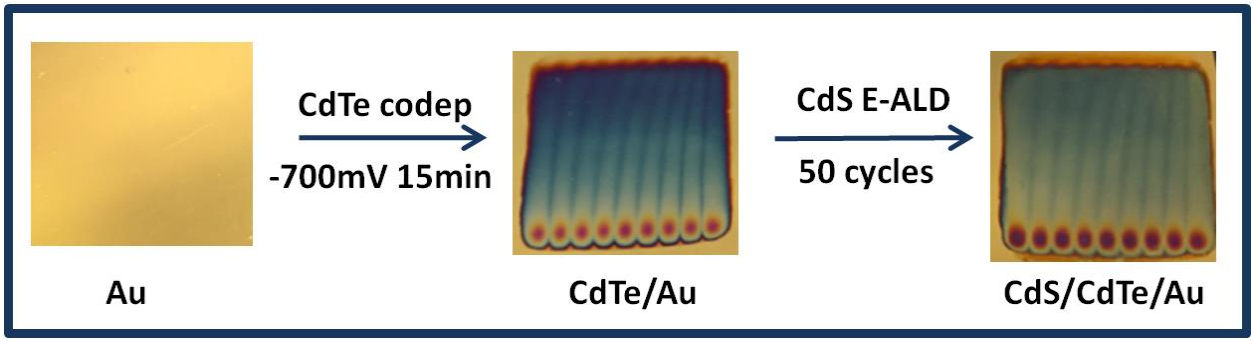

Figure 5.1: Illustration of the process of making CdS/CdTe/Au using CdTe codeposition and CdS E-ALD technique. The pictures from left to right are: clean Au substrate, CdTe on Au after 15 min of codeposition at -700 mV, CdS on CdTe/Au after 50 cycles of deposition (Cd potential = -775 mV; S potential = -500 mV).

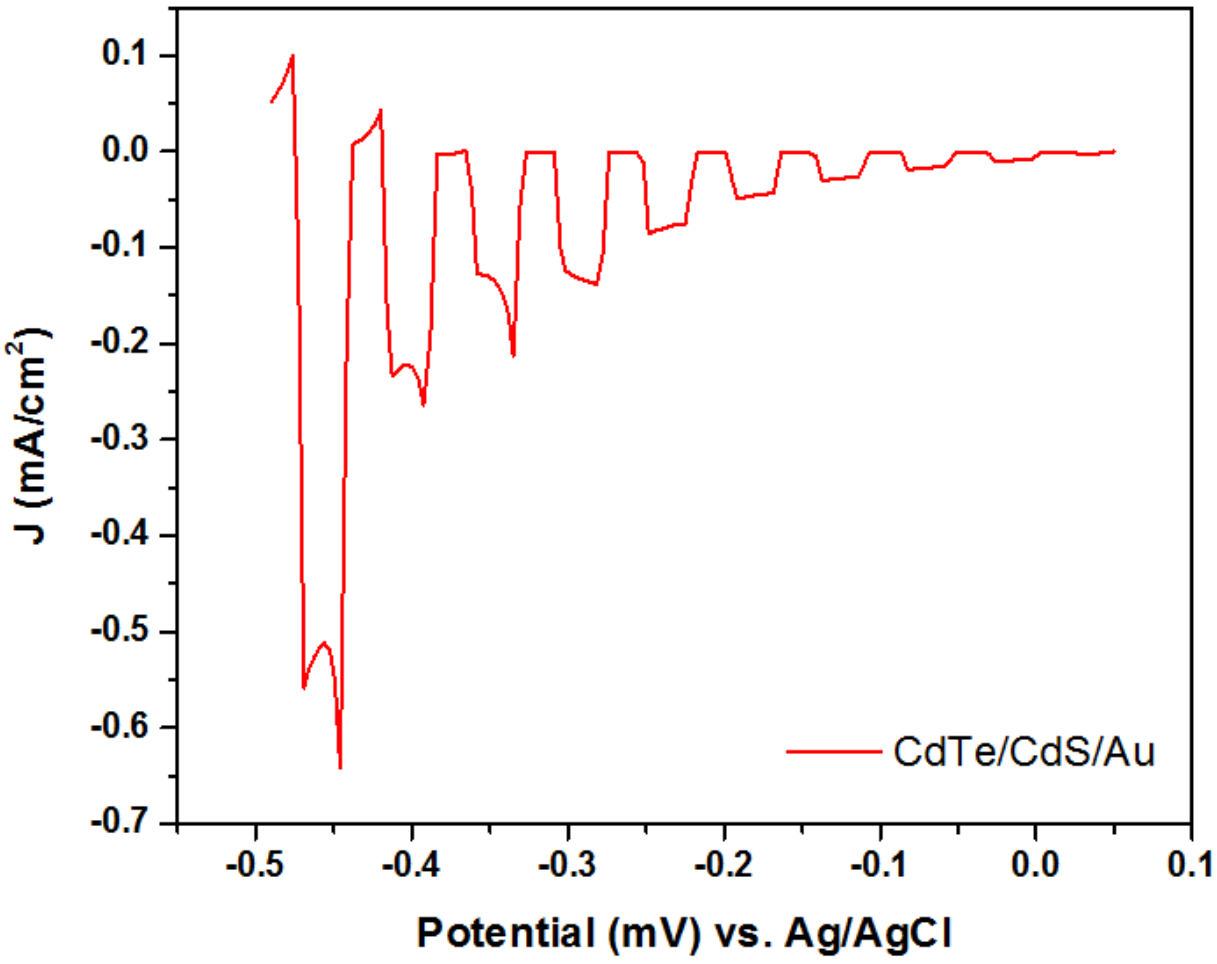

Figure 5.2: I-V curve of CdS/CdTe/Au in methyl viologen solution under 1 sun illumination with AM 1.5 filter. The illuminated area was 0.283 cm^2.

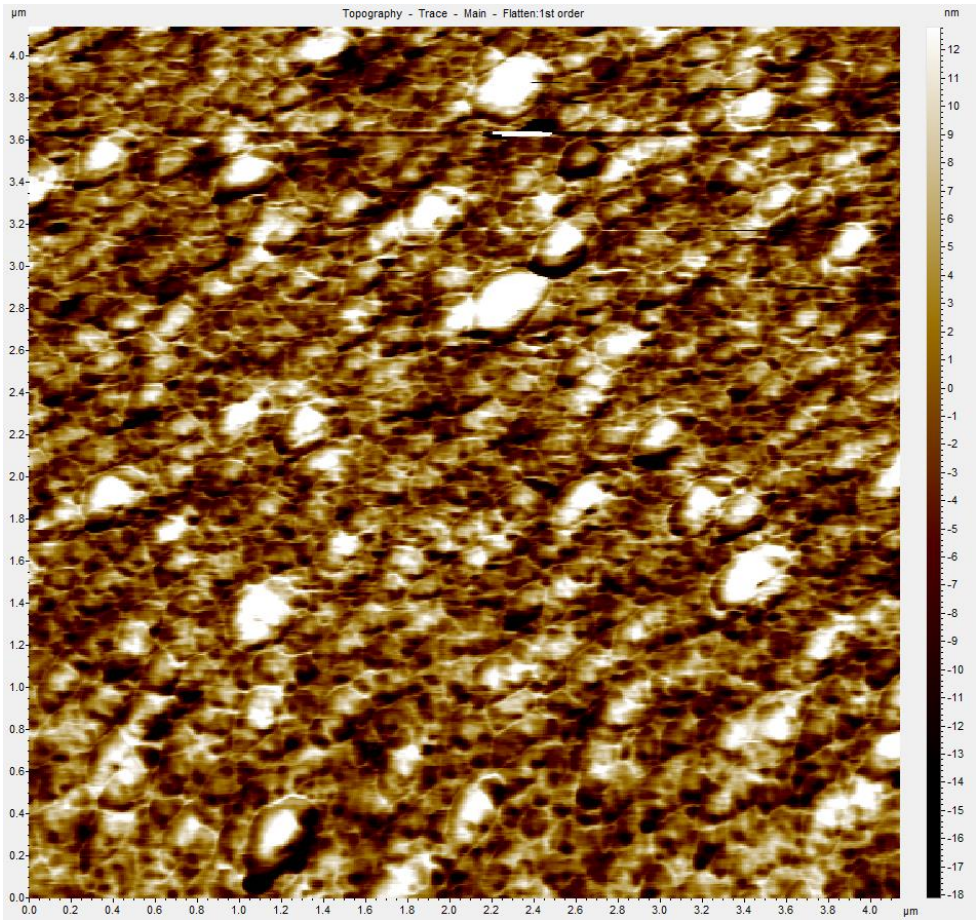

Figure 5.3: AFM topography image of the CdTe/CdS/ITO/Glass. The image area is 4.14 µm.

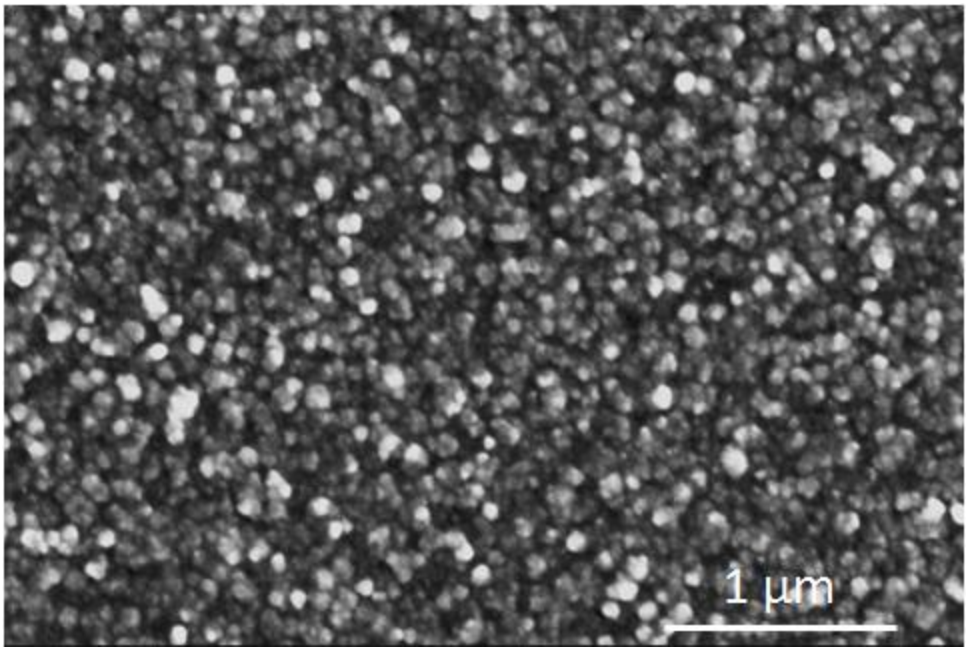

Figure 5.4: SEM image of the CdTe/CdS/ITO/Glass with acceleration voltage of 10 keV. The image area is 4.14 µm.

CHAPTER 6

ULTRA THIN AU DEPOSITION ON TRIPLE JUNCTION AMORPHOUS SILICON SOLAR CELL[5]

[5]S. Shen, J. Stickney, To be submitted to *Journal of the Electrochemical Society*

Abstract

Triple junction amorphous Si solar cell (TJSC) is an ideal photovoltaic for solar water splitting, as it provides a large potential output. However, the front contact ITO layer of a TJSC is unstable in a basic environment needed for oxygen evolution. This chapter investigates the deposition of an ultra-thin Au protective layer on ITO using electrochemical reduction and surface limited redox reaction (SLRR). SLRR is where an atomic layer of a sacrificial metal is exchanged for a more noble metal at open circuit. An ultra-thin Au layer was successfully deposited onto the ITO surface and the coverage increases linearly with respect to the number of cycles performed until a plateau was reached and a complete Au layer was formed. SEM shows that the Au exists on the surface as small particles and covers the entire surface evenly with no clumps. The Au-coated TJSC put out a constant potential in a pH 13 solution for an hour, which is a significant improvement from the unprotected TJSCs.

Introduction

In the last decades, numerous efforts have been made to reduce the use of non-renewable fossil fuels as the world's main energy supply. One possible solution is to use photovoltaics to convert sunlight into electricity to power everyday lives. Another possible option could be burning hydrogen instead of fossil fuels as they are the cleanest and lightest fuels possible. Hydrogen is a storable fuel that can be used to generate power for transportation and grid-scale energy storage[1-3]. An area where these two efforts meet is photoelectrochemical driven water splitting. Water splitting mimics the photosynthetic process within a leaf that converts the energy of sunlight into chemical energy by splitting water to produce hydrogen gas and oxygen gas: $2H_2O \rightarrow 2H_2+O_2$. The free energy for this reaction is $\Delta G = +237$ kJ per mol of H_2 or $\Delta E^0 = 1.23$

V under standard state conditions[4]. To successfully drive this reaction and to compensate for the voltage drop in the light absorbers, a total voltage of 1.6-1.7 V must be generated[5]. This research topic dates back to the 1970s[6-7] and has regained considerable interest during recent years because of the development in tandem and multi-junction solar cells[8-10]. Triple junction amorphous silicon cells (TJSCs) are a promising candidate as their open circuit voltage can exceed 2 V. Many studies have been done using triple junction amorphous silicon cells as the photovoltaic for photoelectrochemical driven water splitting[11-13].

The use of a catalyst is required to the photosynthetic process as the electron-hole pairs are generated one at a time and the water splitting process is a four electron-hole process. Since 2010, there have been significant efforts to replace noble-metal electrocatalysts (e.g. GaAs and GaInP)[13] with those made from less expensive elements. Different reactions take place in the photoanode and cathode, thus different catalyst is required. Typical catalyst used in oxygen evolution is RuO_2, $NiCoO_4$, $NiLa_2O_4$, etc[4, 14-15]. The catalyst that is going to be applied to the TJSC is a Ni-based material according to our collaborator Dr. Syed Mubeen from the University of Iowa.

During the artificial photosynthesis process, the photovoltaic can either be used as an external power supply to power an electrolyzer where water splitting happens, or to be combined with the eletrolyzer system into one integrated unit, where the internal electric field in the solar cell drives the reaction and water splitting occurs on the surface of the solar cell. The second setup not only reduces the instrument size, but also increases the efficiency by using a very low current density on the electrode. As the photovoltaic is in direct contact with the electrolyte solution, the stability of the photovoltaic becomes a crucial factor in evaluating the performance

of the system. TJSC utilizes a tandem-stacked design that not only put out a high voltage, but also allows for the optimization of the different layers of the cell to absorb different parts of the solar spectrum[13]. TJSCs typically use stainless steel as the back contact and a transparent conducting oxide (TCO) layer as the front layer to allow light to pass through. The sunlight enters the TJSC and generates a voltage sufficient to split water. Oxygen is produced at the anodic TCO surface following the oxidation reaction: $4OH^- \rightarrow O_2 + 2H_2O + 4e^-$. This suggests that a basic electrolyte solution environment facilitates the evolution of oxygen. However, as one of the most commonly used TCO layer, Indium-Tin-Oxide (ITO) is prone to corrosion in a basic environment. ITO is an n-type semiconductor with a bandgap between 3.5–4.3 eV. It usually consists of In_2O_3 with 10 wt% SnO_2[16]. Thus, an extra protection layer is needed to protect the ITO layer from corrosion from the electrolyte. The protection layer should firstly be transparent thus to allow light to pass through the cell. Secondly the layer should be conductive so that the electron-hole pairs generated in the cell can move to the surface. Thirdly, the protection layer should be compatible with the photocatalyst that grows on the surface and provide good adhesion. An ideal protection coating would be an ultra-thin precious group metal that is transparent and conductive. This chapter is focused on the idea of depositing an ultra-thin Au layer on TJSC using electrochemical reduction and surface limited redox replacement (SLRR). This study shares the same idea with Chapter 4 in terms of ITO reduction for the purpose of forming some sacrificial In metal, which could later be exchanged for a more stable metal. Pt nanofilms on Au has been successfully deposited using SLRR[17]. SLRR is where an atomic layer of a sacrificial metal is exchanged for a more noble metal at open circuit[18-20]. The driving force for SLRR is the metal reactivity difference between the two elements, where a more reactive metal can reduce the ionic form of a more noble metal to its elemental state. In this study, the sacrificial is

obtained from electrochemically reducing ITO to small and dispersed In metal, which upon flowing in Au^{3+}, reduces the Au^{3+} to Au. The indium metal is oxidized to In^{3+} and flushed out from the system, leaving a fraction of a monolayer of Au on the ITO surface. This process is repeated until the surface is completely covered with Au and no ITO is exposed.

Experimental

The Au solution was 0.1 mM $AuCl_3$ (Sigma-Aldrich) in 18 MΩ nanopure water. The pH was measured 3.2 without any adjustments. The Cu solution was 0.5 mM $CuSO_4$ (J.T.Baker) in 0.5 M $NaClO_4$, pH 3. The precursor concentrations were in the mM range because only a fraction of a monolayer (ML) of deposition is desired in each step. A monolayer (ML) in this study is defined as one adsorbate atom per Au atom. The pH 3 acidic blank consisted of 0.5 M $NaClO_4$ and were used to rinse cell of any precursor left with the same pH. The pH 13 basic blank solution also consisted of 0.5 M $NaClO_4$ and was used to mimic the basic working environment for water splitting catalyzing process. All solutions were made using 18 MΩ nanopure water filtered through Millipore Advantage 10. The substrates used were commercially available triple junction amorphous solar cell, provided by Dr. Mubeen from the University of Iowa. The TJSC substrates were cut, etched and cleaned with the following procedure before sent to the author.

1. Cut large sheet of TJ-Si into 2x2 cm pieces.
2. Etch the cut edges with concentrated phosphoric acid by placing a thin bead of phosphoric acid along the edges, 1 mm or less in width. Let it sit for 30 min, then rinse the edges with DI water.
3. Clean the etched samples by sonicating for 10 minutes in each of the following: 1% Alconox, acetone, isopropanol, DI water

4. Dry with clean dry nitrogen gas

All electrochemical experiments were performed using an automated flowcell system (Electrochemical ALD, L.C., Athens, GA). Solution bottles were connected to a distribution valve, which controls the species flowing into the cell. The solutions were pumped through the distribution valve to a flowcell, of which the potential was measured by a potentiostat. The pump and potentiostat were automated using a program developed in-house named Sequencer. The auxiliary electrode used was a gold wire embedded in the cell wall and the reference electrode was 3 M Ag/AgCl (BASi, West Lafayette, IN). The exposed electrode area was 0.32 cm^2, as defined by a quarter-inch diameter green donut shaped tape. The flow rate was kept at 11 mL/ min for solution exchange. Cyclic voltammetries (CVs) were performed at a scan rate of 10 mV/s, with the solution flowing at 2 mL/ min. Prior to all experiments, nitrogen gas was flown into the system to purge away all the oxygen gas in the bottles and in the tubes.

Results and discussion

Figure 6.1 depicts a window opening of a clean TJSC in pH 3 blank solution. No obvious reduction was observed until the negative potential limit was pushed to -900 mV, where the indium oxide was reduced to metallic indium. In the positive-going scan, a prominent oxidation peak was observed starting at -650 mV, corresponding to indium re-oxidation to Indium (III). As the negative potential limit was pushed more negative, a hysteresis loop was observed, indicating a typical nucleation and growth process. The size of oxidation peak in the reverse scan also grew as more nucleation and growth took place. The idea of the reduction process in this study was to create a minimum amount of In necessary to Au SLRR process, without changing the nature of the ITO layer. Thus, a conservative potential of -900 mV was chosen for the reduction of ITO. The reduction time was determined 10 s based on past experience from chapter 4.

After the reduction, Au solution was flown in for SLRR. This process was repeated multiple times until a full coverage was achieved. Figure 6.2 describes the process of a complete cycle. The black and red curves correspond to the potential and current, respectively. The cycle started with 10 s of quiescent reduction at -900 mV, followed by 10 s Au exchange at a flow rate of 11 ml/min at open circuit, then the flow stopped and the substrate was left in the Au solution for another 170 s, after which 10 s of blank solution was pumped into the cell at 11 ml/min to prepare the environment for the next cycle. No potential was applied in a cycle except for the first 10 s.

One way to quantify the presence of Au on the surface is by scanning a CV in pH 3 blank solution and integrating the oxidation and reduction peak. Figure 6.3(a) depicts the CV on TJSC after Au SLRR, compared with a regular Au slide (Figure 6.3(b)) used in chapter 2. Both CV exhibited the same shape, as expected for an Au covered surface. As the oxidation potential was push more positive, the reduction peak at -800 also increased. 1400 mV was shown to be too extreme for the TJSC and lead to the broken-down of the substrate. Thus reduction at the 1300 mV scan was used to determine the Au coverage and the number is calculated to be 1.12 ML. This number is a rough estimated because the layer structure is Au on ITO instead of Au on Au, thus the 220 $\mu C/e^{*}cm^{-2}$ assumption during calculation is not entirely accurate. However, the scan did prove the existence of an Au layer on the surface and the substrate showed much higher stability during the scan compared with an untreated TJSC. Figure 6.4 depicts the CV of an untreated TJSC in pH 3 solution. An abnormal oxidation peak was observed in the negative-going scan and the current dropped back to 0 when the initial OCP was reached. This oxidation current is possibly the oxidation of the amorphous Si underneath the ITO. The substrate showed

cracking and delamination after the CV, with the stainless steel layer exposed. This behavior was not observed with the Au-coated TJSC, suggesting a much higher stability.

A second method was used to quantify the Au coverage by using Cu solution. Cu is known to form UPD on metal surfaces such as Au, but not on metal oxide surfaces such as ITO. Figure 6.5 is the window opening of Cu solution on (a) regular Au slide and (b) 10 cycles Au-coated TJSC. The shapes of the 2 CVs are not exactly the same, but they represent the same behavior. In both CVs, the reduction peak at 200 mV represents the UPD formation of Cu on Au, and the oxidation peak at 300 mV represent the stripping of UPD Cu from Au. The constant current at negative potentials corresponds to the bulk deposition of Au, and the oxidation peak with the onset potential of 0 mV is the stripping of bulk Cu. In both cases, no bulk stripping peak was observed when the potential was reversed at 0 mV. All Cu was stripped when potential reached 400 mV. Thus, by stepping between 400 mV and 0 mV, UPD amounts of Cu was stripped and deposited. 0 mV is the E^0 of bulk Cu formation and stripping and can allow the maximum amount of UPD Cu formation. Because UPD Cu can only form on Au surface, not on ITO surface, the UPD Cu coverage can correlate with the Au coverage and give insights into what fraction of the TJSC is coated with Au.

Figure 6.6 shows the example of a current density-time trace of stepping between 400 mV and 0 mV in Cu solution. The black and red curves represent a regular Au slide and an 18 cycle Au coated TJSC. The positive spikes correspond to stepping to 400 mV, and negative spikes 0 mV. The initial step was to 400 mV to make sure that the surface is free of any Cu deposit. Each time the current went through an exponential decay and leveled off at a value close to 0 μA, which confirmed that the deposition is of UPD nature, instead of bulk. The reduction

peaks are integrated and average was taken for the 3 steps on each of the substrates. The Cu coverage was 1.17 ML on Au slide and 1.23 ML on Au coated TJSC. The Au coated TJSC has slightly more Cu coverage, which could be due to the roughened surface of TJSCs.

TJSC with different cycle numbers of Au coating were made and Cu coverage was determined on each deposit. The coverage is an average of 3 depositions at 0 mV. Figure 6.7 depicts the Cu coverage with respect to the cycle numbers. A linear trend was observed from 0 all the way to 18 cycles. After 18 cycles Cu coverage stopped increasing and plateaued at 1.2 ML, which is expected for a completely coated rough surface.

To test the stability of the Au-coated TJSC, an 18-cycle deposit was immersed in pH 13 blank solution and the open circuit potential was recorded. A cellphone flashlight was used to illuminate the cell every 5 min for the initial 30 min and at 50 min. The recorded open circuit potential is depicted in Figure 6.8. The dark (with room light) open circuit potential drifted slightly negative during this entire process. The author did her best in positioning the flashlight to achieve a strong and consistent illumination. The illuminated (with flashlight) open circuit potential is consistent during the 50 min process, with a small decrease in the final illumination. This has shown that the Au-coated TJSC has a relatively high stability in a strong basic environment.

SEM was used to characterize the surface morphology of the untreated TJSC and the TJSC after Au coating and is shown in Figure 6.9. The untreated TJSC has large grains on the surface with small textures on each grain. After the Au coating, there is no major change in the morphology of the surface, but tiny bright spots can be seen all over the surface following the

morphology of the original TJSC surface. No pits or dent was observed from reducing the ITO. EDS results in Figure shows the atomic percent of Au on the surface is

Conclusion

A thin layer of Au has been successfully coated on triple junction amorphous Si solar cells using electrochemical reduction and surface limited redox replacement. The Au coverage on the surface increases as the cycle number increases and eventually plateaued after reaching a full monolayer. The Au layer covers the TJSC surface evenly with no visible defects under SEM. The Au-coated TJSC is stable in pH 13 solution for over an hour. Future studies can be done on characterizing the PEC performance of the Au-coated TJSC for catalyst attachment and water splitting. The Au exchange duration in the cycle can potentially be shortened to reduce the effect of acid etching on ITO during deposition. Different metals such as Pt, Ru can also be tested for best results.

Acknowledgement

Support from the National Science Foundation, DMR 1410109, is gratefully acknowledged. Thanks are extended to Dr. Syed Mubeen and his students from University of Iowa for providing the substrates. Thanks are extended to the Georgia Electron Microscopy for use of their SEM.

References

1. Edwards, P. P.; Kuznetsov, V. L.; David, W. I. F.; Brandon, N. P., Hydrogen and fuel cells: Towards a sustainable energy future. *Energy Policy* **2008,** *36* (12), 4356-4362.

2. Wang, Y.; Chen, K. S.; Mishler, J.; Cho, S. C.; Adroher, X. C., A review of polymer electrolyte membrane fuel cells: Technology, applications, and needs on fundamental research. *Applied Energy* **2011,** *88* (4), 981-1007.

3. Evans, A.; Strezov, V.; Evans, T. J., Assessment of utility energy storage options for increased renewable energy penetration. *Renewable and Sustainable Energy Reviews* **2012,** *16* (6), 4141-4147.

4. Walter, M. G.; Warren, E. L.; McKone, J. R.; Boettcher, S. W.; Mi, Q.; Santori, E. A.; Lewis, N. S., Solar Water Splitting Cells. *Chemical Reviews* **2010,** *110* (11), 6446-6473.

5. Ager, J. W.; Shaner, M. R.; Walczak, K. A.; Sharp, I. D.; Ardo, S., Experimental demonstrations of spontaneous, solar-driven photoelectrochemical water splitting. *Energy & Environmental Science* **2015,** *8* (10), 2811-2824.

6. Fujishima, A.; Honda, K., Electrochemical evidence for the mechanism of the primary stage of photosynthesis. *Bulletin of the chemical society of Japan* **1971,** *44* (4), 1148-1150.

7. Fujishima, A.; Honda, K., Electrochemical photolysis of water at a semiconductor electrode. *nature* **1972,** *238* (5358), 37-38.

8. Yoneyama, H.; Sakamoto, H.; Tamura, H., A Photo-electochemical cell with production of hydrogen and oxygen by a cell reaction. *Electrochimica Acta* **1975,** *20* (5), 341-345.

9. Nozik, A., p-n photoelectrolysis cells. *Applied Physics Letters* **1976,** *29* (3), 150-153.

10. Ohashi, K.; McCann, J.; Bockris, J. M., Stable photoelectrochemical cells for the splitting of water. *Nature* **1977,** *266* (5603), 610-611.

11. Khaselev, O.; Bansal, A.; Turner, J. A., High-efficiency integrated multijunction photovoltaic/electrolysis systems for hydrogen production. *International Journal of Hydrogen Energy* **2001,** *26* (2), 127-132.

12. Rocheleau, R. E.; Miller, E. L.; Misra, A., High-Efficiency Photoelectrochemical Hydrogen Production Using Multijunction Amorphous Silicon Photoelectrodes. *Energy & Fuels* **1998,** *12* (1), 3-10.

13. Reece, S. Y.; Hamel, J. A.; Sung, K.; Jarvi, T. D.; Esswein, A. J.; Pijpers, J. J.; Nocera, D. G., Wireless solar water splitting using silicon-based semiconductors and earth-abundant catalysts. *Science* **2011,** *334* (6056), 645-648.

14. Lu, X.; Zhao, C., Electrodeposition of hierarchically structured three-dimensional nickel–iron electrodes for efficient oxygen evolution at high current densities. *Nature communications* **2015,** *6*, 6616.

15. Matsumoto, Y.; Sato, E., Electrocatalytic properties of transition metal oxides for oxygen evolution reaction. *Materials Chemistry and Physics* **1986,** *14* (5), 397-426.

16. Kim, H.; Gilmore, C.; Pique, A.; Horwitz, J.; Mattoussi, H.; Murata, H.; Kafafi, Z.; Chrisey, D., Electrical, optical, and structural properties of indium–tin–oxide thin films for organic light-emitting devices. *Journal of Applied Physics* **1999,** *86* (11), 6451-6461.

17. Jayaraju, N.; Vairavapandian, D.; Kim, Y. G.; Banga, D.; Stickney, J. L., Electrochemical atomic layer deposition (E-ALD) of Pt nanofilms using SLRR cycles. *J. Electrochem. Soc.* **2012,** *159* (10), D616-D622.

18. Brankovic, S. R.; Wang, J. X.; Adžić, R. R., Metal monolayer deposition by replacement of metal adlayers on electrode surfaces. *Surface Science* **2001,** *474* (1), L173-L179.

19. Brankovic, S.; Wang, J.; Adzic, R., New methods of controlled monolayer-to-multilayer deposition of Pt for designing electrocatalysts at an atomic level. *Journal of the Serbian Chemical Society* **2001,** *66* (11-12), 887-898.

20. Mrozek, M. F.; Xie, Y.; Weaver, M. J., Surface-Enhanced Raman Scattering on Uniform Platinum-Group Overlayers: Preparation by Redox Replacement of Underpotential-Deposited Metals on Gold. *Analytical Chemistry* **2001,** *73* (24), 5953-5960.

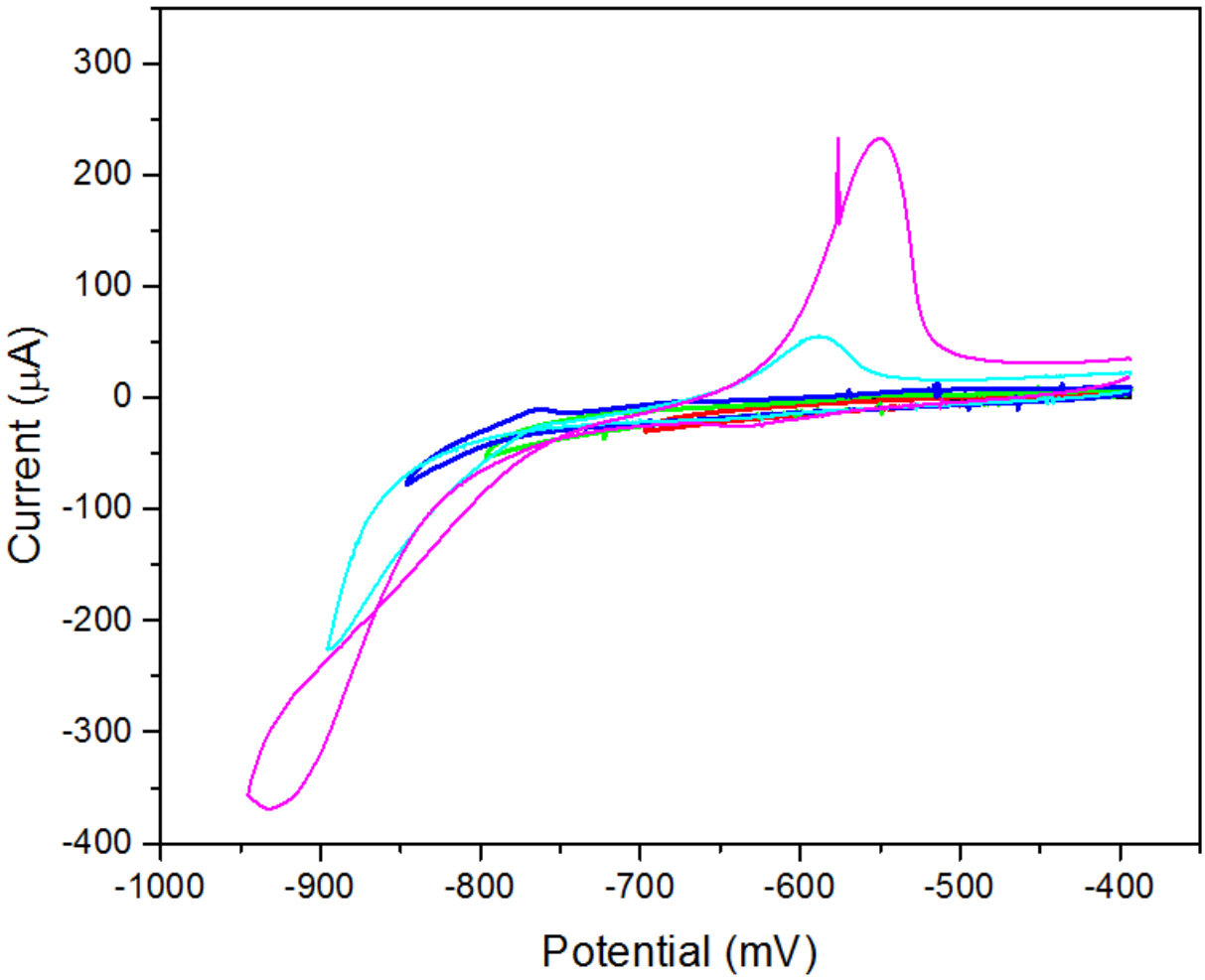

Figure 6.1: Window-opening of TJSC in pH 3 blank solution. The electrode area is 2.1 cm^2

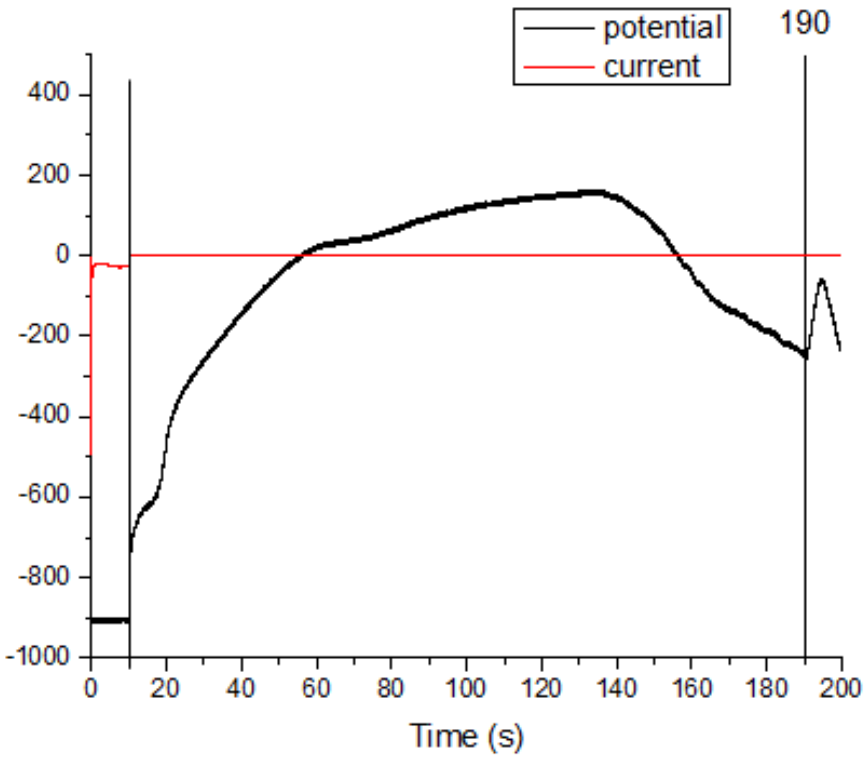

Figure 6.2: Potential-current-time trace of one complete Au deposition cycle. The black lines represent the potential, and the red curves are the corresponding current. The cell is filled with Au solution in between the time scale of the two vertical black lines, and blank outside the black lines. The electrode area is 0.32 cm^2.

(a)

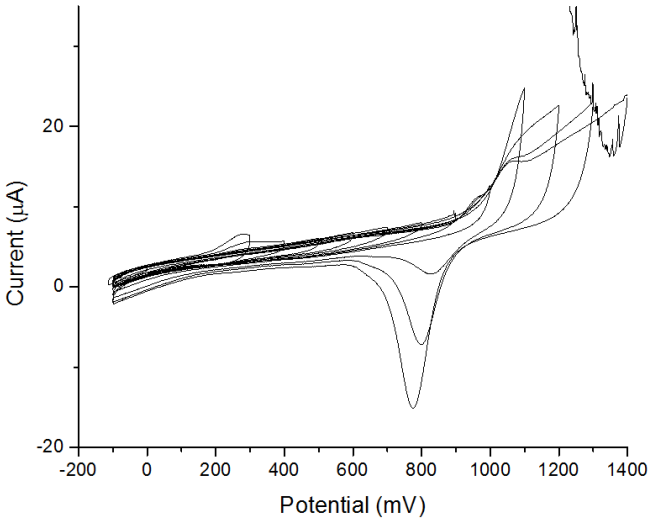

(b)

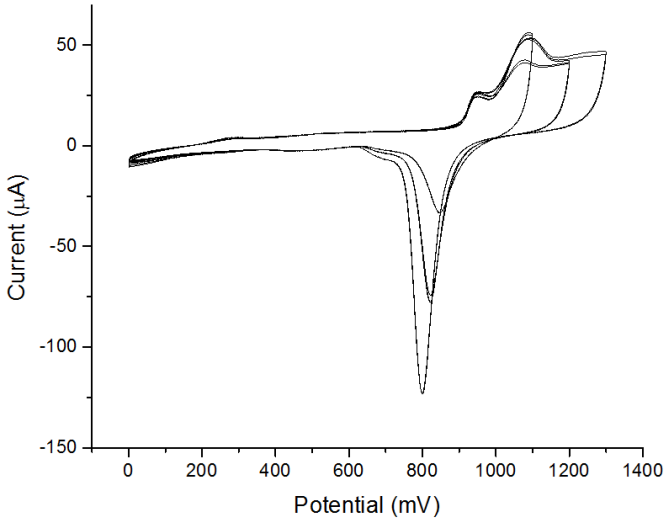

Figure 6.3: (a) Window-opening of 10-cycle Au coated TJSC in pH 3 blank solution. The electrode area is 0.32 cm^2 (b) Window-opening of a regular Au slide in pH 3 blank solution. The electrode area is 2.1cm^2

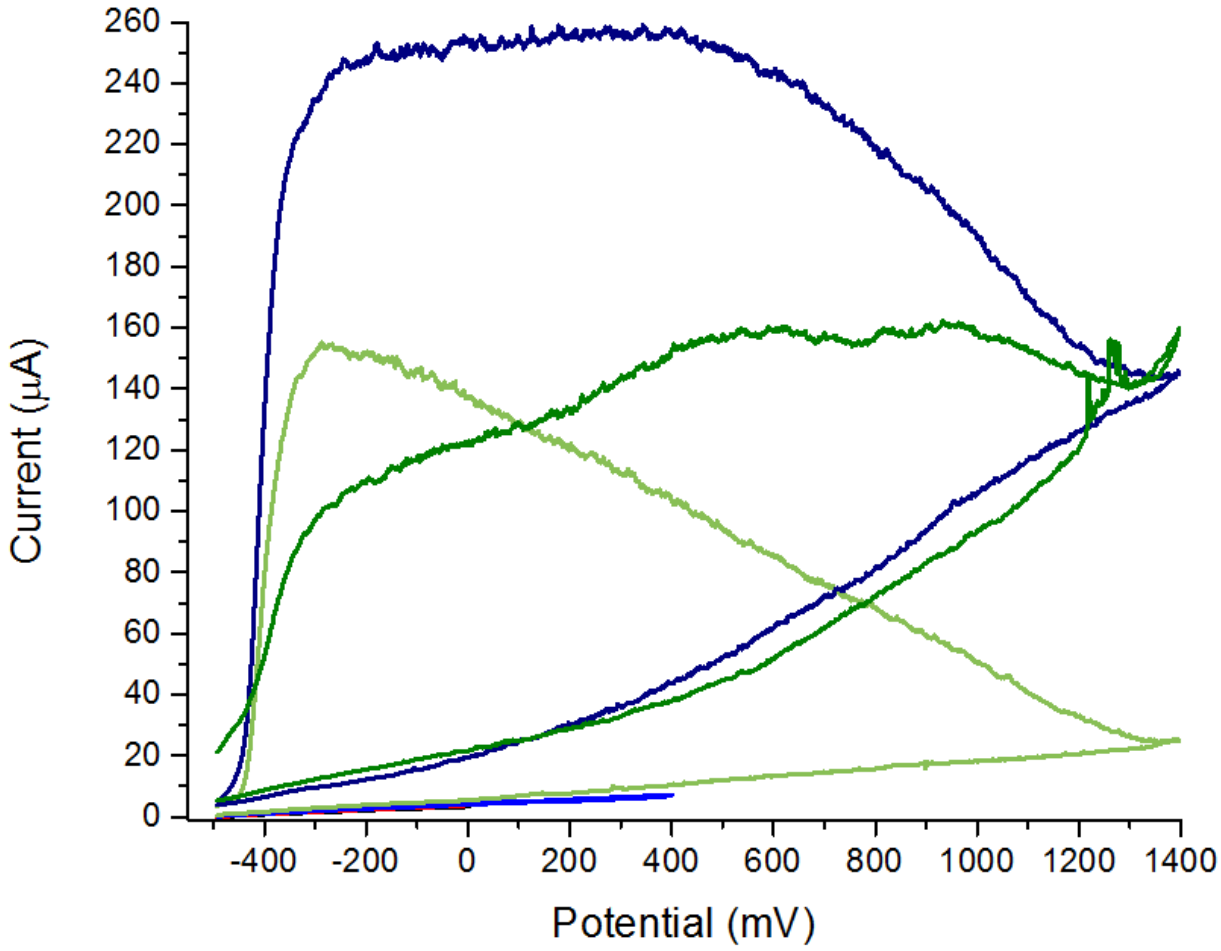

Figure 6.4: Cyclic voltammetry of an untreated TJSC in pH 3 blank solution. The electrode area is 2.1 cm^2

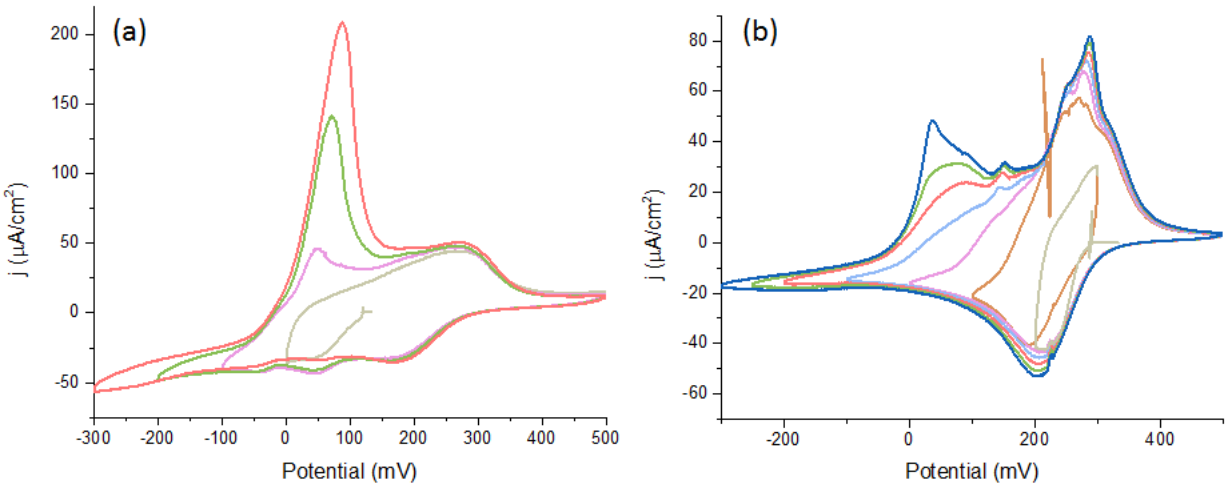

Figure 6.5: window opening of Cu solution on (a) 10 cycles Au-coated TJSC and (b) regular Au slide

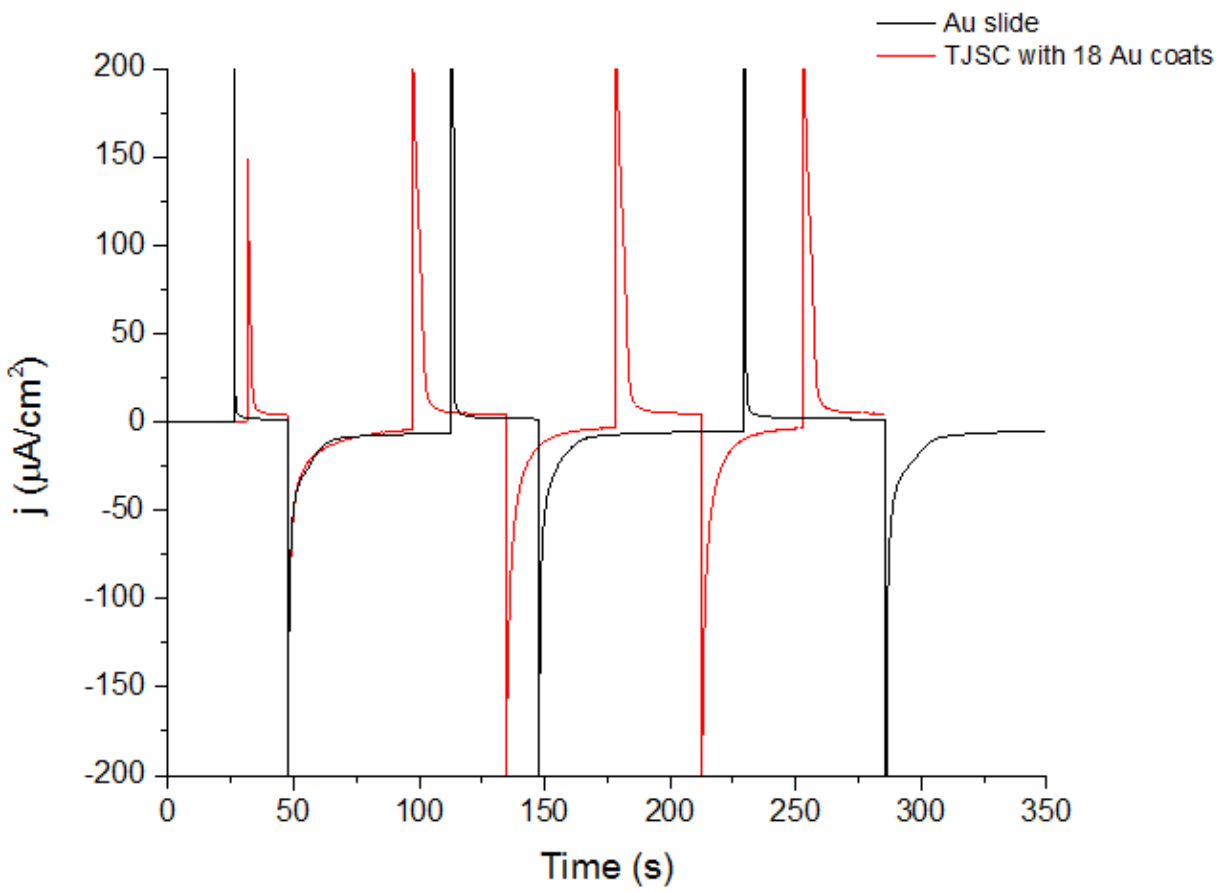

Figure 6.6: current density-time trace of stepping between 400 mV and 0 mV in Cu solution. The black and red curves represent a regular Au slide and an 18 cycle Au coated TJSC.

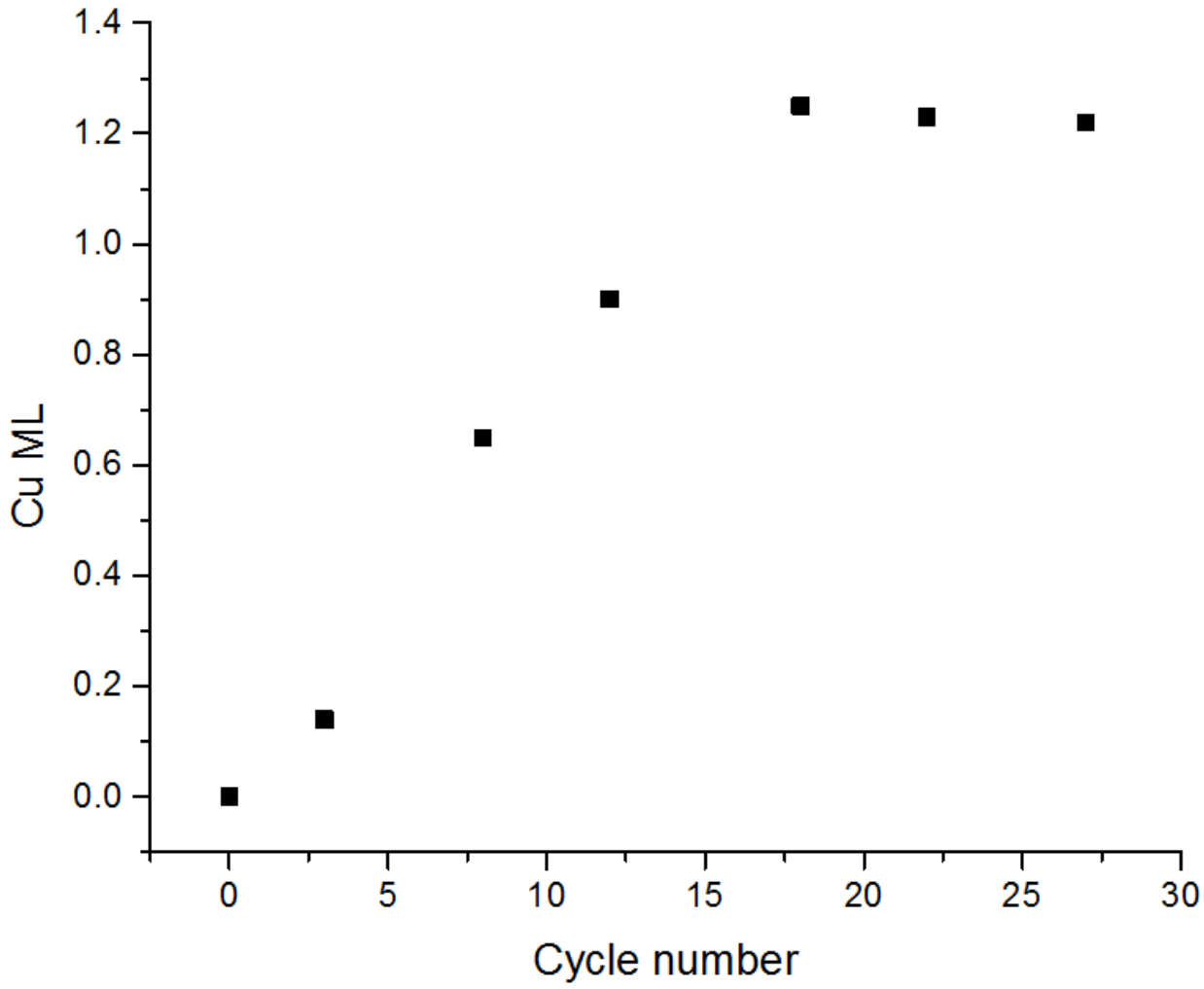

Figure 6.7: Cu coverage with respect to the cycle numbers

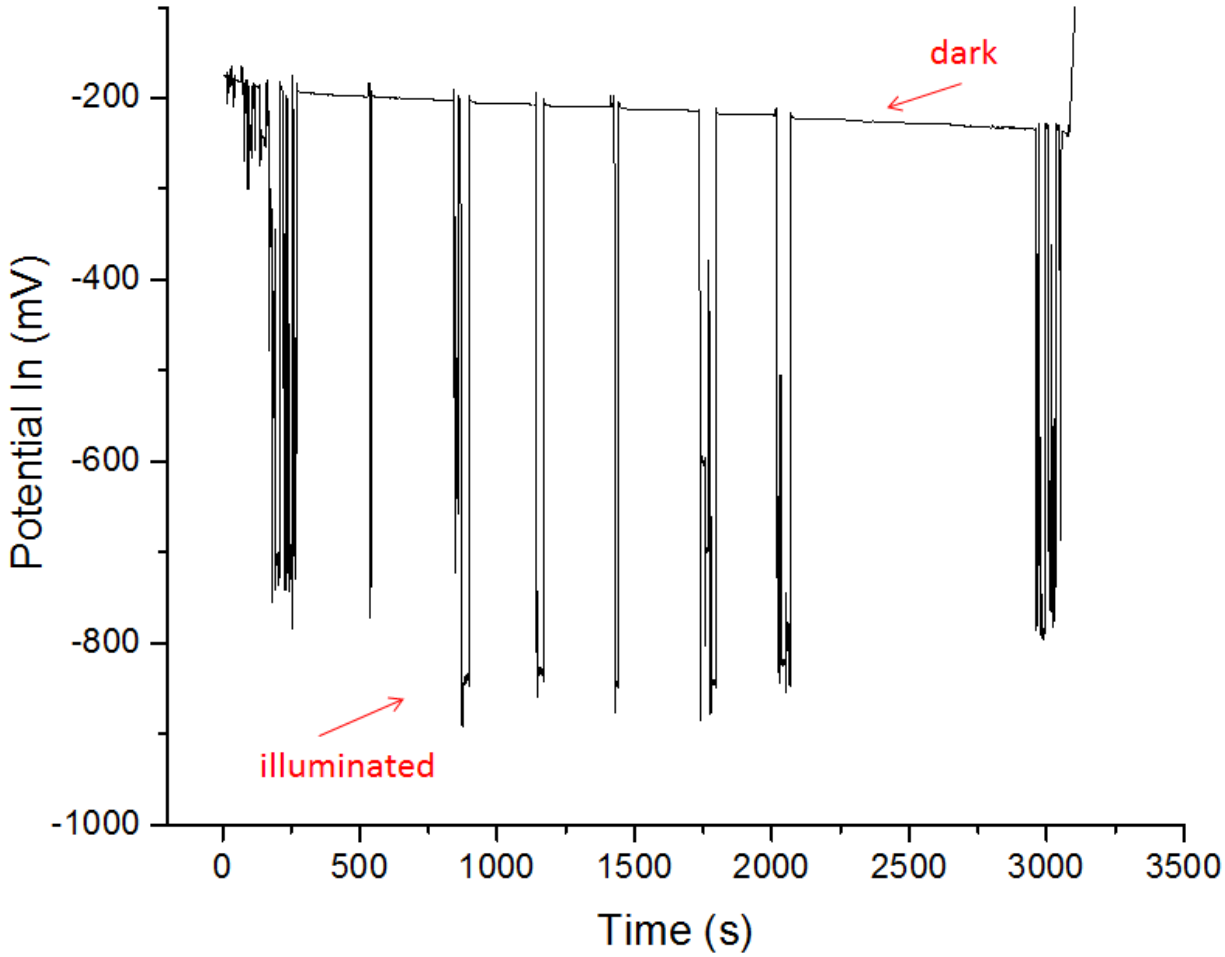

Figure 6.8: OCP-time trace of an 18-cycle deposit was immersed in pH 13 blank solution

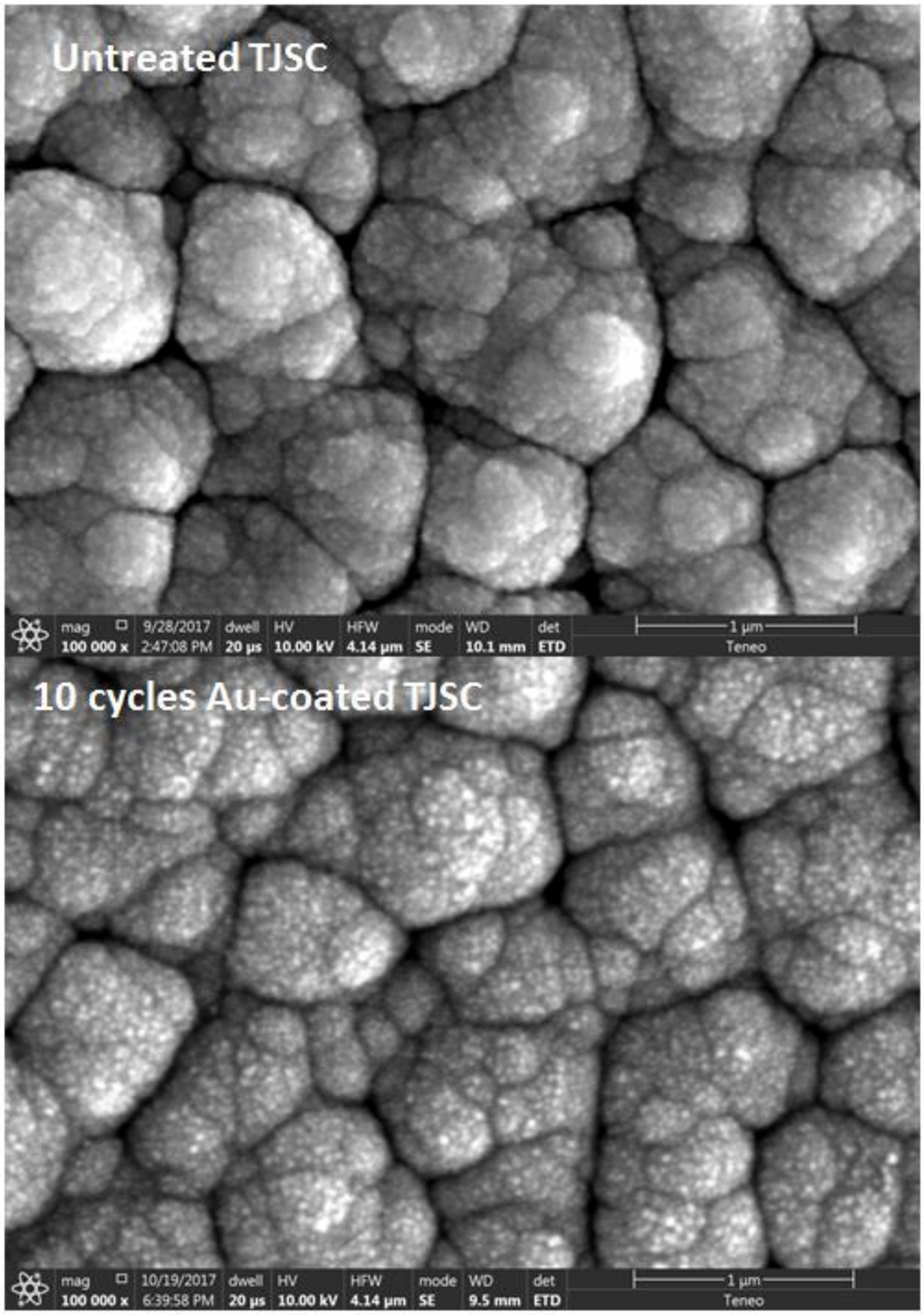

Figure 6.9: SEM of an untreated TJSC and 10 cycles Au-coated TJSC.

CHAPTER 7

CONCLUSION AND FUTURE STUDIES

The focus of this dissertation was the growth of CdS thin films on substrates with different materials and morphologies by electrochemical atomic layer deposition (E-ALD) and the formation of CdS/CdTe solar cells, as well as some preliminary studies of Au ultra-thin film deposition on ITO surfaces. Chapter 2 investigated the growth of CdS thin films on Au over a wide range of conditions using E-ALD. Cyclic voltammetry was used to study the electrochemical behavior of Cd and S individually on Au substrate. After the possible deposition range was narrowed down, the dependence of film composition on Cd deposition potential and S deposition potential was systematically studied using electron probe microanalysis (EPMA). The effect of step duration on the morphology and roughness of the deposit surface was investigated. As the step length increase from 2.5 s to 10 s while keeping the total deposition time constant, flow pattern was significantly reduced and the deposit surface looked visually smoother. The dependence of film thickness was a function of the cycle number. Film thickness, measured from spectroscopic ellipsometry, was shown to be proportional to the number of cycles performed. The linear growth with the number of cycles was consistent with a layer-by-layer growth process and the surface limited reaction mechanism. The optimum potential range for deposition was found to be -200 to -700 mV for Cd, and -200 to -600 mV for S. X-ray diffraction showed the deposits to be single crystal zinc blend <111> structure. The calculated growth rate based on lattice constant and thickness measurement was 0.56 ML/cycle, consistent with the layer-by-layer mechanism. The crystallite size was calculated from Scherer's

equation to be 32 nm. SEM images showed conformal growth of the deposits where film follows the morphology of the Au substrate underneath. Photoelectrochemistry measurement in methyl viologen solution under 1 sun with AM 1.5 filter showed the deposit to be n-type, with a very clean dark current, suggesting good film quality.

In chapter 3, the E-ALD of CdS on both planar Ag films and Ag nanorods on ITO was investigated. The difference between CdS E-ALD on Au substrates and Ag substrate is that Ag is a much more reactive metal than Au. Ag oxidizes easily and can form bulk Ag_2S at open circuit when exposed to sulfide solution. Thus the potential for CdS E-ALD on Ag must be carefully tuned. Cyclic voltammetry was used to study the electrochemical behavior of Cd and S individually on planar Ag substrate. No Cd UPD behavior was found on Ag substrate other than Cd-Ag alloy formation. The UPD formation of S on Ag substrate was limited to a small range from -750 mV to -675 mV. In the actual E-ALD process, Cd deposition potential was kept at -600 mV, and S deposition potential was varied from -675 mV to -600 mV. EPMA measured sulfur-deficient deposit until the potential was pushed to -600 mV. Stoichiometric deposits were formed at a potential of -600 mV for both Cd and S. SEM images showed conformal coating of CdS on planar Ag substrates. The deposition condition was transferred to the Ag nanorods, and under SEM the CdS thin film followed the morphology of the nanorods can coated the points and ridges conformally.

In chapter 4, the formation of CdS on indium-tin-oxide (ITO) substrate using E-ALD was investigated. Because of the heterogeneity nature of the ITO surface, neither S nor Cd showed any UPD behavior on ITO. A method was developed to pretreat the ITO substrate with 90 s pf reduction at -900 mV in pH 3 blank solution, and exchange the In metal formed from reduction with Cu^{2+}, leaving the surface with a small amount of stable Cu metal as the nucleation sites for

CdS UPD growth. The amount of In formed was found to increase linearly with increasing reduction time. The In metal clusters formed preferentially at the grain boundaries, and as the In^{3+} dissolved from the crystal lattice and nucleated to form In, pits were formed and the In cluster resided right next to the pits. After Cu redox displacement with In, the excess Cu bulk was stripped by scanning the potential anodically from open circuit to -200 mV. E-ALD was performed on the pretreated ITO substrate with Cd potential at -700 mV and S potential at -400 mV. SEM images showed that the treatment has significantly increased the number of nucleation site and improved the adhesion between the CdS thin film with the ITO substrate. SEM images taken at 5, 15, and 25 cycles showed progressive growth starting from the metal nucleation sites to smooth ITO surface. The Cd/S atomic ratio was determined by EDX to be 0.8, consistent with the S-deficient n-type CdS.

Chapter 5 focused on the fabrication of CdS/CdTe photovoltaic device with both superstrate and substrate configuration. In the superstrate configuration, the ITO substrate was patterned with 1x1 mm^2 squares using photolithography to separate the 2 cm^2 area into many individual cells. CdS thin film was deposited onto the patterned ITO using methods decribed in chapter 4. CdTe thin film was deposited onto CdS/ITO using pulse plating atomic layer deposition. Finally a Au was layer was electrochemically deposited onto the CdTe/CdS/ITO as the back contact. In the substrate configuration, CdTe was deposited onto Au substrate using cdepostion at -700 mV for 15 miniutes. CdS was deposited onto CdTe/Au using E-ALD with Cd depostion of -775 mV and S potential of -500 mV. The stoiochimetry of CdTe was measured with EPMA to be 1:1, and after CdS deposition, the Cd to (S+Te) was measured again with EPMA with 1:1, suggesting good stoichimetry with both films. XRD diffraction was taken for the CdS/CdTe/Au configuration to show CdTe zinc blend <111> structure and CdS <111>

structure. Photoelectrochemistry measurement of the CdS/CdTe/Au configuration in methyl viologen solution under 1 sun with AM 1.5 filter showed p-type response, which is expected for a p-n junction in an appropriate redox couple solution.

Chapter 6 focused on the deposition of an ultra-thin Au layer on triple junction amorphous solar cells. This is work is an extension of chapter 4 in terms of ITO reduction and inert metal redox exchange at open circuit. This method is not limited to Cu or Au, any metal that is more stable than In should theoretically work, but it depends on the function of the inert metal itself. Future studies can be done on characterizing the PEC performance of the Au-coated TJSC for catalyst attachment and water splitting. The Au exchange duration in the cycle can potentially be shortened to reduce the effect of acid etching on ITO during deposition. Different metals such as Pt, Ru can also be tested for best results.

Future work will be focused on two major aspects. The first is the extension of chapter 3. The E-ALD growth of CdS on Ag nanorods has been optimized. Nanostructured electrode materials are attractive for their unique electrical[1-2], photocatalytical[3] and optical properties[4] and have found applications in energy[5-6], environment[7-8], and electronics[9]. The unique structure of Ag nanorods should present interesting applications. Photoresponse of CdS on planar Ag substrates and on Ag nanorods can be measured and compared. The use of Ag nanorods is expected to enhance the light absorption and charge collection of thin layer photocatalysts such as CdS. Combining chapter 2 and 3, CdS formation on Au nanorods can also be studied as an extension of chapter 2. The dependence of light absorption enhancement on the length and density of nanorods, and on the thickness of the CdS layer thickness can be investigated. Such study is helpful for developing real-world applications such as hydrogen evolution and water splitting using semiconductor photocatalysts on metal nanorods structures.

The second focus should be the further development of a good performance CdTe/CdS solar cell. On the superstrate configuration front, to reduce the likelihood of shorting from the back contact to the front contact, the photoresist width can be increased each time a new layer is put on, so that the top back contact layer has a minimum chance to pass through the CdS/CdTe layer to reach the ITO layer. The choice of back contact material can also be explored, due to the high price tag of Au for large scale PV production. Mo is a popular back contact metal for CdS/CdTe solar cells because it is inexpensive, conductive and is not too mobile to diffuse into the CdS/CdTe layers. Another optimization is the Cl treatment for CdTe solar cell. Cl treatment is known to improve the performance of CdTe/CdS solar cells, although the reason is still unclear. Annealing of the substrate and the thin film may also improve the structure of the deposit, leading to a better performance. Investigating such treatments is an essential step for fabricating a high efficiency CdTe/CdS solar cell.

References

1. Cao, Z.; Ouyang, L.; Li, L.; Lu, Y.; Wang, H.; Liu, J.; Min, D.; Chen, Y.; Xiao, F.; Sun, T.; Tang, R.; Zhu, M., Enhanced discharge capacity and cycling properties in high-samarium, praseodymium/neodymium-free, and low-cobalt A2B7 electrode materials for nickel-metal hydride battery. *International Journal of Hydrogen Energy* **2015,** *40* (1), 451-455.

2. Boles, M. A.; Ling, D.; Hyeon, T.; Talapin, D. V., The surface science of nanocrystals. *Nature materials* **2016,** *15* (2), 141-153.

3. Grassian, V. H., When Size Really Matters: Size-Dependent Properties and Surface Chemistry of Metal and Metal Oxide Nanoparticles in Gas and Liquid Phase Environments. *The Journal of Physical Chemistry C* **2008,** *112* (47), 18303-18313.

4. Wen, X.; Xie, Y.-T.; Mak, W. C.; Cheung, K. Y.; Li, X.-Y.; Renneberg, R.; Yang, S., Dendritic Nanostructures of Silver: Facile Synthesis, Structural Characterizations, and Sensing Applications. *Langmuir* **2006,** *22* (10), 4836-4842.

5. Ouyang, L.; Guo, L.; Cai, W.; Ye, J.; Hu, R.; Liu, J.; Yang, L.; Zhu, M., Facile synthesis of Ge@FLG composites by plasma assisted ball milling for lithium ion battery anodes. *Journal of Materials Chemistry A* **2014,** *2* (29), 11280-11285.

6. Persano, L.; Camposeo, A.; Pisignano, D., Active polymer nanofibers for photonics, electronics, energy generation and micromechanics. *Progress in Polymer Science* **2015,** *43*, 48-95.

7. Tachibana, Y.; Vayssieres, L.; Durrant, J. R., Artificial photosynthesis for solar water-splitting. *Nature Photonics* **2012,** *6* (8), 511-518.

8. Brillet, J.; Yum, J.-H.; Cornuz, M.; Hisatomi, T.; Solarska, R.; Augustynski, J.; Graetzel, M.; Sivula, K., Highly efficient water splitting by a dual-absorber tandem cell. *Nature Photonics* **2012,** *6* (12), 824-828.

9. Ozbay, E., Plasmonics: merging photonics and electronics at nanoscale dimensions. *science* **2006,** *311* (5758), 189-193.